# MICROFLUIDIC DEVICES FOR MEMBRANE PROTEIN NANOPARTICLE FORMATION

by

Hsin-Jui Wu

B.S.,M.S., Da-Yeh University, 2004

M.S., University of Colorado Boulder, 2009

A thesis submitted to the

Faculty of the Graduate School of the

University of Colorado in partial fulfillment

of the requirement for the degree of

Doctor of Philosophy

Department of Mechanical Engineering

2013

This thesis entitled:
Microfluidic Devices for Membrane Protein Nanoparticle Formation
written by Hsin-Jui Wu
has been approved for the Department of Mechanical Engineering

_____
Professor Michael H. B. Stowell

_____
Professor Yung-Chen Lee

Date_____

The final copy of this thesis has been examined by the signatories, and we
Find that both the content and the form meet acceptable presentation standards
Of scholarly work in the above mentioned discipline.

## Abstract

Wu, Hsin-Jui (Ph.D., Mechanical Engineering)

Microfluidic Devices for Membrane Protein Nanoparticle Formation

Thesis directed by Associate Professor Michael H. B. Stowell and Professor Yung-Chen Lee

Microfluidic devices, so-called BioMEMs, or Lab on a chip, have been widely used to improve the science and technology, especially in biological applications. The analysis of protein structure formation is currently one of the most interesting research areas in biology. The analysis of protein structure not only aid scientists in realizing the interaction of molecule biology but also can be applied to improve in the development of the drug design in pharmacology. Our main focus is on the membrane proteins that are estimated to be more than 30% of total protein number. These membrane proteins can be a transport channel for controlling molecule transportation, a sensor and a receptor to communicate between cells. The existing structures of membrane proteins are embedded with lipid bilayer structure where they are naturally formed by hydrophobic reaction. Consequently, the best way to analyze the single membrane protein structure is from the purified single membrane-detergent complex added with lipid and then removing the detergents to form a nature structure of membrane protein with lipid bilayer which is called a reconstitution, or membrane protein crystallization. The current method of membrane protein crystallization is using dialysis membrane in between protein-detergent-lipid solution and a buffer solution to dialyze and remove the detergents. The main drawbacks in the current methodology include time-consuming hand pipette, large volume of protein sample consumption (microliter), and slow diffusion of dialysis process (days). We

present a new method of membrane protein crystallization by using microfluidic device to achieve the reconstitution. This microfluidic device is designed and fabricated by using a soft lithography which is one of MEMs techniques. Based on this new microfluidic device we can reach break-through improvements compared to the current method with dialysis membrane. First, hand pipette is no longer required because the input fluids are all driven by controllable syringe pumps. Secondly, micro channels allow a lower volume of protein sample consumption, nanoliter to picoliter. The third advantage is the diffusion process in microfluidic device can be completed in few seconds without dialysis membrane to form membrane protein crystals.

## ACKNOWLEDGEMENTS

I would first like to deeply thank my two advisors, Prof. Michael Stowell in MCDB and Prof. Y. C. Lee in Mechanical Engineering, for their support and guidance over the past years. Working with Michael and Y. C. was the best experience and I definitely enjoyed the time in their labs and leaned from them as well.

Also, I would like to thank all of people who has helped me for years. To the all members of Michael's group in MCDB, thanks for all of help and teaching me the fundamental knowledge of biology, especially Dr. Tamara Basta, Dr. Steve Eisenberg, and Dan Adams. To the all members of Y.C.'s group in Mechanical Engineering, thanks for all of help, technique sharing and collaboration, especially Dr. Rick Chuang, Dr. Martin Lin, Dr. Leo Cheng, Dr. Li-Anne Liew, Ching-Yi Lin, and Paul Schroeder. I am so grateful to have all of you for the past few years.

Finally, I would like to thank all of my family and friends in Taiwan who has always been there supporting me. And special thank to my parents, brother, and sister, really thank you all for your patience, encouragement, and unending love that support me to finish my doctoral thesis and complete this unforgettable doctoral journey.

CONTENTS

CHAPTER

TABLES

FIGURES

# CHAPTER 1

# INTRODUCTION

## 1.1 Overview

In the past few decades microfluidic techniques have been widely applied in different fields such as chemical, biological and mechanical areas. Basically, microfluidics are used to manipulate and control a small volume amount of various fluids in small scale channel patterns to do experiments, a process also referred to as “Lab on a chip” [1,2]. The amount of fluid is usually within microliter/nanoliter/picoliter and dimensions of channel are between millimeter (mm) to micrometer (um). One of the advantages of using microfluidic devices is to reduce the consumption of fluid and therefore, the cost. For example, in biological experiments some of the samples, such as the well-purified proteins are difficult to produce and expensive. Therefore it’s a major consideration for scientists to reduce the amount of samples needed during the process.

If we can convert the current experiment into a small scale then the problem of saving sample consumption can be solved by only using nanoliter or less amount of samples in microfluidic device. This could be addressed by transplanting the current process onto microfluidic devices such that experiments can be done in smaller scale and only nanoliter (or less) amount of samples are needed.

### 1.2 Size matters in Microfluidics

When the sizes of fluids reduce to a micron scale, some physical phenomenons of fluids in microfluidic system are changed [3]. One of dimensionless numbers is Reynolds number which is a major number in the fundamental physics of fluids to determine flow is laminar or turbulence scheme. Reynolds number presents the relative ratio of inertia force to viscous force. Here is a equation, where **ρ** is the density of fluid (kg/m3), **υ** is the mean velocity of fluid (m/s), **L** is the dimension of channel width (m), **μ** is the dynamic viscosity of fluid (kg/(ms)), and **η** is the kinematic viscosity (**η = μ/ρ**) ($m^2/s$).

$$Re = \frac{\rho v L}{\mu} = \frac{v L}{\eta} , = \frac{inertia\ force}{viscous\ force} \quad (1)$$

Basically, laminar flow occurs when Reynolds number < 2000 and turbulence flow occurs when Reynolds number > 4000. Following from the Reynolds number equation, decreasing dimension of channel width L, especially in micrometer scale, leads to Reynolds number becoming smaller. Applying appropriate parameters which are from the micron scale into Reynolds number equation, the Reynolds number is far smaller than 2000, Reynolds number in our case are only between 0.02 to 20. Because of size reduction from micron scale, most of them, using liquid fluid to be major flows such as water and oil, are laminar flow except compressible gas.

Because turbulence flow barely occurs in microfluidic system only laminar flow and convections need to be considered. Although convection is the key importance to increase mixing efficiency by turbulence flow in the large scale, diffusion of laminar flow also can play same role in the micro scale. When there is an interface between in two different concentration fluids, the mixing processes naturally diffuse from high concentration to low concentration. Diffusion time **t** (s) related with the distance **d** (m) to travel and diffusion coefficient **D** ($m^2/s$). For instance, if particles in a fluid have same diffusion coefficient but in different traveling distances, such as 5 mm and 5 um, and the diffusion time in 5um will be $10^6$ faster than diffusion time in 5mm. Thus some experiments in large scale, which have to wait for diffusion process and need to use large

volume of precious liquid, when converted into the small scale are not only reducing material consumption but also reducing time for completing processes [4].

$$\boldsymbol{t = \frac{d^2}{D}} \tag{2}$$

In the microfluidic system the dimensionless Capillary number (Ca) also needs to be considered especially for droplet formation in two-phase immiscible flow such as water droplet in oil or oil droplet in water by generating designs of T-junction and flow focusing. The capillary number is the ratio of viscous stress and surface tension between two immiscible flows.

$$Ca = \frac{U\mu}{\gamma}, \ = \frac{Viscous\ stress}{Interfacial\ tension} \tag{3}$$

**U** is the velocity of continuous phase; **μ** is the dynamic viscosity of continuous phase, and **γ** is the surface/interfacial tension between two immiscible fluids. Above a critical Ca number, a droplet will be formed due to the inner fluid being sheared and extended by continuous flow. When inner flow has extended long enough, surface tension is allowed to break the flow into droplet formation. In addition, by adding surfactants in one of phases, it can reduce interfacial/surface tension between two phases and keep droplets in more stable situation.

### 1.3 Microfluidics in biological applications

Developed applications by microfluidic techniques have been applied to biological field such as polymerased chain reaction (PCR) chip. There are also other interesting areas including droplet generating, chemical trial mixing, and biological sample screening [5,6]. Two phase flow water-based droplet formation is a common methods for generating droplets. Water is injected into a continuous oil flow to form a water-based droplet due to surface tension break viscous stress. Using this method the biological sample can be isolated in water droplet and delivered by carrier oil through micro channels.

One of the methods to form droplets is called T-junction [7] where water flowing perpendicular injects to continuous oil flow and then shear stress of oil breaks off viscous of water to form water droplet. In addition the water-based droplet not only can be mixed with different water-based components and conditions before oil is isolated but can also make hundreds to thousands number of droplets sequentially, so-called high throughput microfluidic system. Bo Zheng et al has demonstrated screening of protein crystallization by using T-junction of

microfuildic devices with few nanoliter of protein solution. Figure 1.1 and 1.2 present these microfluidic systems where mix buffer, protein, and other components with different ratio by changing each input flow rate [8-10]. Moreover, 100 sample droplets with different trials were delivered to glass capillary tube for protein structure analysis screening by X-ray diffraction.

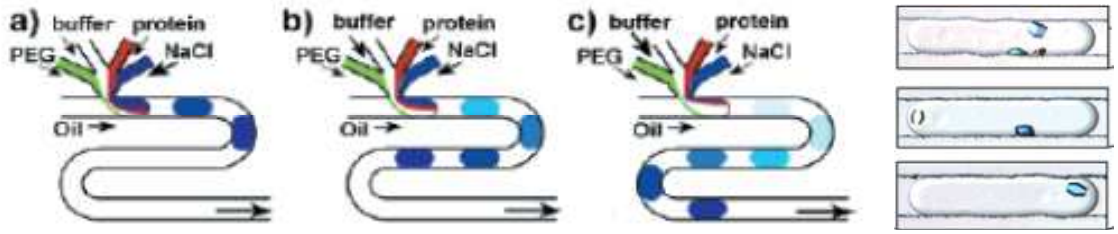


Figure 1.1 shows a microfluidic system for protein crystallization. (a-c) gradient droplet colors present each protein sample has different conditions by controlling flow rate. (e) Protein crystallizes [8].

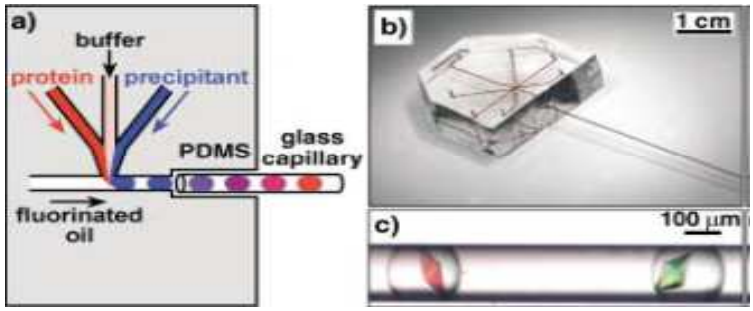


Figure 1.2 shows the mixing with buffer, protein and precipitant with different conditions and formed droplets by continuous oil in T-junction. Then droplets are delivered to glass capillary for X-ray screening [9].

Another method, the flow focusing system, also has been demonstrated to generate droplets in microfluidic devices of biological applications [11]. This method consists of a continuous center water flow injected into a main channel and break off to form water-based droplets by a shear stress creating from the oil flows of the both sides. Figure 1.3 shows the droplet generation of multi-step mixing method by using flow focusing where two water-based flows carry with the sample and are mixed before injection into continuous oil [12]. Adjustment of the flow rate ratio for two inputs from syringe pumps, allows the mixing ratio of two samples can be controlled. Based on these methods, it is not difficult to manipulate and control mixed droplet with different mixing ratio .

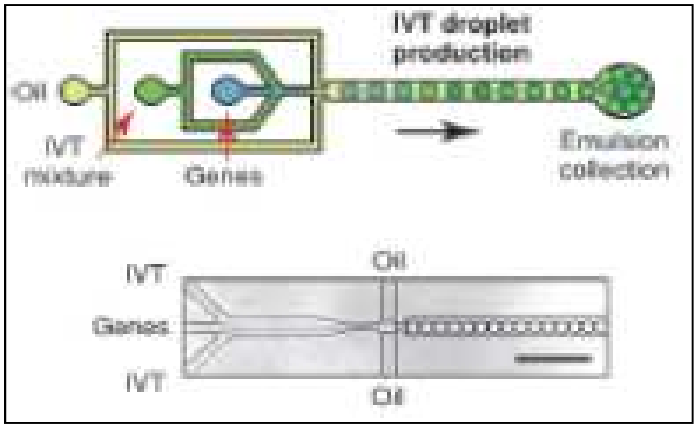


Figure 1.3 shows the generation of the Multi-step mixing droplets by flow focusing method. To change mixing ratio by controlling flow rate ratio of two water-based inputs [12].

However, to keep in one certain mixing ratio with same size droplets and generate hundreds to thousands of droplets with specific same mixing ratio is difficult. This is because is not easy to hold the stable flow rate and stable pressure in microfluidic devices when there are 2 or more input resources. In such a small scale of channels, slight changes will cause different results and obviously occur if flows are driven by changing pressures. The syringe pumps provide flow rate related with pressures for driving fluids forward. During changing flow rates from syringe pumps, the unstable pressures into channels will create a pressure gradient from pump to channel. In this period, pressures are in transition and thus mixing ratio and droplet size are also not in stable.

The water-based droplets can be formed in T-junction by two immiscible flows and can be delivered by controlling carrier flow such as continuous oil. In contrast the T-junction also has been demonstrated for the separation of droplets of different sizes [13]. During the continuous flow, oil carries water droplet to go into T-junction channel, the continuous oil separates into two opposite directions inducing the surface tension between water and oil sheared to break the viscous of water droplet (Figure 1.4). Therefore one water droplet is forced to become two droplets. The flow resistance concept is used to determine the size of droplet after droplet break up.

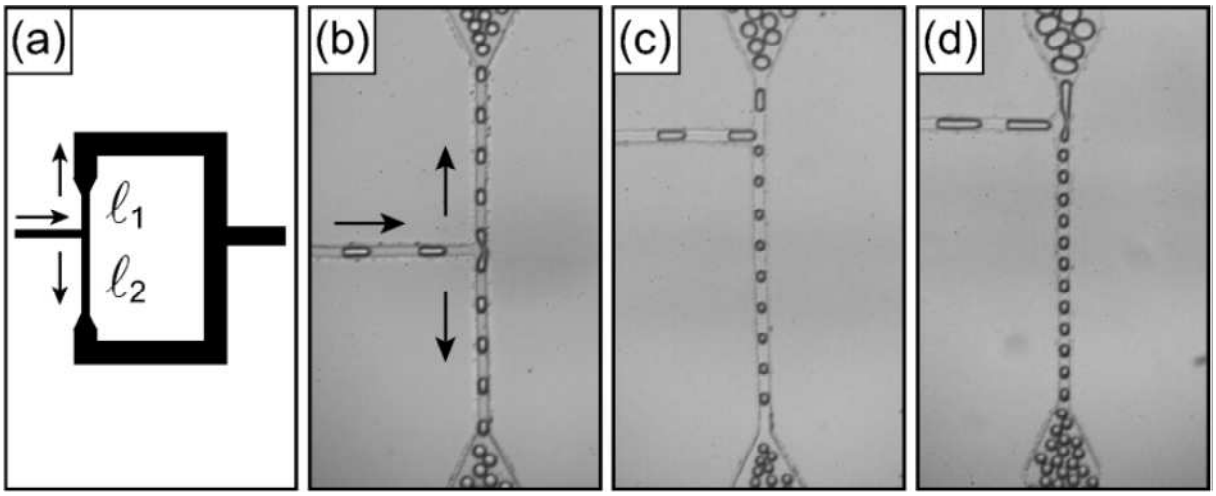


Figure 1.4 shows the method of the droplet break up in T-junction. b) same lengths of channels with same break up droplet size; c,d) longer length of channel has smaller droplet due to higher flow resistance [13].

In addition, the microarray for delivery and localization of droplets by using flow resistance concept are the significant application as well (Figure 1.5). Water-based droplets are generated from T-junction or flow focusing and then the oil carries water droplets in the micro channels. Different geometry designs can be used to make different flow resistances for droplet delivery and localization [14, 15].

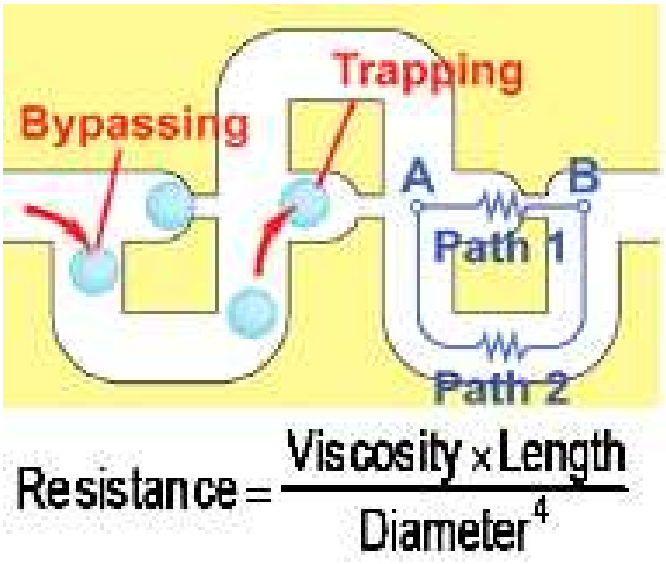


Figure 1.5 shows the schematic and equation of the flow resistance. The droplet is delivered and localized into a trap whit two paths, path 1 and path 2. The droplet will choose path 1 and after it is localized. The following droplet will bypass through path 2 and sit in the next trap [14].

As the carrier oil flow goes from point A to B, there are two paths it can go; path 1 and path 2. The path chosen will be determined by flow resistance to see which has more oil flow going through as well as current in the electric circuit. Thus carrier flow will go through path 1 first because of the equation of the flow resistance the short length will have the smaller flow resistance. After the carrier flow carries the water, the droplet becomes stuck in the trap. The flow resistance of path 1 will increase to be larger than path 2 due to the channel diameter changed when droplet is trapped. Then the second water droplet will bypass and go to the path 2 and trapped in the next designed trap.

Following this process continuously, it can be formed the microarray of the water-based droplets (Figure 1.6) [16]. By using this flow resistance concept, we not only can be localized the droplet but also isolate individual droplets in microarray device for biological sample screening.

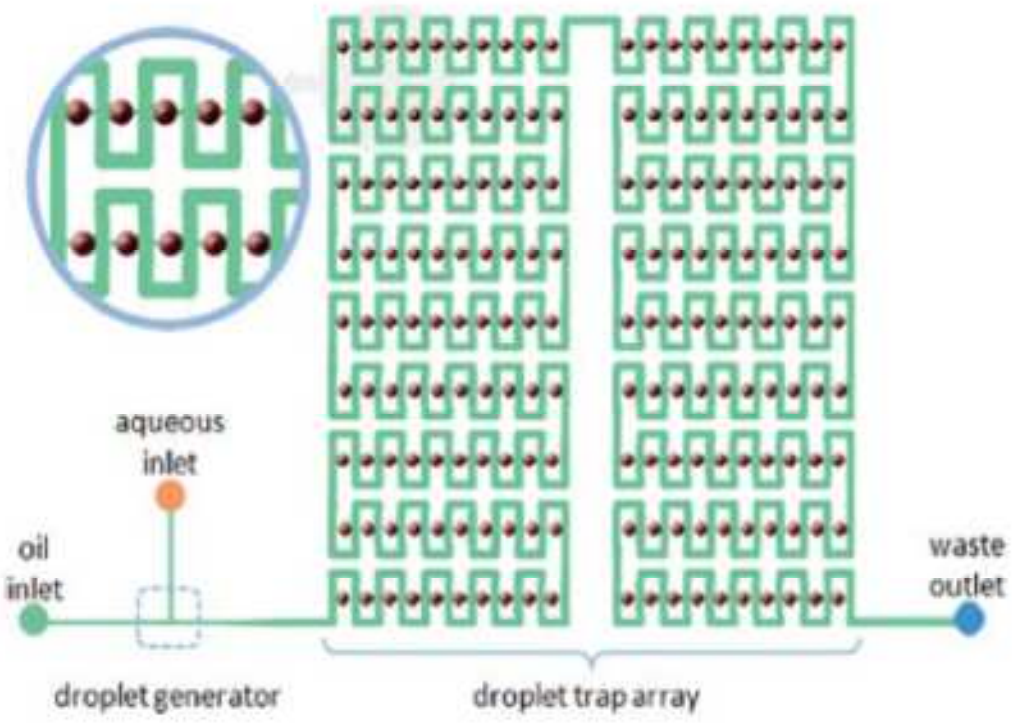


Figure 1.6 shows the scheme of the microarry by using the flow resistance concept. Eventually droplets located and isolated in each trap for experiment [16].

Besides the two-phase flow (water/oil) of droplet-based in T-junction or flow focusing systems,

there is another famous application in biological areas, a single-phase flow. When the two continuous flows with different concentrations mix in a micro channel, the final concentration can reach an equilibrium stage by diffusion process. This diffusion mechanism in microfluidic channels is usually designed for filtering, diluting and mixing in some chemical reaction applications.

The membraneless H-filter is the best example of filtering that can be applied to removing or collecting the chemical particles as a purification process without a membrane filter. The diffusion coefficients of the particles are dominated by their size. The large particle size has a large diffusion coefficient so it needs a longer diffusion length (L) to be transported or removed during the diffusion procedure. Consequently, the way to collect or remove different sizes of chemical particles in flow is controlled by changing and designing a certain diffusion length. Figure 1.7 shows the design geometry of H-filter. The sample and solution with particles are injected from both sides and then merged in the initial across of main channel. The large particles remain on the stream and deliver to waste output because the particles along the designed length (L) have no time to be diffused. Thus the purified solution without particles was mixed with sample and delivered to outlet of the left-hand side. This simple H-filter not only can be mixed with sample and solution with particles in initial intersection but can be removed the unwanted

from the particles in main channel by diffusion process.

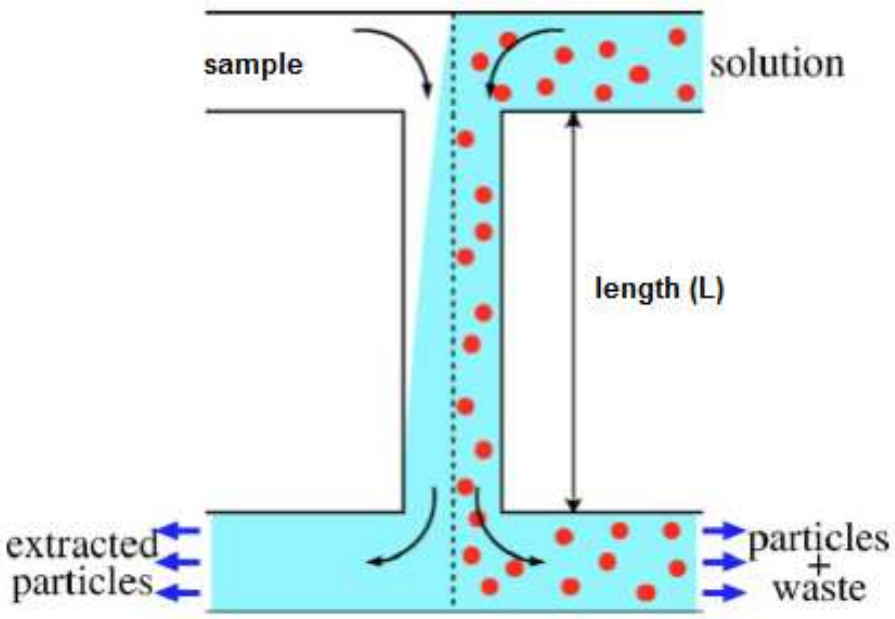


Figure 1.7 Presents a membraneless H filter. Sample and solution with particles mixed in initial intersection of main channel. The lack of diffusion length (L) does not allow time for particle to diffuse. Thus the particles remain in the initial stream and are delivered to the waste outlet. The sample with purified solution without particles is sent to the outlet of left-hand side.

The flow scheme of our membraneless device is the laminar flow that present the stable streams in the channel, and not crossed with each other. According to stable streams in laminar flow we can modify the design of the output as illustrated in the diagram (Figure 1.8) below using three separate channels. The middle output will act as the collector channel for the samples of

membrane protein crystals. The other two are waste channels for buffer solution where they are mixed with removed detergents during diffusion [34]. Thus we can increase the density of membrane protein crystals by simply collecting from the middle output.

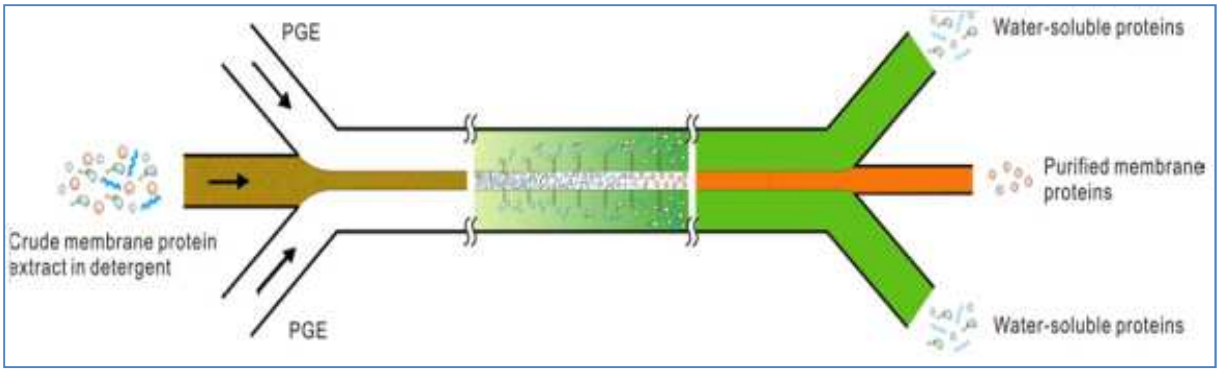


Figure 1.8 shows that the design of output can be used for collecting the membrane protein crystal samples [34].

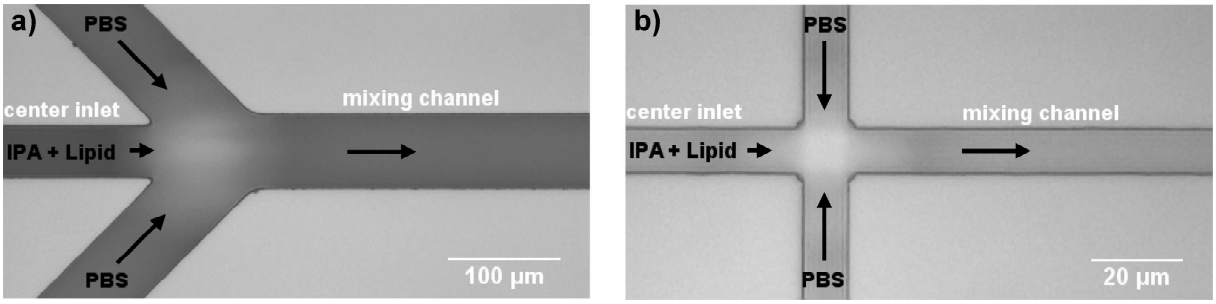


Figure 1.9 presents the flow focusing method applied on forming a lipid vesicle. The higher concentration of lipids were diluted by convection-diffusion and bellowed its CMC to reconstitute vesicle structure.

Figure 1.9 shows the single phase of flow focusing applied to the diluting approach where the isopropyl alcohol (IPA) with lipid injected into center of main channel and merged with the physiology buffer solution (PDS) from both sides.

When the center stream merges the outer buffer solutions, the higher concentration of center flow being diffused to the outer lower concentration flow by convection-diffusion phenomena. Due to this process the high concentration flow can be diluted and eventually reach an equilibrium. Additionally the diluting speed also can be controlled by varying the Flow Rate Ratio (FRR) of horizontal (IPA+Lipid) and perpendicular (PBS) inputs. A higher FRR creates a stronger convection-diffusion effect to force a faster mixing speed. Therefore, this method provides lipids diluted from their initial concentration to finally attain its critical micelle concentration (CMC) to form a lipid vesicle structure.

# CHAPTER 2

# MEMBRANE PROTEIN

## 2.1 Overview

Membrane proteins are permanently embedded in the lipid bi-layer and are essential in biology because they play major functional roles in membrane cells. For instance, membrane proteins are transport channels that allow ions, small or macro molecules pass through membrane cell. And they are also signal receptors and sensors to communicate between cells. Thus, many membrane proteins are aimed at drug design and drug delivery for diseases.

Membrane proteins are estimated to represent more than 30% of the protein encoded in the genomes of the organism. While only containing less than 1% of the structure entries in the Protein Data Bank. The first structure of membrane protein was solved more than 20 years ago.

They only around 140 membrane protein structures corresponding to around 80 unique types of membrane protein have been elucidated to date [17,18].

Unfortunately the process to obtain 2D membrane protein structure is difficult because they require crystallization in not only a certain conditions but also in a nature hydrophobic environment with a lipid bilayer. Therefore, it is important to develop a new method that can generate and obtain the crystal structure of membrane proteins more efficiently. Moreover, optimization of finding initial conditions for membrane protein crystallization is the crucial final goal.

## 2.2 Methods for membrane protein crystallization

Currently there are several methods for growing crystal structure of 2D membrane proteins and 3D proteins [19]. Figure 2.1 shows the membrane protein structure determination procedure. The first step is to obtain membrane fragments from crude cell of tissue which is called the extraction. Depending on the types of membrane fragments desired, there are several extraction methods that could be used, such as sonication, and filtration.

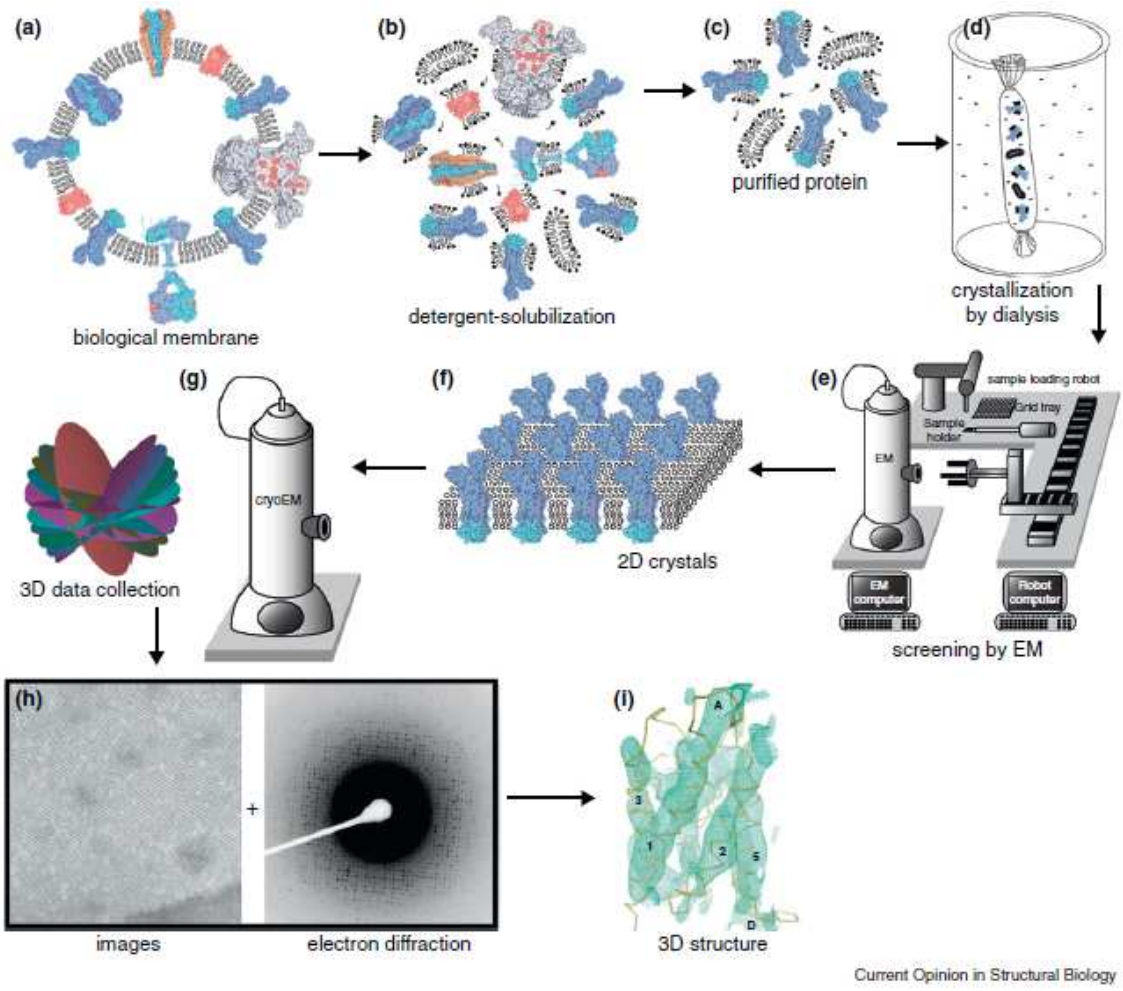


Figure 2.1 shows the membrane protein structure determination procedure from the cell membrane to 3D structure, a) biological membrane, b) using detergent to solubilize membrane, c) purifying the membrane protein to collect a single type of membrane protein, d) crystallization by using dialysis method to remove detergent and form lipid bi-layer structure aggregated with membrane protein, e) screening by electron microscopy (EM), f) if 2D crystals achieved, then g) collect image data by cryoEM, h) tomography analysis, i) 3D structure.

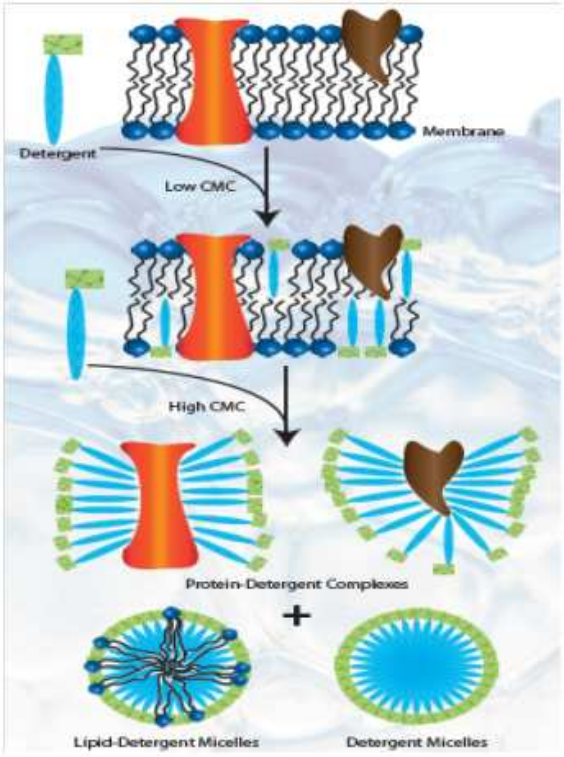


Figure 2.2 shows purification of membrane protein by detergents with critical micelle concentration. At high critical micelle concentration of detergent the membrane protein would be extracted from lipid bilayer structure and become protein-detergent complex formation.

Purification is the next step which purifies protein sample and removes unwanted molecules from membrane fragments. Obtaining protein samples is not as easy as it seems. It is estimated that there are hundreds to thousands of different proteins in a single cell. The most useful techniques to separate and isolate membrane proteins is by using detergents and filter to obtain the certain desired protein. Since the membrane proteins are held in the lipid bilayer structure by

hydrophobic interactions, they maintain a native conformation when separated from cells. The protein can be released from the lipid bilayer by adding detergents because the detergent's micelles have similar properties as lipid.

The solubilization of proteins from lipid bilayers depends on the Critical Micelle Concentration (CMC) of detergents which is defined as a concentration of surfactants above that where micelles are formed (Figure 2.2). At low CMC of detergent, the detergents solubilize the lipid bilayer and integral membrane proteins to form a complex consisting of detergent, protein and lipid molecules. At high CMC of detergent, the lipid bilayer becomes saturated with detergent and lipid bilayer brakes apart. Thus, the resulting products are protein with the detergent complex where the hydrophobic regions of detergent bind to hydrophobic domains of protein protecting them from aggregation (Figure 2.3).

Next the protein samples are formed into protein and detergent complexes. The two categories for obtaining protein crystals after purification process, crystallization are 3-Dimension (3D) and 2-Dimension (2D). For the 3D crystallization, the protein samples have to further remove detergents and be pure enough for growing protein crystal. When proteins are crystallized, protein structures can be analyzed by X-ray diffraction crystallography to obtain the 3D protein

structure. However, the membrane proteins are more difficult to be crystallized in 3D structure due to native membrane protein environment with lipid bilayer.

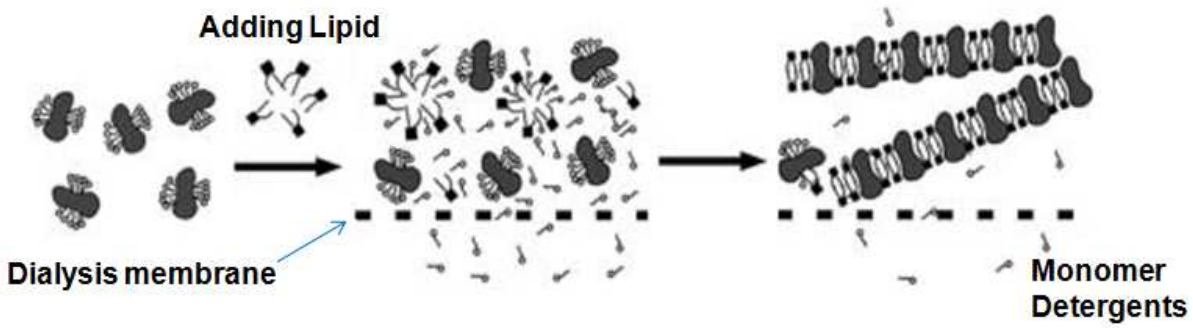


Figure 2.3 2D membrane protein crystallography by using dialysis. The membrane proteins mixed with lipids and the detergent is allowed to be removed and the lipids form a bilayer where the protein can be incorporated and form 2D crystals [20].

To resolve this issue, the structures of membrane proteins embedded with a lipid bi-layer. The 2D membrane protein crystals is a current method using electron microscopy. The processes of the obtaining 2D membrane protein crystallography are start with a purified membrane protein with detergents where protein samples are mixed with lipids and slowly remove detergent by natural diffusion with the dialysis membrane. Upon complete removal of detergents, membrane protein is reconstituted with lipid bilayer structure forming into 2D membrane protein crystal. The 2D membrane protein crystals obtain the images by electron microscopy showing in Figure 2.4. A

collection of 2D membrane protein images with various angles can produce the 3D image of structure utilizing software, which is called tomography [20].

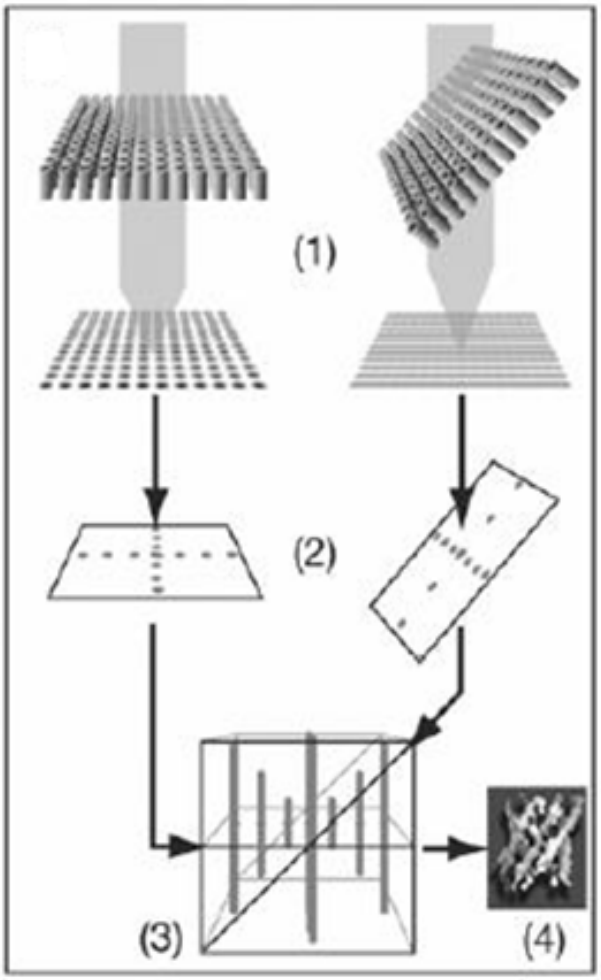


Figure 2.4 shows the tomography method to create 3D structure from 2D membrane protein crystals by image processing which extracts the information from high-resolution images and electron diffraction patterns for mergeing it into a 3D potential map.

## 2.3 Comparison of 3D and 2D protein crystallization

There are several benefits of using 2D membrane protein crystallography versus 3D crystallography. First, membrane proteins require conditions that make their membrane spanning regions soluble. In 3D crystallography, the protein sample must be purified enough to form crystals of only protein [21]. In 2D crystallography, the membrane protein only needs to be soluble by lipids and will form sheets of crystallized protein within lipid bilayers. Second, the membrane proteins can form crystals fairly rapidly using 2D membrane protein crystallography. In 3D crystallography, pure proteins are placed in specific crystallization conditions and left to sit until crystals are formed, this could take weeks to months if crystals even form at all. In 2D membrane protein crystallography, crystals are formed rapidly because the limiting step is detergent removal. Upon detergent removal, lipids can form bilayers where proteins can gain order and form crystals. Lastly, the 2D membrane protein crystallography followed by high-resolution electron microscopy can produce atomic level 3D images of membrane proteins [22].

## 2.4 Current conventional dialysis method

The current and most common technique to obtain 2D membrane protein crystallization is diffusion which removes detergents in microliter scale by using dialysis membrane [26]. Figure 2.5 shows the method of using the dialysis membrane.

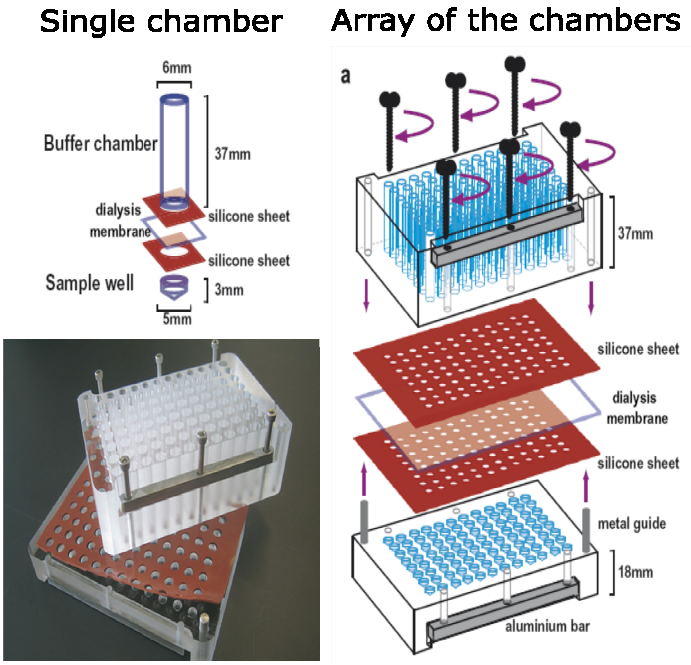


Figure 2.5 shows currently the common method for 2D membrane protein crystallization. The equipment consists of buffer chamber on the top, dialysis membrane in the middle, and sample well at the bottom. Detergents will be removed to buffer chamber by natural diffusion process and dialysis membrane will keep the large molecules in sample well [26].

The equipment consists of three parts from top to bottom in which are buffer chamber, dialysis membrane and sample well. Membranes protein-detergent complex samples are mixed with lipids in the buffer liquid and pipetted into the sample well. Due to the difference of detergent's concentration between the buffer chamber and the sample well, a gradient of concentration is formed between the buffer chamber and the sample well. During diffusion process, the gradient changes and the Critical Micelle Concentration (CMC) of detergent in sample well also decreases until equilibrium. The protein-detergent complex starts to break up and the detergents are released from protein and become monomers to diffuse out of sample well. The lipids will form membrane bilayer and the protein will be embedded with bilyaer structure to form the membrane protein which is a native environment. After the membrane protein integrated with lipid bilayer, it cannot pass through dialysis membrane which only allows small molecules, such as detergent monomers, to pass through into buffer chamber.

There are still some disadvantages with current method, such as the lager volume of protein samples need ("a few microliter"), compared to nanoliters as in the microfluidic devices, longer time period to completing dialysis process ( "usually few days"), and pipetting by hands.

# CHAPTER 3

# FABRICATION OF MICROFLUIDIC DEVICE AND FLOW VISUALIZATION

## 3.1 Overview

The fabrication processes of microfluidic devices consist of few steps which are mask design, wafer patterning and device making. Currently, several MEMs techniques have been applied to microfluidic devices such as photolithography, and soft lithography [23]. By using these techniques, researchers have designed different functional microfluidic devices to control fluids such as micro mixers, micro valves, droplet generations and droplet separations. Furthermore, the sizes of microfluidic channels are getting smaller and smaller, commonly below a hundred micrometers, which improve mixing efficiencies and minimize the amount of fluids used. Figure 3.1 shows a global view of our current design schemes including the mixing device(a), the mixing device with designed outlet for increasing density (b), flow focusing lamina flow device

(c), and flow focusing lamina flow device with designed outlet for increasing density (d). Moreover, because the membrane protein samples and the buffer solution are all transparent, barely to be observed by microscope, we tried to use blue-dye in the pre-test examination for flow visualization to demonstrate the flow focusing phenomena in microfluidic device

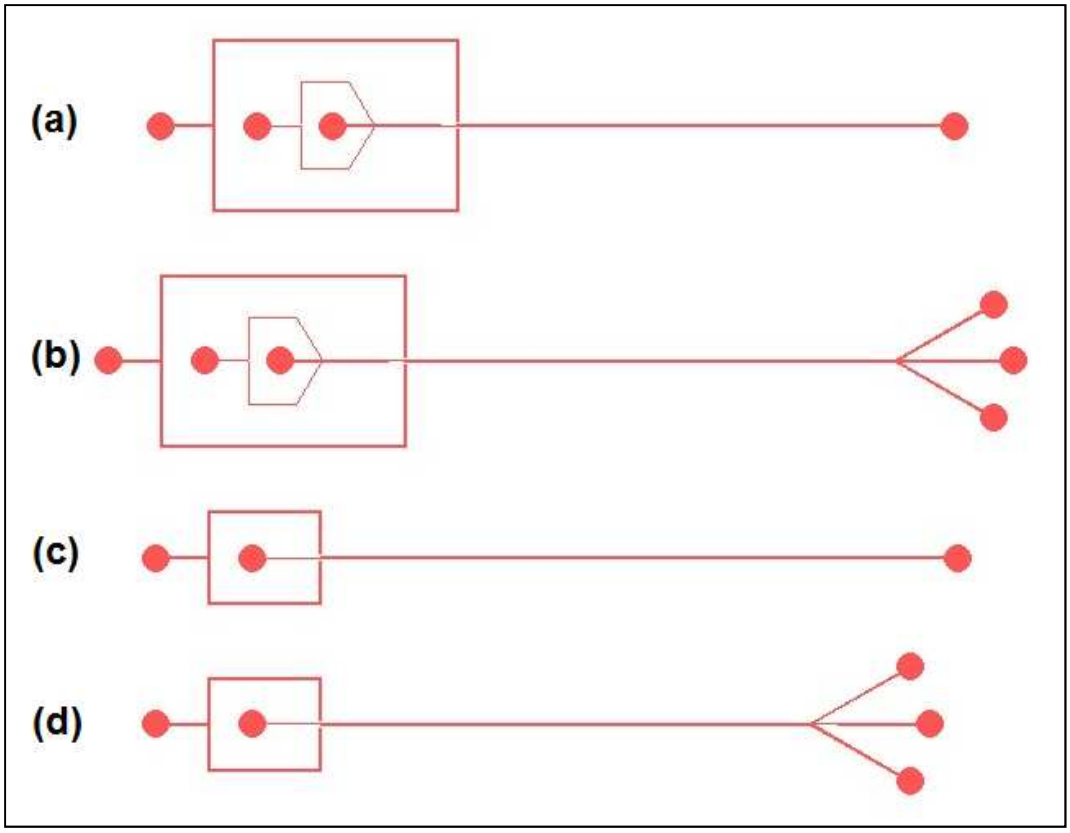


Figure 3.1 shows the global view of four designs, top to bottom are a mixing device, mixing device with designed outlet for increasing density, flow focusing lamina flow device (c), and flow focusing lamina flow device with designed outlet for increasing density (d).

### 3.2 Photolithography

The fabrication process was derived from photolithography and softlithography method, a common Bio-MEMS technique that has advantages such as low cost and ease of fabrication. Photolithography starts from the three inch silicon wafer with one-side polished as a based substrate for the first preparation stage (Figure 3.2).

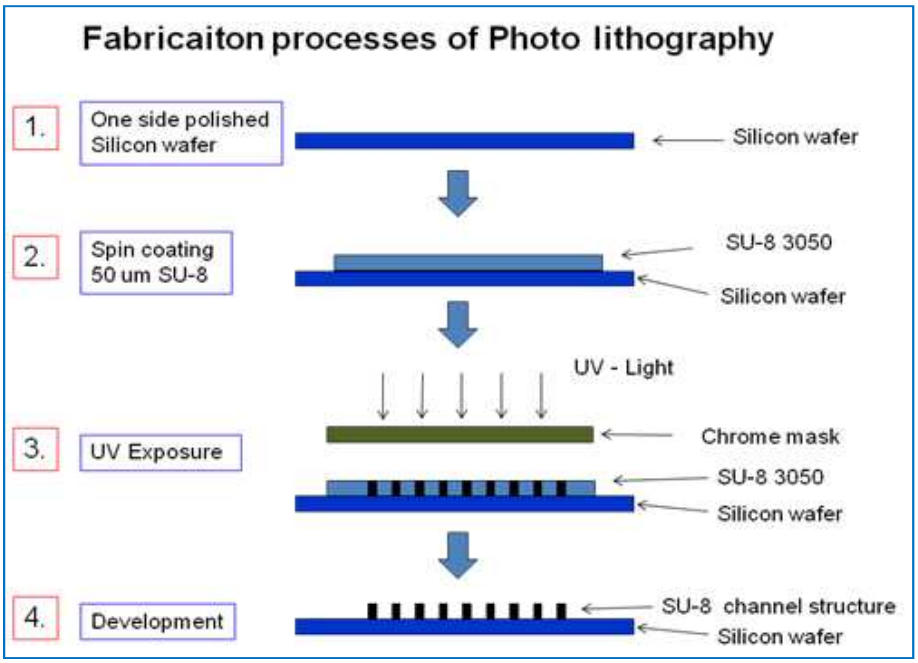


Figure 3.2 Fabrication processes of photolithography. 1. Preparation of one-side polished silicon wafer. 2. Pour SU-8 on the top of silicon wafer and spin coating at certain speed. 3. UV exposure. 4. Development for removing un-crosslinked SU-8.

Next the light-sensitive epoxy based negative photo resist SU-8 is used for the structure material on the silicon wafer. Different types of SU-8 have different bonding strength and viscosity such as the 3000 series having a better bonding strength with a silicon wafer compared to the 2000 series and 3050 series with a higher viscosity than 3010. Moreover, higher viscosity SU-8 under high spin coating speed can reach more stable flat surface due to centrifugal force effect. Based on above considerations and after testing we chose SU-8 3050 from Microchem company, which has high bonding strength with silicon and allows high speed spin coating to achieve flat surface to be our pattern structure material. To increase the bonding strength of silicon wafer with SU-8 and create a high quality SU-8 surface, preparation of the silicon wafer has to go through a cleaning process which includes Piranha, acetone, isopropanol alcohol(IPA), and a de-ionized water rinse. After the wafer cleaning process, liquid SU-8 is dispensed onto the polished surface of silicon wafer and is spun at a certain speed 3000 rpm to create a 50um thickness of SU-8 structure. After spin coating, a soft bake process follows in which the silicon wafer is placed on a leveled hotplate for 15 minutes at 95 degree Celsius to evaporate solvent in the SU-8 resist and then gradually cool-down to room temperature to avoid wrinkles. Now the resist has become hardened and is ready to go to ultraviolet (UV) exposure. When UV light passes through the transparent area of chrome mask, the patterned resist is crosslinked due to chemical reaction. The

next step is the post exposure bake on the hotplate for 1 minute at 95 degree C and then gradually cool-down to room temperature similar to the soft bake. The final step is the development process which removes the un-crosslinked resist by dissolving in Microchem's SU-8 developer liquid. Eventually the mold for microfluidic channels is made of SU-8 patterned structure on 3 inch silicon wafer surface. (Figure 3.3).

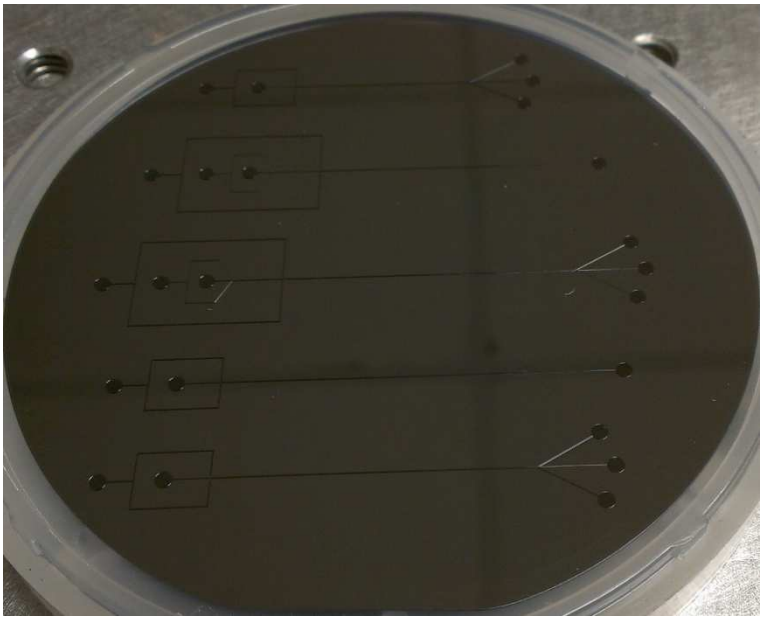

Figure 3.3 shows the illustration of the SU-8 structure on the silicon wafer.

### 3.3 Softlithography

After completing the process of making the SU-8 channel structure on silicon wafer, the next step is fabrication of a microfluidic device by printing in Polydimethylsiloxane (PDMS) which is two-part silicon-based elastomer and also is thermal cured polymer. It is low cost, easily handled and manufactured. Moreover, PDMS is a biocompatible and a clear transparent material that commonly use in biological application such as Bio-MEMs. We used Sylgard 184 from Dow Corning which uses mixing ratio of PDMS and curing agent as recommended 10:1. After mixing the PDMS with a curing agent and fully stirring, place the PDMS into a vacuum chamber for degassing process. We carefully pour the PDMS onto the SU-8 structure mold wafer and avoid generating bubbles.

The curing time of PDMS can be decreased by increasing the curing temperature. For Sylard 184, the curing time in room temperature is approximately 24 hours as recommended. However in a hotplate/oven at 100 degree C the time can be reduced to approximately 1 hour while still maintaining acceptable quality a. Once PDMS is cured, it can be peeled off from the silicon wafer substrate. During peeling, isopropanol alcohol is applied into the gap of PDMS and silicon wafer to reduce the adhesion and avoid the damage to the SU-8 channel structure (Figure 3.4).

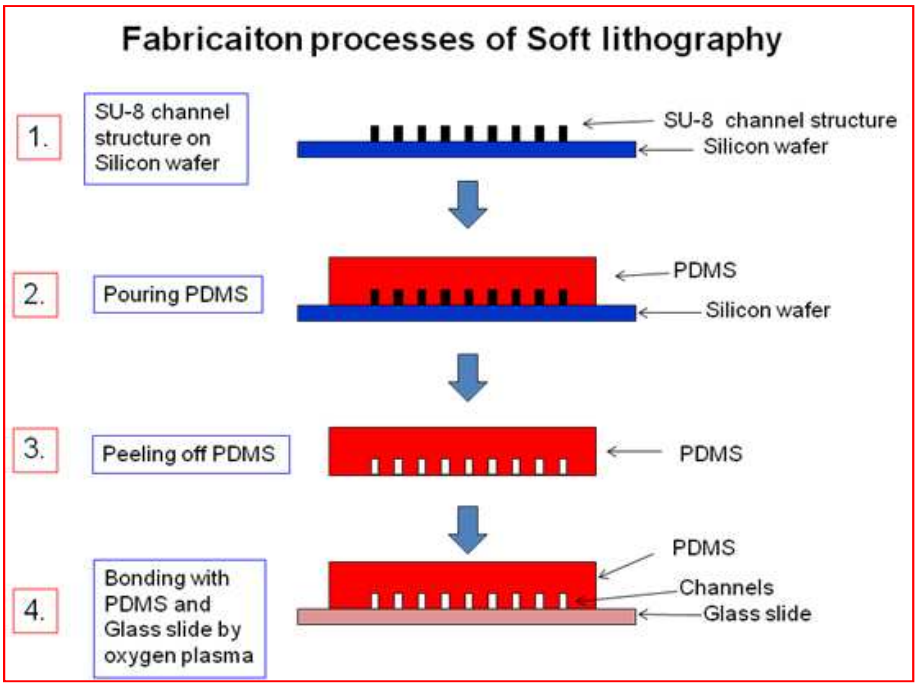


Figure 3.4 Fabrication Processes of Soft lithography. 1. Preparation of SU-8 channel structure on silicon wafer. 2. Carefully pour PDMS on silicon wafer avoiding bubbles. 3. Peel off PDMS from silicon wafer. 4. Bonding PDMS with glass slide by using oxygen plasma.

### 3.4 Assembly of microfluidic device

After releasing the PDMS from the silicon wafer substrate, the next process is to assemble and bond PDMS with a glass slide to make a microfluidic device. Holes are made on PDMS by 1.2

mm diameter punch pen for connecting input tube from the syringes before bonding process. The cured PDMS has a hydrophobic surface property that can be changed to hydrophilic surface by using oxygen plasma surface treatment (Figure 3.5). Prior to oxygen plasma treatment, the surfaces of PDMS and glass slides must be carefully cleaned because the unclean surfaces might reduce the bonding strength between PDMS and glass.

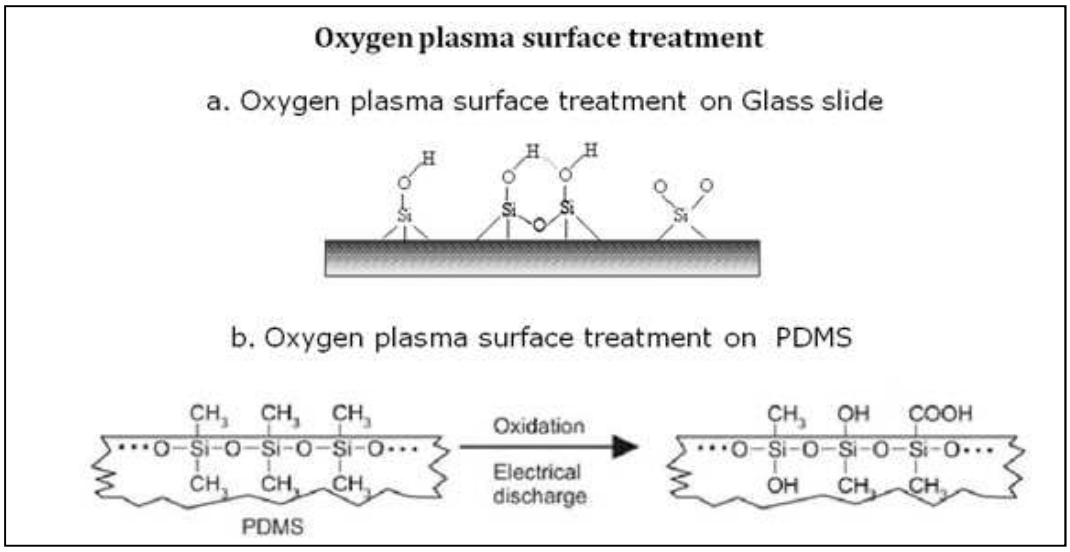


Figure 3.5 shows the chemical reactions of glass slide and PDMS after oxygen plasma surface treatment. Glass slide after surface treatment will obtain OH on the surface and reactive a Si-O covalent bonding interface with treated PDMS.

PDMS slots and glass slides are placed into oxygen plasma chamber at 75 watts for 30 seconds,

and immediately assembled after oxygen plasma process. Then we move the assembled device on the hotplate and heat it up to 85 degree C for 20 minutes to enhance the bonding strength between the PDMS and glass slide (Figure 3.6)

Figure 3.6 shows the image of the microfluidic device that PDMS bonds with glass slide

### 3.5 Experimental set up

Figure 3.7 shows the microfluidic experiments, our testing vehicle consists of 4 individual controllable syringe pumps with a main controller to drive fluids that can precisely adjust flow rate down to 1nl/min and a CCD camera with microscopy for capturing images for data analysis. Figure 3.8 shows the exact equipment set up on the optic table.

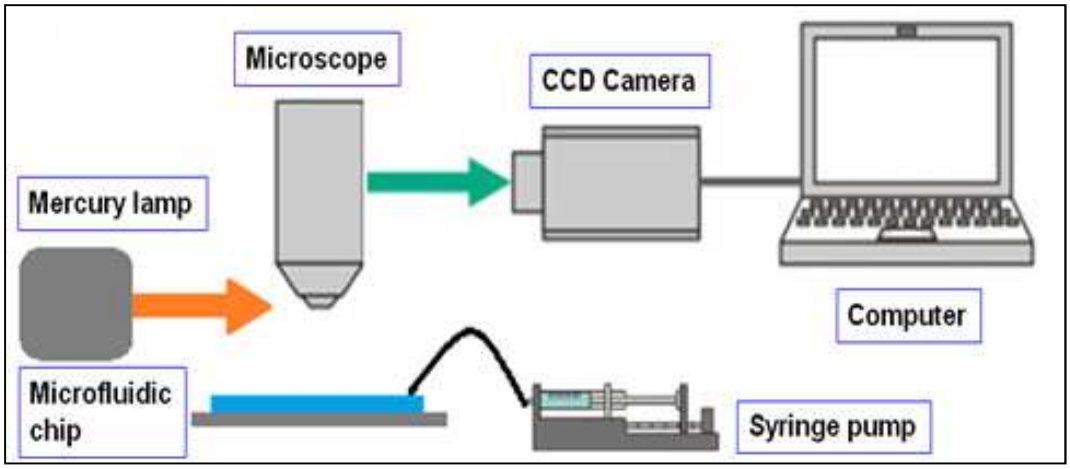


Figure 3.7 shows the experiment sep up consist of syringe pumps with controller which can precisely adjust the flow rate down to 1nl/m and CCD Camera with microscope capture images for data analysis.

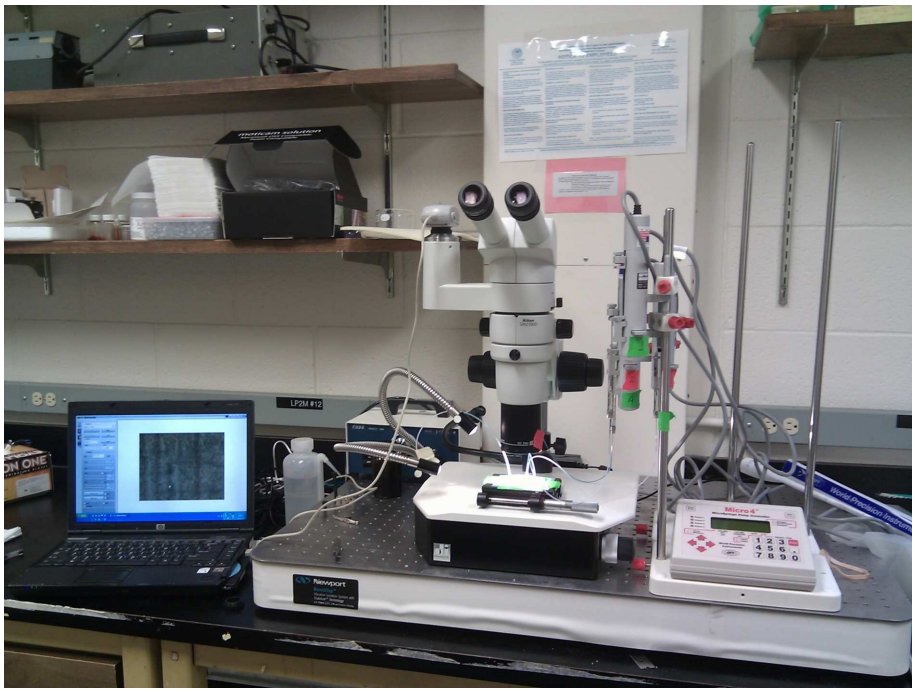

Figure 3.8 shows the exact equipment of experiment in the testing table.

### 3.6 Flow visualization testing with water and blue dye

The membrane protein samples and the buffer solution are all transparent, barely to be observed by microscope, so we used the blue-dye pre-test examination to demonstrate the flow focusing phenomena in the microfluidic device. Figure 3.9 shows the schematic diagram illustrating the designed geometry using for experimental device.

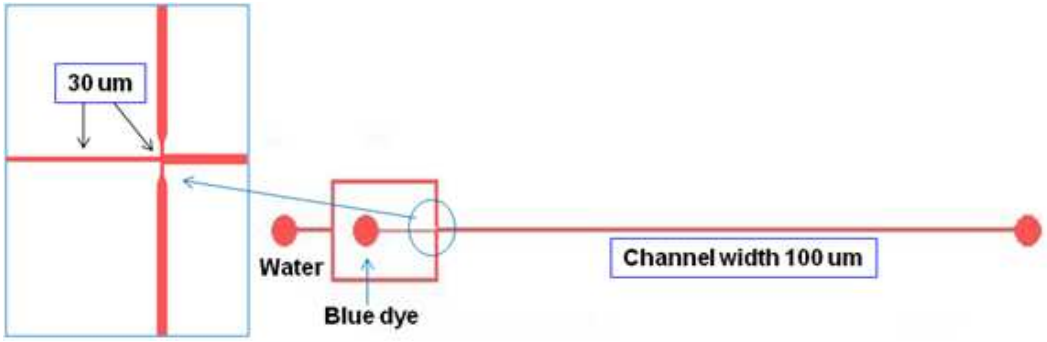


Figure 3.9 The experimental device for the study on membraneless laminar flow. The channel widths are 100μm for the main mixing channel and 30μm for T-junction channels.

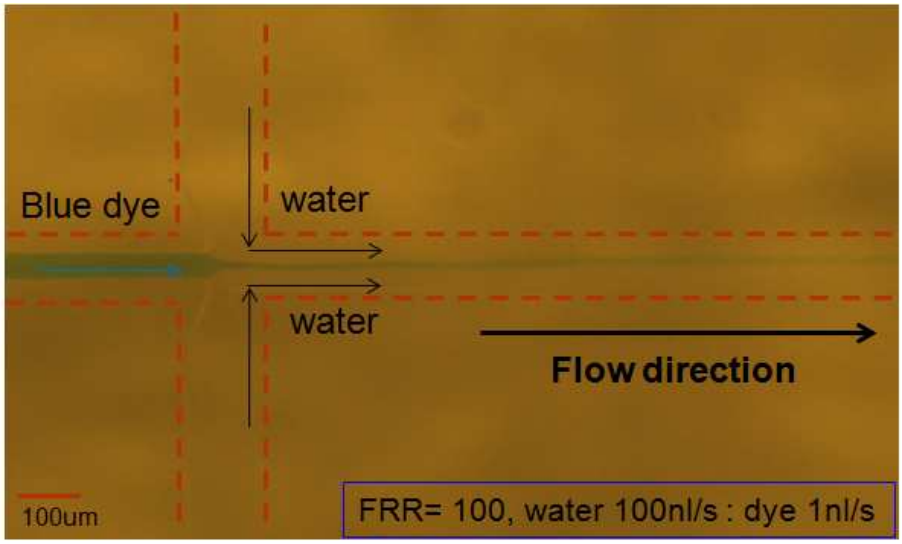


Figure 3.10 shows the flow pattern of flow focusing at FRR of 100. The water flows being injected from both perpendicular sides into the main channel and the dye flow being injected into the middle of the main channel

The flow focusing pattern was formed by water flows being injected from both perpendicular sides into the main channel and the dye flow being injected into the middle of the main channel in Figure 3.10.

As shown in Figure 3.11, when the flow rate ratio of water and dye was 10:1, the dye stream was thicker than expected. When the flow rate ratio was increased to 100:1, the dye stream became thinner. The increased water flow rate changed the ratio as expected. Correspondingly, the water-to-dye volume ratios were changed as well. Comparison of the numerical simulation and

experiment results, both of these pre-testing tests successfully revealed the same flow pattern and concentration distribution.

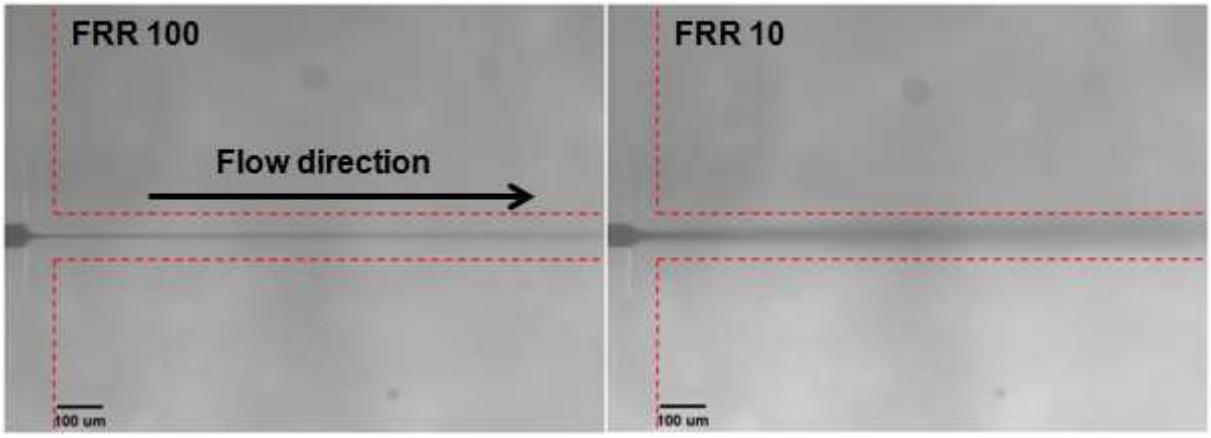


Figure 3.11 The laminar flow in the microfluidic channel. The thickness of the dye flow is controlled by changing the water-to-dye flow rate ratio (FRR). The left image shows a case with a flow rate ratio of 100, the dye stream was very thin. The right image shows another case with a flow rate ratio of 10 with a thick dye stream. The red dashed line represents the physical walls of the device.

Figure 3.12 shows the concentration variation as a function of FRR at start point and at 2.5mm away from the initial two flows merging area. All images were captured by CCD camera and data analysis was processed and converted by software Image J for measuring the length and concentration. Here RGB code presents the concentration intensity from “255” white color to “0”

black color. Comparing the flow rate ratios, the higher flow rate ratio has a faster diffusion speed because of the large surface to volume ratio due to the thinness of dye stream and a higher percentage increase in diffusion. In contrast, the lower flow rate ratio has a lower diffusion speed. The dye stream was surrounded by the outer water flows with an interface formed. The inner dye diffused naturally toward the outer water flow. Following along the main channel, the dye concentration at the center decreased and the water concentration increased correspondingly. Eventually both concentrations reached the same levels.

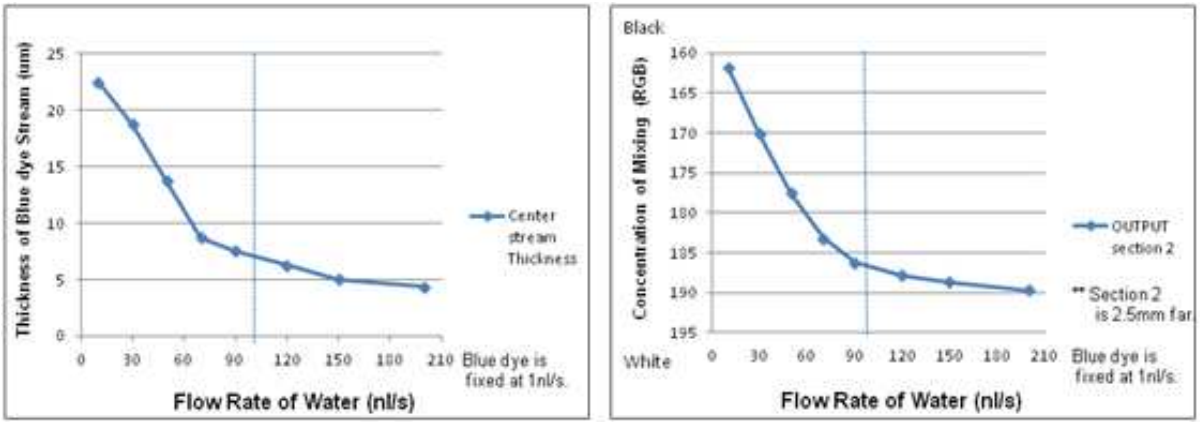


Figure 3.12 shows the different thickness of blue dye stream changed with various FRRs in left diagram. A higher FRR has thinner thickness of blue dye inducing fast diffusion due to the large surface to volume ratio. The right diagram shows the increasing flow rate ratios gradually diminished concentration with faster diffusion speed.

# CHAPTER 4

# MEMBRANELESS MICROFLUIDIC DEVICE FOR MEMBRANE PROTEIN NANOPARTICLES FORMATION

## 4.1 Overview

The structural and functional studies of membrane protein lipid nanoparticles in native biological membrane are relatively important research areas. This virus-like nanoparticle formed by a self-assembly crystallization process of membrane protein and lipids is critical to pharmaceutical industrial. These nanoparticles have a variety of potential applications in drug delivery and in drug design that can carry specific the membrane protein on aim or release control. The previous studies stay on an inefficient method with a standard dialysis process that has low-throughput, time consumption(weeks), and protein sample waste. However, the interdisciplinary cooperation between in biology and Micro Electro Mechanical Systems

(MEMS) has been tremendous developed. Here we demonstrate a new concept with a high-throughput membraneless microfluidic device to fast produce the reconstitution of membrane protein nanoparticles. The reconstitution process in continuous micro flow dominated by convection-diffusion phenomena in microfluidic channel can be completed in “seconds” to form membrane protein lipid particles, and also can save protein sample consumption down to only nanoliter or picoliter. Therefore, this novel microfluidic device has an ability to rapidly form uniform membrane protein lipid nanoparticles and will make a transformative impact to commercial applications in variety of areas from biology to pharmacology**.**

## 4.2 Introduction

Membrane proteins represent more than 30% of the proteins encoded in the all genomes and play a major rule in physiological environment controlling irons/molecules, energy and information through cell-to-cell membrane bilayer. In addition, more than 50% of drug designs aim at membrane proteins in pharmaceutical industry. This novel membrane protein nanoparticle has potential applications in drug delivery and drug release control carrying with specific proteins.

However, the first structure of membrane protein was found 25 years ago but currently only around 754 membrane protein structures with 266 unique types of membrane proteins have been identified and recorded. That is only around 1% of entire protein structure in Protein Data Bank [35]. Therefore, to investigate and understand the structure of membrane proteins become an important research area [36].

The reason for this slow development of membrane protein analysis technique is that is difficult to optimize and find the correct combination to obtain the membrane protein from few controllable parameters such as protein to lipid ratio, ph, and NaCl concentration. And other problem is from the inefficient standard method whose equipment has disadvantages including the time consuming, sample intensive, and low-throughput [26]. The scheme of standard method to reconstitute membrane proteins in a native bilayer lipid environment consists of a sample well, a buffer solution well and a dialysis membrane in the middle. The higher concentration of detergents from protein/lipid/detergent complex sample well through a dialysis membrane to the lower concentration of buffer solution well [37]. And the designed pores of dialysis membrane only allowed a small molecular such as detergents to pass through and remind a large one such as membrane proteins in sample well. Once the detergents fully removed by diffusion process the membrane protein aggregated with native lipid bilayer structure to from membrane protein

nanoparticles. The major disadvantage, time consuming, is because the diffusion process from sample well to buffer well is driven by nature diffusive phenomena that takes “ 7 days to weeks” for slowly removing detergents to completely achieve the reconstitution process for membrane protein nanoparticle crystallization. Sequentially, this slow diffusion not only caused time consuming problem but made the low-throughput performance in this conventional standard method

Recently, the interdisciplinary collaboration has been developing on diversity of fields especially between engineering and biology [30]. Microfluidic and Bio-MEMS are good examples for this such interesting topic [4,38]. In the past few decades, Microfluidic has been rapidly applied into the biology area to manipulate and control a small volume for both simple or complex experiments such as mixing, and diluting processes [39,40]. Sequentially, it can enhance the efficiency of biological experiments. In this small scale, typically the characteristic channel size of microfluidic device is from several micrometers to few hundred micrometers, there is some advantages of Microfluidic including super low Reynold number, less sample required, and fast chemical reaction [41,42]. Based on these benefits we can obtain a stable laminar flow pattern in microfluidic channels where allow people to have a solid device without any influences. In the past studies of microfluidic, the single phase flow focusing system has been widely used for

mixing, diluting and filtering of some chemical reaction experiments [43]. When the two continues fluids with different concentrations injected into the flow focusing system, they can be rapidly mixed or diluted to completely reach the final concentration equilibrium in seconds due to a very short diffusive channel width [44,45]. Moreover, for example, this system can be also applied for filtering to sort the different sizes of particles without any membrane filter [46].

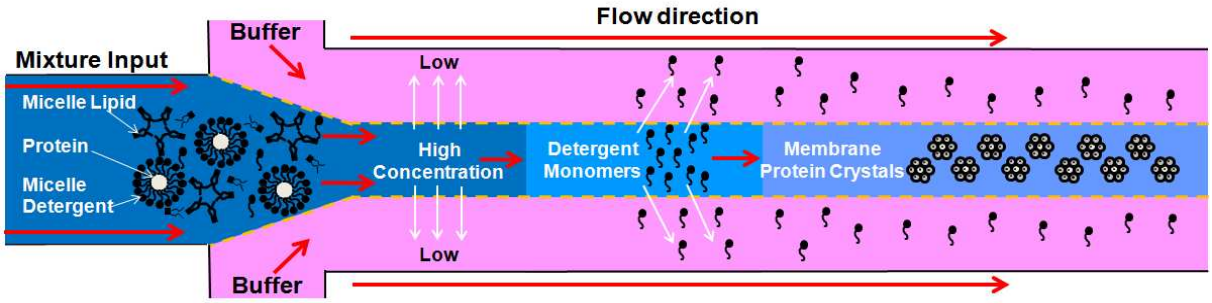


Figure 4.1 Examples of successes in membrane protein crystallization by a conceptual breakthrough using controlled convective-diffusive transport in microfluidic channel to boost the crystallization process. The interfaces between the center mixture and the side buffer streams can create concentration gradients where detergent can be removed and membrane protein aggregated with lipids to form the nanoparticles

The diffusion coefficients of particles depend on size of itself that causes the diffusion lengths for vary of particle sizes are different as well. Based on this concept, the diffusion length can be

calculated by a diffusion equation considering the diffusion coefficients of particles. Therefore the certain particle can be removed by a designed diffusion length as a function of the filter [47].

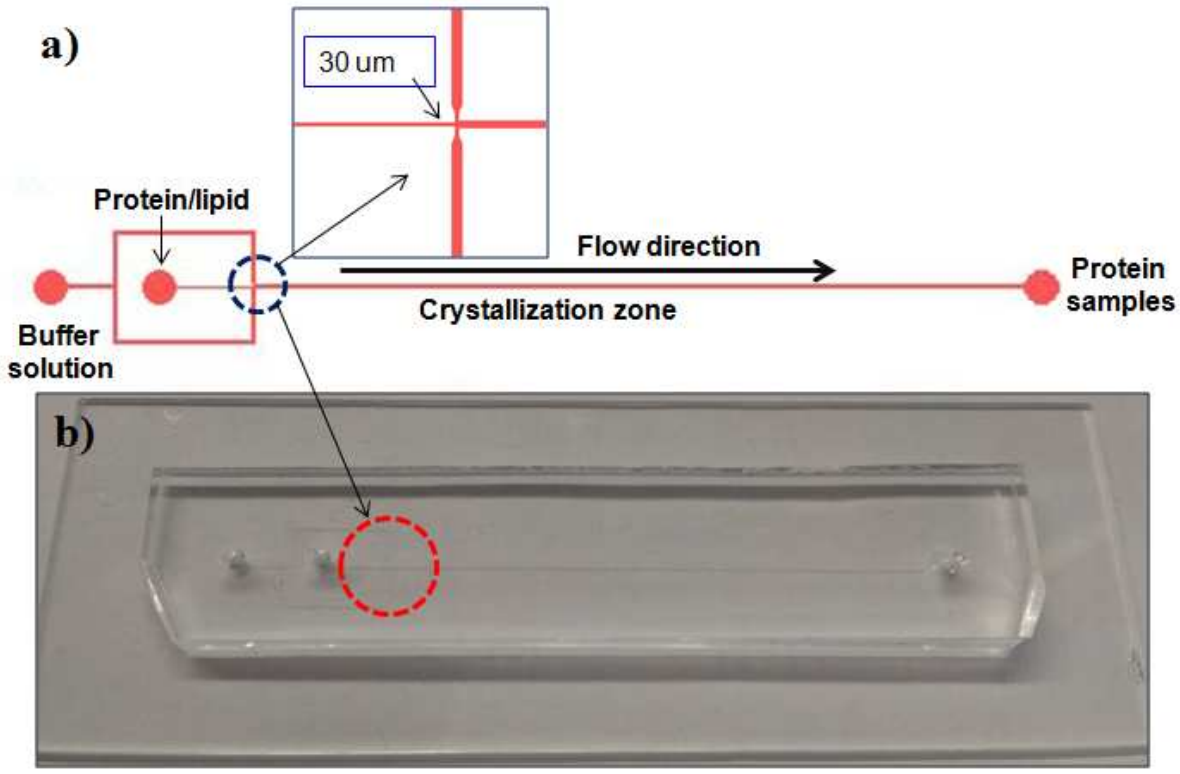


Figure 4.2 a) Channel design pattern that is accomplished by using controlled flow focusing to boost the crystallization process and additional outputs for removing unwanted detergents, b) Device image shows the exact chip size as same as glass slide.

Figure 4.1 shows our new concept for super-fast evaluation of membrane protein crystallization and we demonstrate a successful membrane-less microfluidic device converted a traditional

dialysis membrane method to a novel method that can achieve the fast response time for reconstitution of membrane protein nanoparticle from days to “seconds” with nanoliter or less sample required. In addition, it added the sorting function in the output that allows to remove unwanted detergent monomers out with buffer solution and obviously increases the density of membrane protein nanoparticles we wanted. Figure 4.2a shows the designed PDMS channels range from 30 to 100 micrometers and Figure 4.2b shows the total size of our microfluidic device is the full 25 by 75 mm of the glass slide.

### 4.3 Sample preparation

In this study we used *E. coli* mechanosensitive channel of small conductance (MscS) [48-50], detergents Fos-Choline (FC-14) with initial concentration 2.5mM (millimolar) and diffusion coefficient $7.5X10^{-9}$ $cm^2/s$ and lipids Phosphocholine (PC-14) with initial concentration 0.16mM and diffusion coefficient $3X10^{-8}$ $cm^2/s$ [51,52]. The initial mixture sample consists of pre-mixed 1mg/ml protein and 0.1mg/ml PC-14 lipid with lipid to protein/detergent ratio of 10:1. The sample preparation process is that the purified small conductance mechanosenstive channel (MscS-HT) were used to form membrane protein lipid polyhedral nanoparticles (MPPs) at a

concentration of 1mg/ml. Lipid, PC-14 (**1,2-dimyristoyl-*sn*-glycero-3-phosphocholine**) purchased from Avanti Polar Lipids, was dissolved at 5mg/ml in 1% CHAPS and used at concentration of 0.1mg/ml. Typical MPP solution contained 50mM Tris pH7.0, 100mM NaCl, 1mM sodium azide, 1mg/ml MscS-HT and 0.1mg/ml PC-14.

### 4.4 Electron Microscope sample preparation

All images were took by transmission electron microscope (TEM). After collected the protein samples from microfluidic experiment, those samples have to pre-treated and transfer to EM grid. The EM grid is a 3.05 mm diameter, thin copper mesh with the thickness range from 10um to 25um. In this study we used mesh 300 which is defined by the number of holes in 1 inch. Before placing the protein sample on the EM grid, the EM grid has to be coated a Formvar thin film that can produced by mixing Formvar powder with ethylene dichloride. The thickness of Formvar film is controlled by concentration of Formvar powder. Usually the thickness of Formvar film would be around 60nm in order to have the clear images during TEM process. Then the EM grid has to be coated the carbon layer by carbon evaporator to create a hydrophilic surface allowing protein sample to self-attached on the grid. The final step is negative stain that a small drop of

sample (5ul) is deposited on the carbon coated EM grid, allowed to settle around 1 minute, dried by filter paper, and then covered with a small drop of stain (2% uranyl acetate). After approximately one minute, then dried by filter paper as well, and the sample is ready to be viewed by TEM.

### 4.5 Results

Because the membrane protein sample and the buffer solution both are transparent that are invisible under the microscope. Therefore, we demonstrated the methods for pre-examination to observe the flow pattern of flow focusing phenomena in microfluidic device. One method is using water and blue dye instead of buffer solution and protein sample in pre-test experiment. The water flows were injected from both perpendicular sides into the main channel and merged with injected blue dye from middle of main channel. The flow pattern of flow focusing phenomena using water and blue dye can be observed clearly in main channel.

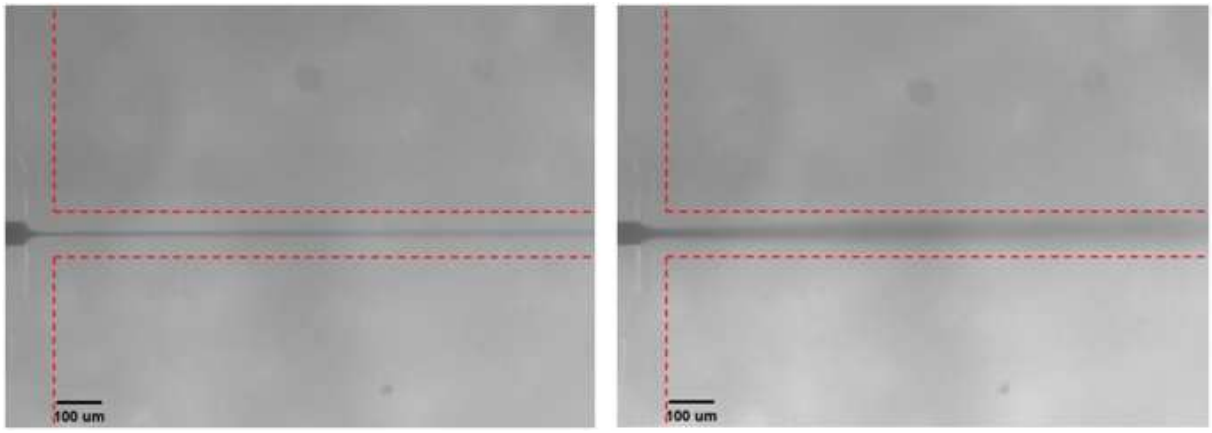


Figure. 4.3 shows the laminar flow in the microfluidic channel. The interfaces between the center mixture and the side buffer streams can create concentration gradients. This thickness of the dye flow is controlled by changing the water-to-dye flow rate ratio (FRR). The left image shows a case with a flow rate ratio of 100, the dye stream was very thin. The right image shows another case with a flow rate ratio of 10 with a thick dye stream. The red dashed line represents the physical walls of the device.

Figure 4.3 illustrates microfluidic channel and flow pattern by using blue-dye on this study. The thickness of the dye flow is controlled by changing the water-to-dye flow rate ratio (FRR). When the flow rate ratio of 100, the dye stream was very thin. When a flow rate ratio of 10, the center stream became a thick dye stream.

Other is numerical simulation for helping us obtain the initial data with vary parameters and optimize the condition as well before experiments. The numerical result of the mixing concentration distribution of the injected central protein/lipid complex stream merging by two side adjoining buffer solution streams were simulated with two-dimensional laminar flow model using COMSOL Multiphysics 4.2a ( COMSOL, Inc., Burlington, MA). The laminar flow and mixing behaviors were governed by the continuity and Navier-Stoke equations for the single phase incompressible flow combining with convection-diffusion equation for the concentration transport of diluted species in flow focusing [33]. The following equations were set up and solved at steady-state.

$$-\nabla \cdot \eta(\nabla u + (\nabla u)^T) + \rho u \cdot \nabla u + \nabla p = 0 \quad (4)$$

$$\nabla \cdot u = 0 \quad (5)$$

$$\nabla \cdot (-D\nabla c + cu) = 0 \quad (6)$$

Where η, u, ρ, and p represent the viscosity, velocity, density and pressure in Equation 4 and 5. D is diffusion coefficient and c is concentration in Equation 6. Because the most liquid component of the sample and buffer solutions is pure water, the above parameters were based on the properties of water. Therefore, the viscosity and density of water are 1 centipoises and 1000 $kg/m^3$. The velocity can be calculated from flow rate (nl/s) divided by cross-section area of channel (micro-meters). For the diffusion coefficient D, we used $7.5X10^{-9}$ $cm^2/s$ for detergent

FC-14 and $3X10^{-8}$ $cm^2/s$ for lipid PC-14. Then apply the no-slip boundary condition to all boundaries except inlets and outlet; it presents the velocity is zero at the walls as well as zero diffusive flux through the wall. Figure 4.4 shows the concentration distribution of the numerical simulation results during the different flow rate ratios within the flow focusing region. For a given set of concentration factors optimized by other studies, the formation of the crystals is affected by the flow rate ratio (FRR) between the buffer (phosphate buffered saline) and the mixture streams.

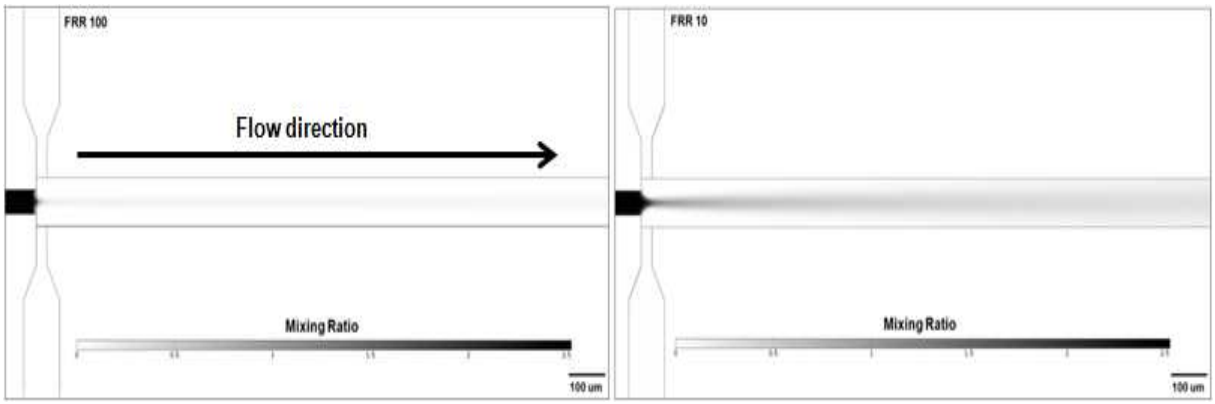


Figure 4.4 shows the numerical simulation results for flow focusing laminar flow in microfluidic channel. The left image shows the concentration diffusion distribution of a flow rate ratio of 100 with a thin center stream. The right image shows another case of flow rate ratio of 10 with a thick center stream.

The higher concentration of protein/lipid/detergent complex being injected into the center of main channel merging by two buffer solutions with equal flow velocity from both perpendicular sides. The contact interface in between a center and both side streams generated a concentration gradient in which the diffusive transport happened from the higher concentration of a center protein/lipid/detergent complex stream to the low concentration of buffer solution stream in both sides. The mixing phenomena in the main channel of center stream and both side buffer solutions were dominated by convective-diffusive transport. Such gradients offer us an opportunity to form membrane protein crystals.

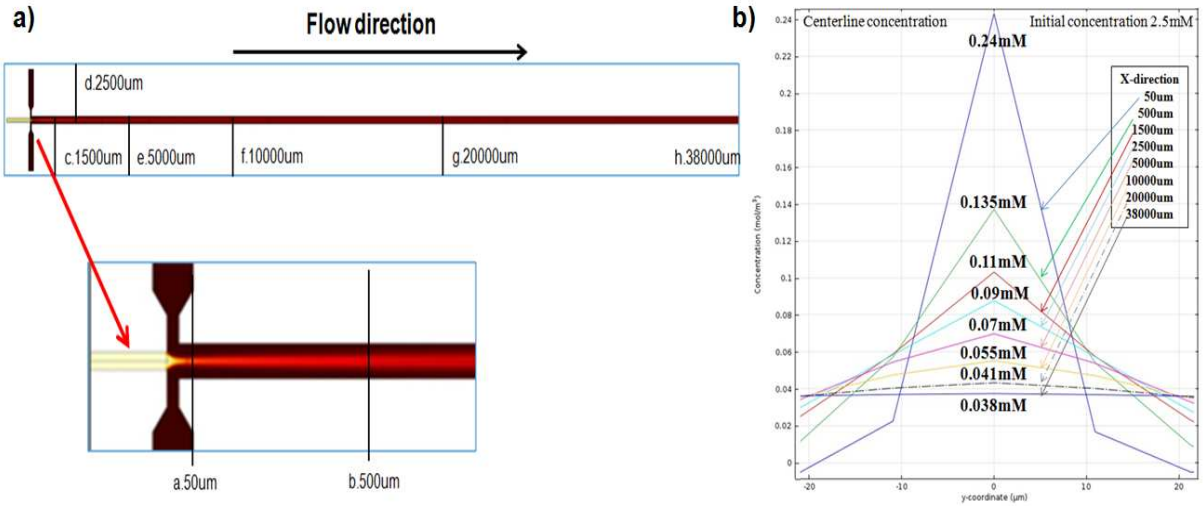


Figure 4.5. a) shows the total 8 measuring points at different distance in X-direction from 50um to 38000um. b) shows the distribution of center flow concentration at different measuring points.

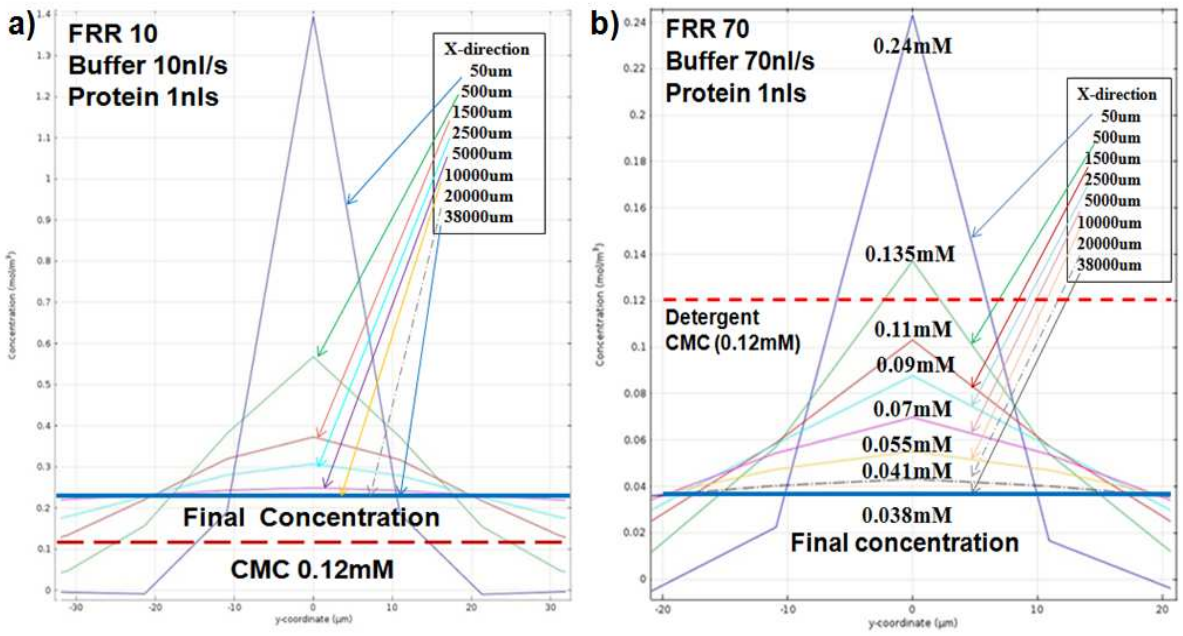


Figure 4.6 the left diagram shows the distribution of detergent FC-14 concentration when FRR at 10. The final concentration is higher than its CMC that means detergents are still in micelle formation. The right diagram shows the distribution of detergent concentration when FRR at 70. The final concentration is smaller than CMC which means the detergents form monomer structure.

Figure 4.5a shows the total 8 designed point for measuring center flow concentration at different distance in x-direction from 50um to 380000um and plot the distribution map in Figure 4.5b. The high concentration, 2.5mM (millimolar), of the micelle detergents Fos-Choline (FC-14) encapsulating proteins *E. coli* mechanosensitive channel of small conductance (MscS) decrease quickly along the mixing channel resulting from the center-to-side convective-diffusive transport.

When the concentration reaches below the critical micelle concentration (CMC) of detergents , 0.12mM for the case studied, micelles become monomers. The monomer detergents are removed to the side buffer stream by diffusion. Figure 4.6 presents the simulation results of detergent FC-14 concentration with the diffusion coefficient $7.5X10^{-9}$ $cm^2/s$. Figure 4.6a shows the final concentration is higher than its CMC that means detergents are still in micelle formation. The right diagram in Figure 4.6b shows the distribution of detergent concentration when FRR at 70. The final concentration is smaller than its CMC which means the detergents form monomer structure.

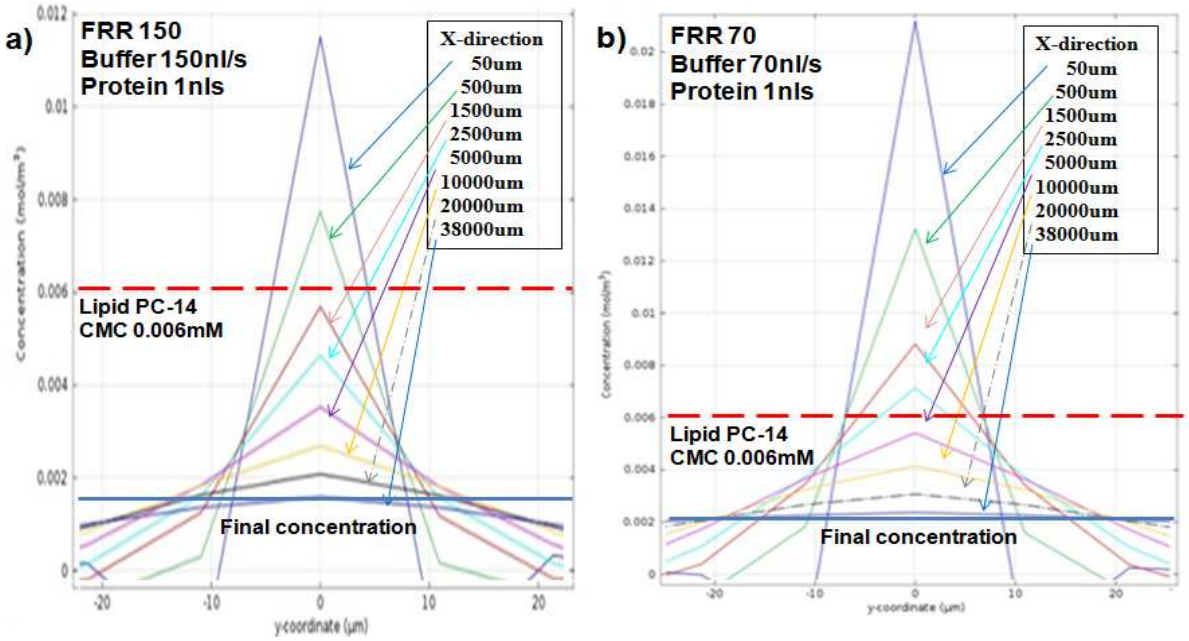


Figure 4.7 the left diagram shows the distribution of lipid PC-14 concentration when FRR at 150. The center flow concentration is mostly lower than its CMC that means lipids become monomer

structure. The right diagram shows the distribution of lipid concentration when FRR at 70. The concentration is larger than its CMC which means the lipids still keep in micelle structure.

Meanwhile, the micelle lipids Phosphocholine (PC-14), with the initial concentration 0.16mM, are transformed into bi-layer structures and simultaneously aggregate with the proteins to form membrane protein crystals. However, the lipid concentration is also a key issue for protein crystallization process in this microfluidic device.

While controlling the FRR to adjust the diffusive speed of detergent concentration, it made lipid concentration change as well. When the FRR is too high, lipid concentration reached or bellowed its CMC of 0.006mM inducing the lipid structure became from a micelle to a monomer. In order to allow membrane protein to be aggregated with lipid bilayer structure, lipid micelle structure is definitely being required. Therefore, the lipid CMC has to be carefully considered in this numerical simulation. Figure 4.7a shows the concentration changing along the center flow. At higher FRR of 150, the concentrations in most of measure points are smaller than lipid (PC-14) CMC that is unable to keep a micelle structure as well as bi-layer membrane. When FRR at 70, the concentrations in most of points are larger than its CMC which means the lipids still keep in micelle structure to form lipid bi-layer membrane.

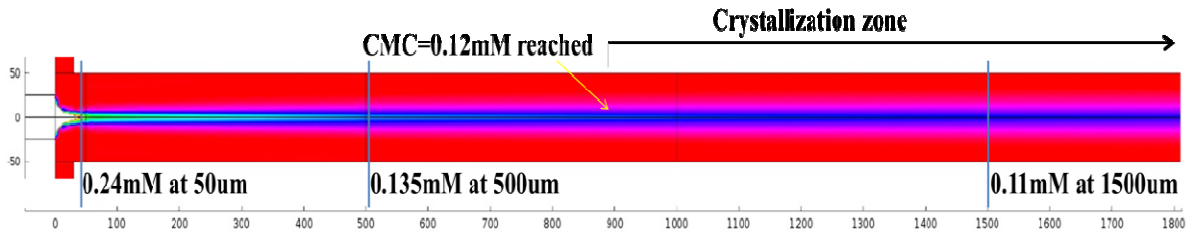


Figure 4.8 shows numerical simulation of a successful crystallization run (FRR=70) with the micelle detergents encapsulating proteins disassembled into monomers at around 900 µm along the mixing channel with a total length of 38,000 µm.

Figure 4.8 shows the concentration distribution of the numerical simulation results during the flow rate of 70 within the flow focusing region from 50um to 38000um. according to the simulation results of detergent and lipid by applying initial concentrations and diffusion coefficients. The crystallization zone can be predicted.

All membrane protein nanoparticle samples were treated and placed on EM grid and the images were captured by transmission electron microscopy. Figure 4.9 presents exciting membrane protein crystals formed as polyhedral nanoparticles by the microfluidic device with FRR=70. The image results shows the crystalline structure is the same as that obtained from using a conventional dialysis approach.

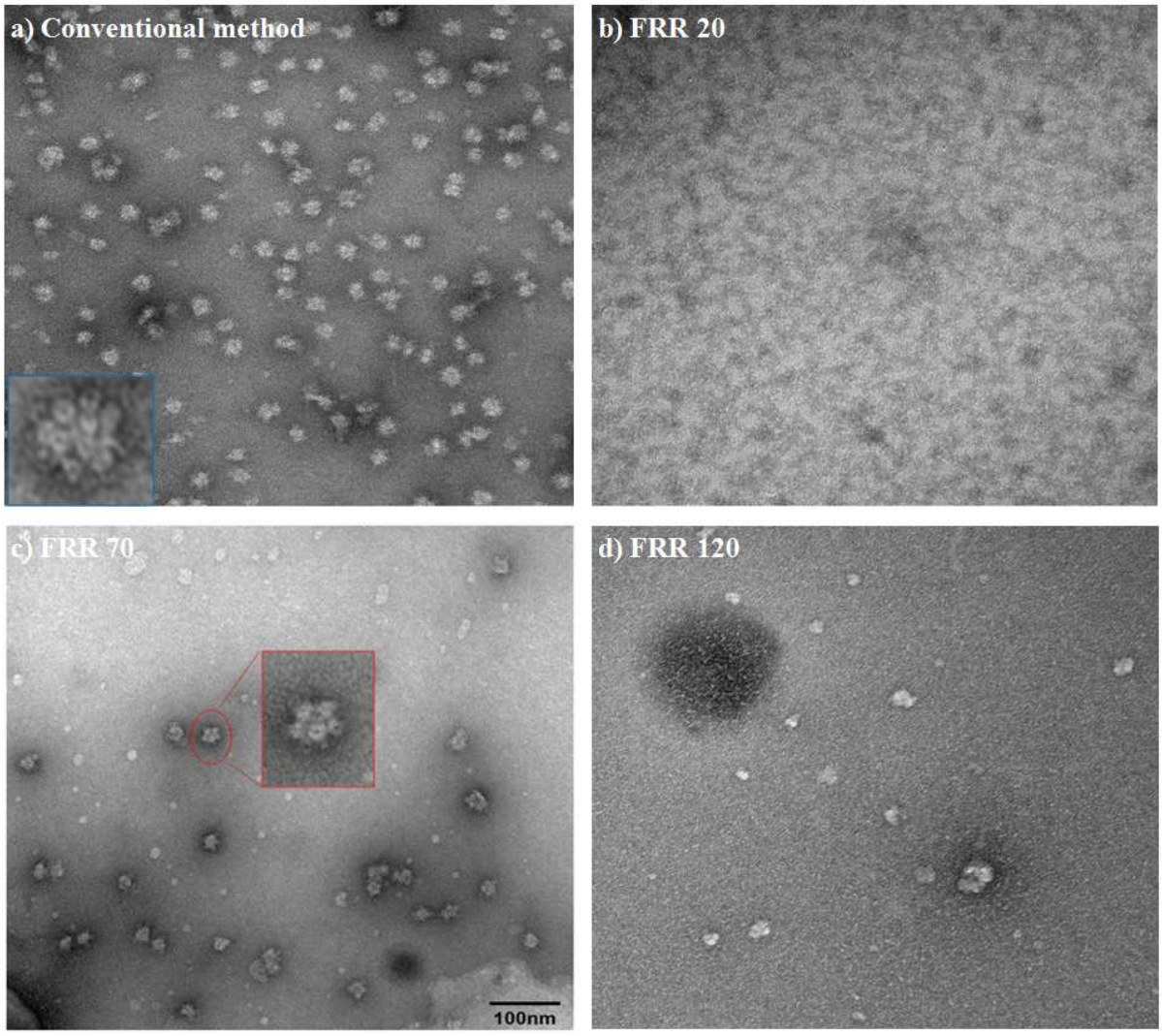


Figure 4.9 shows the images by electron microscope of membrane protein crystals with the membrane protein polyhedral nanoparticles (MPPs) formed by the MPPs formed by using a conventional dialysis membrane method (a), the microfluidic device with FRR=20, no nanoparticles (b), the microfluidic device with FRR=70, well structure of nanoparticle (c), and the microfluidic device with FRR=120, barely see nanoparticle (d).

On the other hand, because the inappropriate physiological environment for membrane protein nanoparticle crystallization the nanoparticles were barely observed when FRR is 20. Besides the experiment results also show the membrane protein nanoparticles only observed within the FRR range from 30 to 120 that strongly supported and confirmed the numerical simulation result following theory of convection-diffusion.

According to the experimental and simulation results, Figure 4.10 presents the FRR window for successful crystallization was between 30 and 120 for the case studied. When the FRR is too low, the crystallization would fail because the concentration of the micelle detergents could not reach levels lower than the CMC of 0.12mM required for releasing the proteins. When the FRR is too high, the crystallization would fail also because the concentration of the micelle lipids could quickly reach levels below the CMC of 0.006 mM and become lipid monomers. Therefore, based on this modeling we can predict the best region of flow rate ratio by knowing the initial concentration and CMC of detergent and lipid.

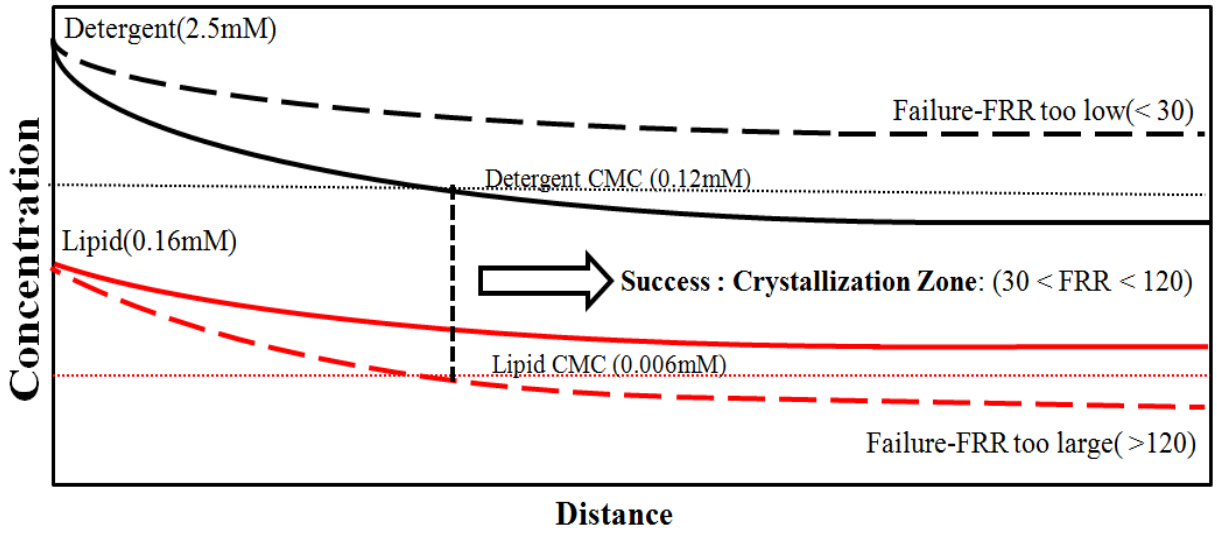


Figure 4.10 shows when the FRR is too low, the crystallization would fail because the concentration of the micelle detergents could not reach levels lower than the CMC of 0.12mM required for releasing the proteins. When the FRR is too high, the crystallization would fail also because the concentration of the micelle lipids could quickly reach levels below the CMC of 0.006 mM and become lipid monomers.

**Hypothesis confirmed** The crystalline structure is the same as that obtained from using a conventional dialysis approach. Besides the experimental results also show the membrane protein nanoparticles only observed within the FRR range from 20 to 120. Moreover, in order to carefully confirm the hypothesis that numerical simulation strongly support the experimental result. We increased the both initial concentrations of detergent and lipid by 5 times more that detergent and

lipid were from 2.5mM and 0.14mM to 12.5Mm and 0.7mM. Applying this initial concentration of detergent into the simulation modeling allowed to obtain the distribution of concentration and predict the approximate range of flow rate ratio for experimental reference. Figure 4.11a shows the detail distribution of the numerical simulation result with detergent concentration 12.5mM at FRR of 450. The result shows the pattern of concentration at FRR of 450 is as similar as that at FRR of 70. Figure 4.11b shows the detail distribution of the numerical simulation result with lipid concentration 0.7mM at FRR of 400. The concentrations in most of points are larger than its CMC that provide micelle lipid to form membrane protein nanoparticles with bi-layer lipid structure.

Based on this simulation results, we applied this approximate range of FRR from 350 to 460 into the experimental test. Figure 4.12 shows the EM image that the membrane protein nanoparticle occurred at FRR of 440. When the FRR is below 360, no nanoparticle were found due to the concentration of detergent did not match the its CMC. When the FRR is above 460, no nanoparticle were found either because the concentration of lipid reached the CMC so that lipids cannot form bilayer structure to associate with membrane protein.

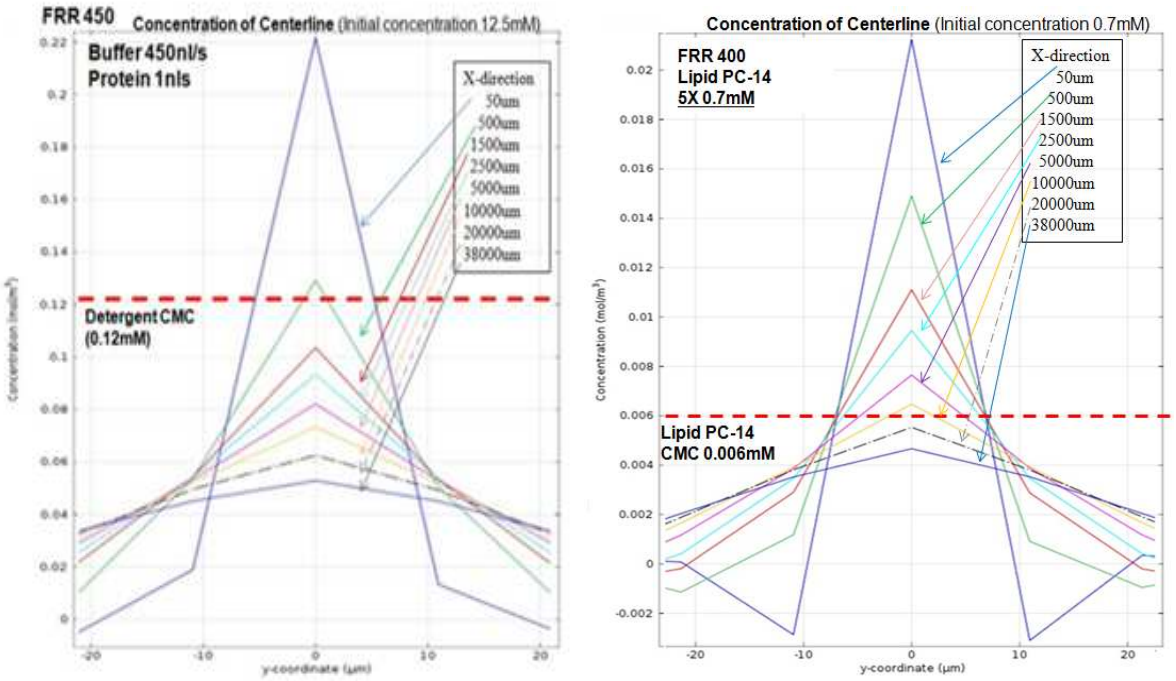


Figure 4.11 shows in the left diagram the simulation result of the distribution of detergent concentration at the FRR of 450 at 5 times more concentrations of detergent; right diagram shows the simulation result of the distribution of detergent concentration at the FRR of 400 at 5 times more concentrations of lipid increased. In this case, the initial concentrations of detergent and lipid are 12.5mM and 0.7mM.

Figure 4.13 shows the repeated results of obtaining membrane protein nanoparticle in FRR range of 400 to 440. According to these cases, the experiment results can be strongly confirmed the numerical simulation result following the theory of convection-diffusion.

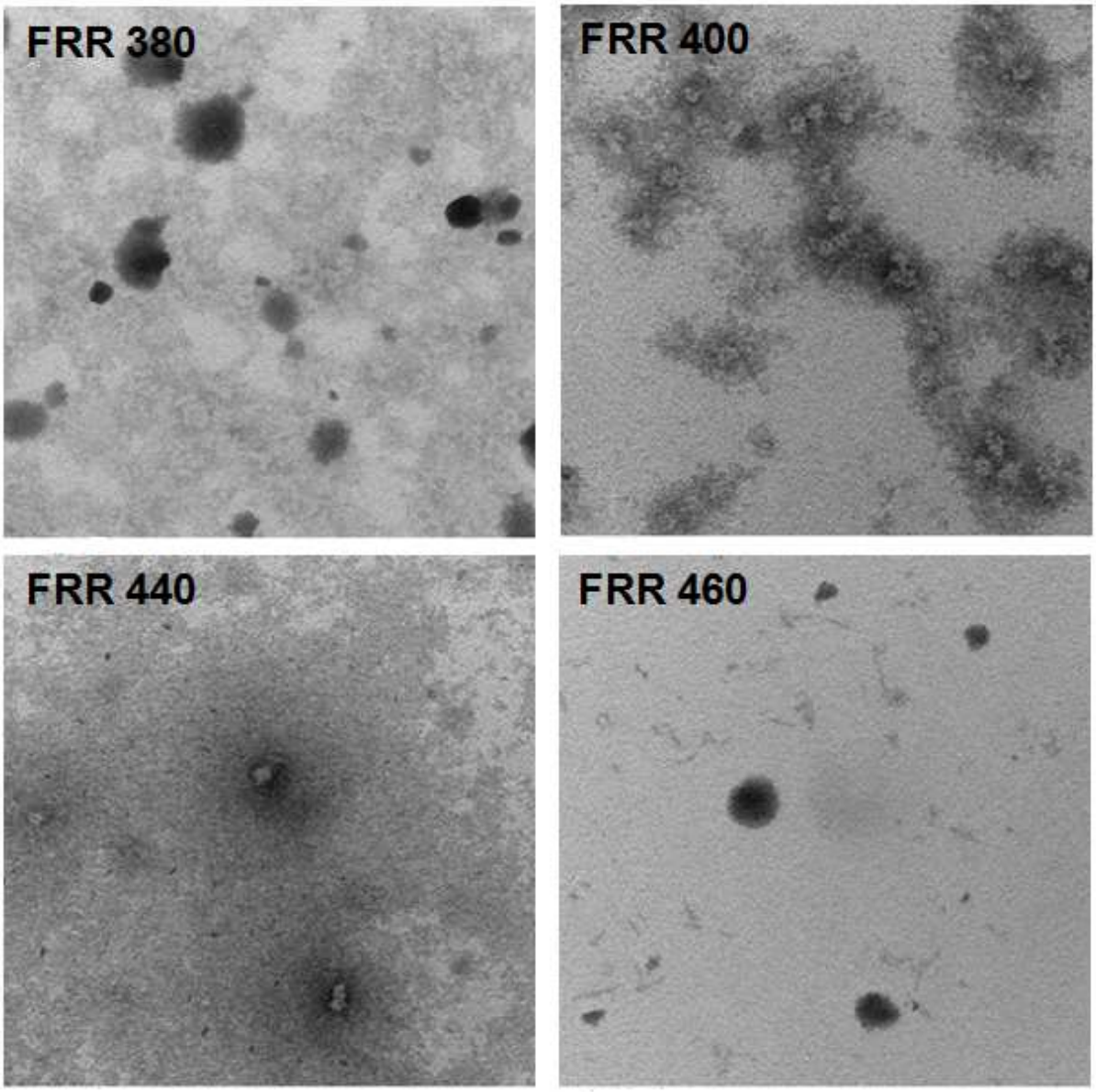


Figure 4.12 shows the FRR test results from 360 to 460. No nanoparticles found when FRR is smaller than 380 and larger than 440.

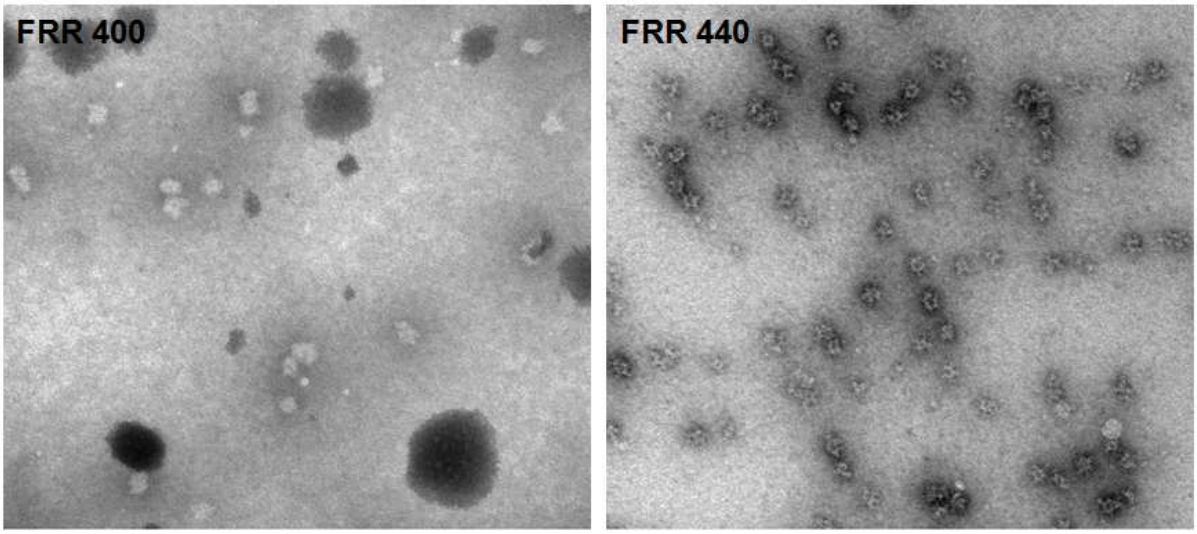


Figure 4.13 shows the repeat result of membrane protein lipid nanoparticle occurred between FRR 400 to 440 with increased 5 times concentration.

**Slow speed** Furthermore, to obtain the better uniformity of membrane protein nanoparticle is also a big challenge for optimizing this novel microfluidic device. According to the prior experiments of conventional standard method with dialysis membrane, the smooth slope of diffusive gradient allowing to obtain better homogenous structure of membrane protein nanoparticle during period of reconstitution. As demonstrated results from previous numerical simulation and experiment, the FRR of 70 showed the well structure of nanoparticle. Here we further varied the different combination of flow speed with fixed FRR of 70 in simulation.

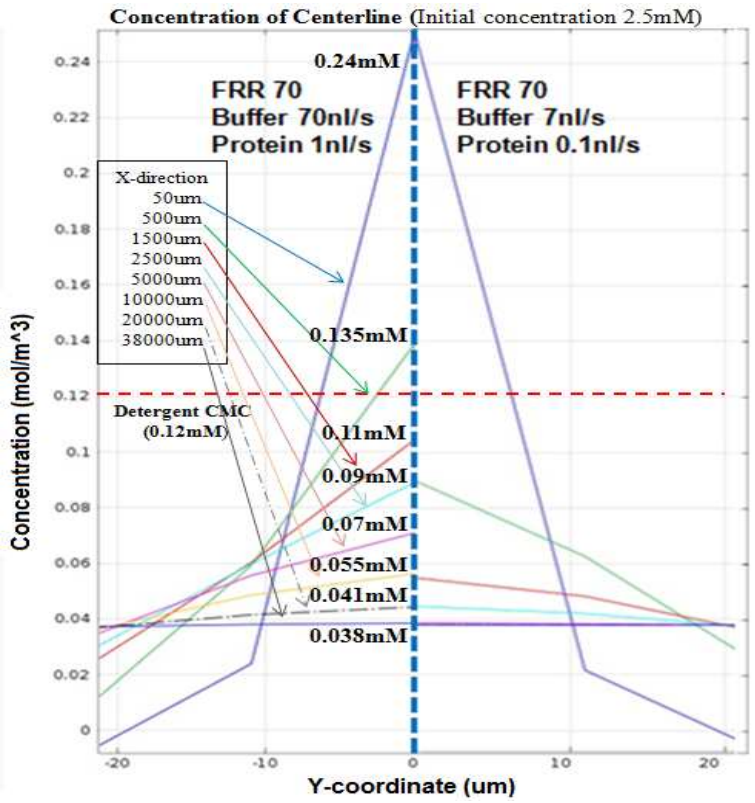


Figure 4.14 shows the distribution of detergent concentration at the flow rate ratio of 70 with two different flow speed. The concentration of center flow is decreasing along the X-direction due to convention-diffusion phenomena. The left part of diagram shows the faster flow speed with the steep slope of diffusive gradient, the buffer solution and protein sample solution are 70nl/s and 1nl/s. The right part of diagram shows 10 times slower flow speed that are 7nl/s for buffer solution and 1nl/s for protein sample solution

The result of both cases as illustrated in Figure 4.14, the left part of diagram shows the flow speed of buffer solution and protein sample solution are 70nl/s and 1nl/s. The right part of diagram shows

10 times slower flow speed that are 7nl/s for buffer solution and 1nl/s for protein sample solution. In this comparison, it demonstrates that the faster flow speed of FRR of 70 generates a quick diffusive reaction. This may not have an enough time period to form well nanoparticle structure. In contrast, the slower flow speed of FRR of 70 induces a smoother slope of diffusive gradient where allows the reconstitution process of membrane protein and lipid to gradually form more uniform nanoparticles.

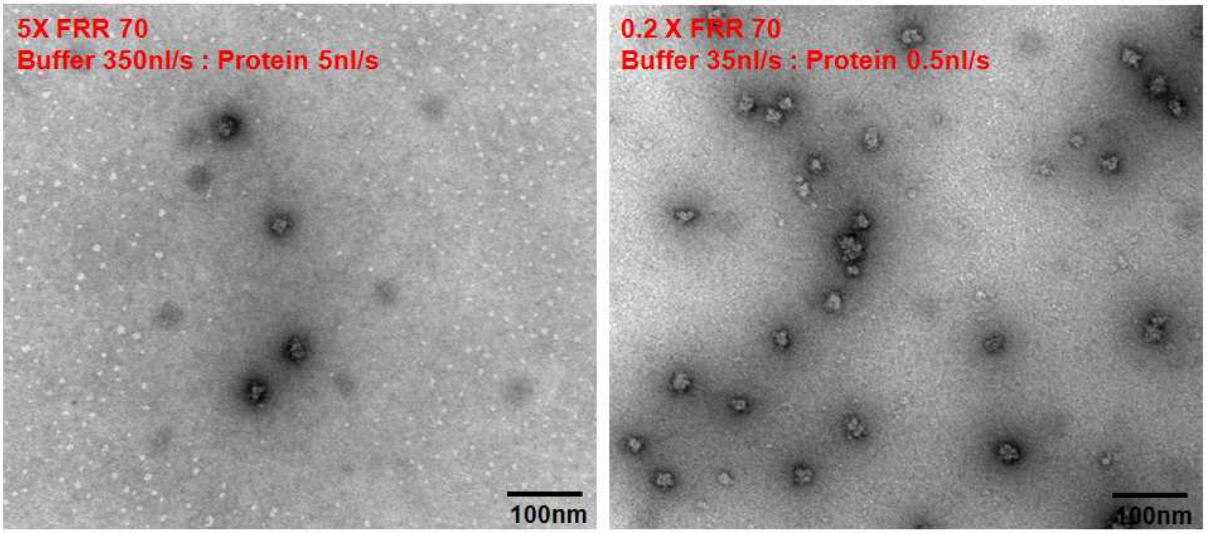


Figure 4.15 illustrates the EM image results of the membrane protein nanoparticles generated by same FRR of 70 with different flow speed. The left image shows few nanoparticles generated by “5X faster” (buffer 350nl/s ; protein 5nl/s) than the original FRR of 70 (buffer 70nl/s ; protein 1nl/s) ; The right image shows more uniform nanoparticles generated by “5X slower” (buffer 35nl/s ; protein 0.5nl/s) than the original FRR of 70.

As shown in Figure 4.15, the two images show “5 times faster” and “5 times slower” than original flow speed at FRR of 70 (Buffer 70nl/s; protein 1nl/s). The right image of slower speed appears more uniform nanoparticles after the reconstitution process of membrane protein crystallization. Although the experiment of slower flow speed takes more time for completing the membrane protein crystallization process, it still reduces the time consuming from “weeks” to “minutes” comparing with the convectional standard method.

**Density chip** In addition, obtaining more membrane protein nanoparticle is also a critical target for improving this novel microfluidic device. According to the theory of stable laminar flow in micro channel, the flow stream lines do not cross each other.

Based on this concept we modified the output design by adding two extra outlets on the two sides to remove the unwanted detergents with buffer solution in order to increase the density of nanoparticle (Figure 4.16). The ratio of the sample outlet and total outlet widths is 40% that can approximately enhance 40% of nanoparticle density comparing to the result with a single outlet as illustrated in Figure 4.17.

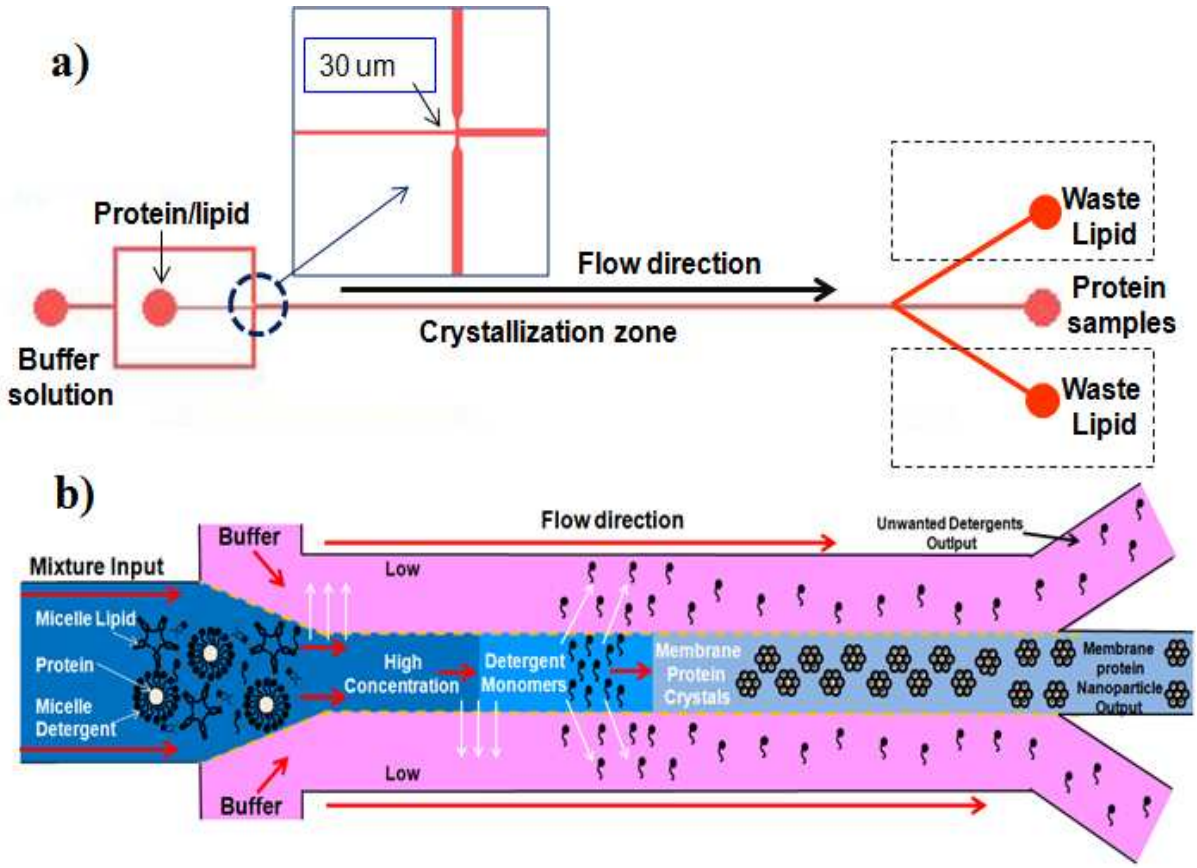


Figure 4.16. a) shows a channel design with one output for the collection of protein samples and two additional outputs for the removal of unwanted detergents. b) shows the microfluidic device developed for membrane protein nanoparticle formation accomplished by adding two additional outputs.

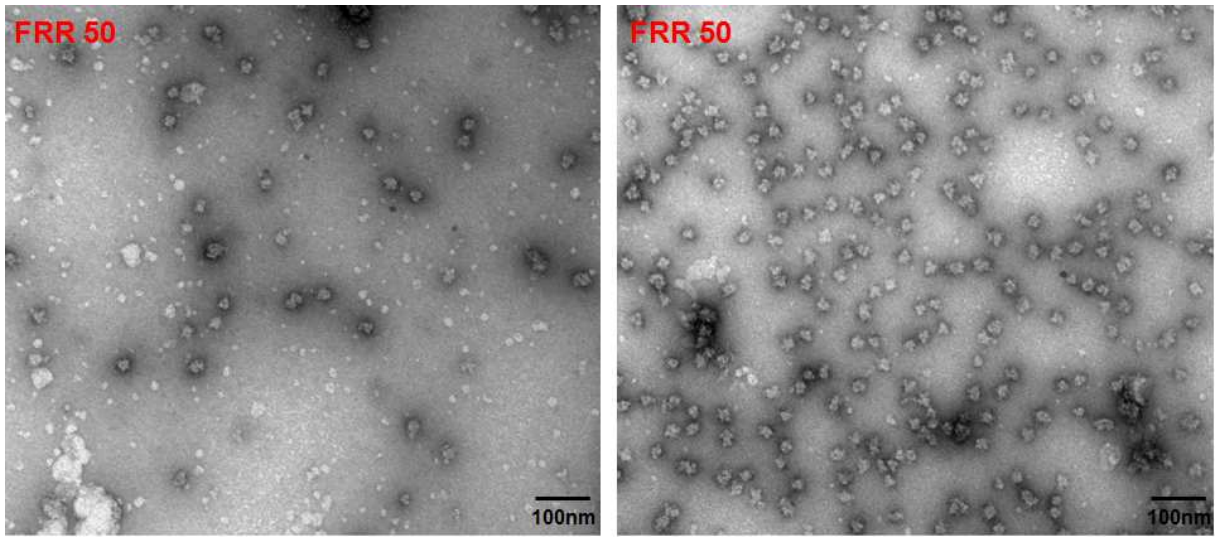


Fig. 4.17. presents the density of membrane protein nanoparticle increased by modifying the output design. The left image shows the result of the nanoparticle density from a single output. The right image shows the result with two extra outlets that can remove unwanted detergents and buffer solution. Approximately, the density of membrane protein nanoparttcle in new output design has been increased 40%.

# CHAPTER 5

# MIXING CHIP FOR MEMBRANE PROTEIN NANOPARTICLE FORMATION

## 5.1 Overview

To generate the perfect condition for membrane protein crystallization is not easy. Success in forming membrane protein crystallization is affected by a combination of several conditions such as protein to lipid ratio, pH and salt concentration in both buffer and protein solutions. Using a sample well and a buffer solution well with a dialysis membrane in between, it takes about seven days to a few weeks to form membrane protein nanoparticles if the processing conditions are good. Usually it would take about a year with over hundreds of trials to achieve one successful at membrane protein crystallization. What is needed is a new microfluidic device for fast evaluation of playing different conditions in order to obtain a successful membrane protein nanoparticle diminishing the time and the protein sample consumptions.

## 5.2 Introduction

In the previous chapter we demonstrated a new method of 2D membrane protein crystallization without a dialysis membrane. Note that the protein sample is pre-mixed with lipid at a certain ratio during the preparation. If we can design a reliable mixer for mixing variable ratio of protein samples and lipids, by controlling flow rate ratio in syringe pumps, without the need for a hand pipette, it would help scientists find the exact conditions for 2D membrane protein crystallization. For instance, scientists may want to attemp 100 trials from mixing ratio 1~100 of sample A and sample B to find conditions such that membrane protein can be crystallized. In the old pipette method they would need to mix them and pipette each different condition into sample wells 100 times. But there is a more efficient way by using mixer of microfluidic device, with a microfluidic device, they might only need to adjust the number of flow rates of syringe pumps. Ideally it is faster and easier. Various mixer designs have been used to control the mixing ratio. As described in [8-10], pre-mixing can be done in Y-channel before the mixed samples are injected into main channel. Here we demonstrated a new method with mixed function for forming membrane protein nanoparticle that help trying any possible

combinations and finding the proper conditions. Figure 5.1 shows the conceptual illustration for membrane protein nanoparticle formation with adjustable mixing ratio control function. In the new design of input section, the protein sample with micelle detergent and micelle lipid is imported from two individual channels. With controllable syringe pumps adjusting each flow rate of inputs for the mixing at the correct ratio is accessible to be achieved. Therefore the flow rate ratio of protein sample and lipid can be verified as well as the mixing ratio of protein to lipid ratio (PLR).

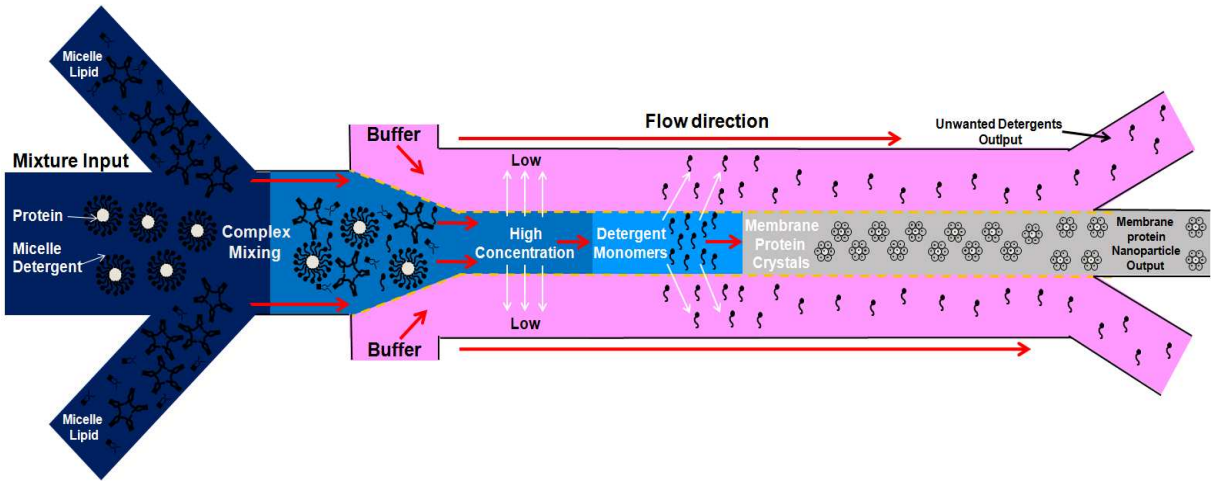


Figure 5.1 Example of membrane protein nanoparticle formation with mixing function. The protein sample with micelle detergent can be adjustably mixed with lipid by using controllable syringe pump.

## 5.3 Blue dye pre-test

Because the fact that protein sample and buffer solutions are invisible, the blue-dye pre test is necessary. In this blue-dye test, we not only obtain the flow visualization but also calibrate the stability of mixing ratio. Therefore to generate combinations of mixing ratios there is a method similar to the multi-step flow focusing [12]. Figure 5.2 shows such a scheme where we used blue dye and water for demonstration purposes. Following the previous successful results of 2D membrane protein crystallization, the flow rate ratio of buffer solution and protein-lipid mixture is 100:1. As illustrated in the figure, there are three inputs, two waters and one blue dye. The first water input has a flow rate fixed at 100nl/s since it plays the same role as the buffer solution in membrane protein crystallization. The flow rate of the remaining two inputs can be adjusted as desired.

Figure 5.3 shows the close view of mixing zone when flow rate ratio (FRR) at 10 and 2. While blue dye started to merge into water in the very beginning, the interfaces between these two flows are obviously observed as well as the thickness of streams which can be measured in order to confirm the initial flow rate ratio provided by syringe pump.

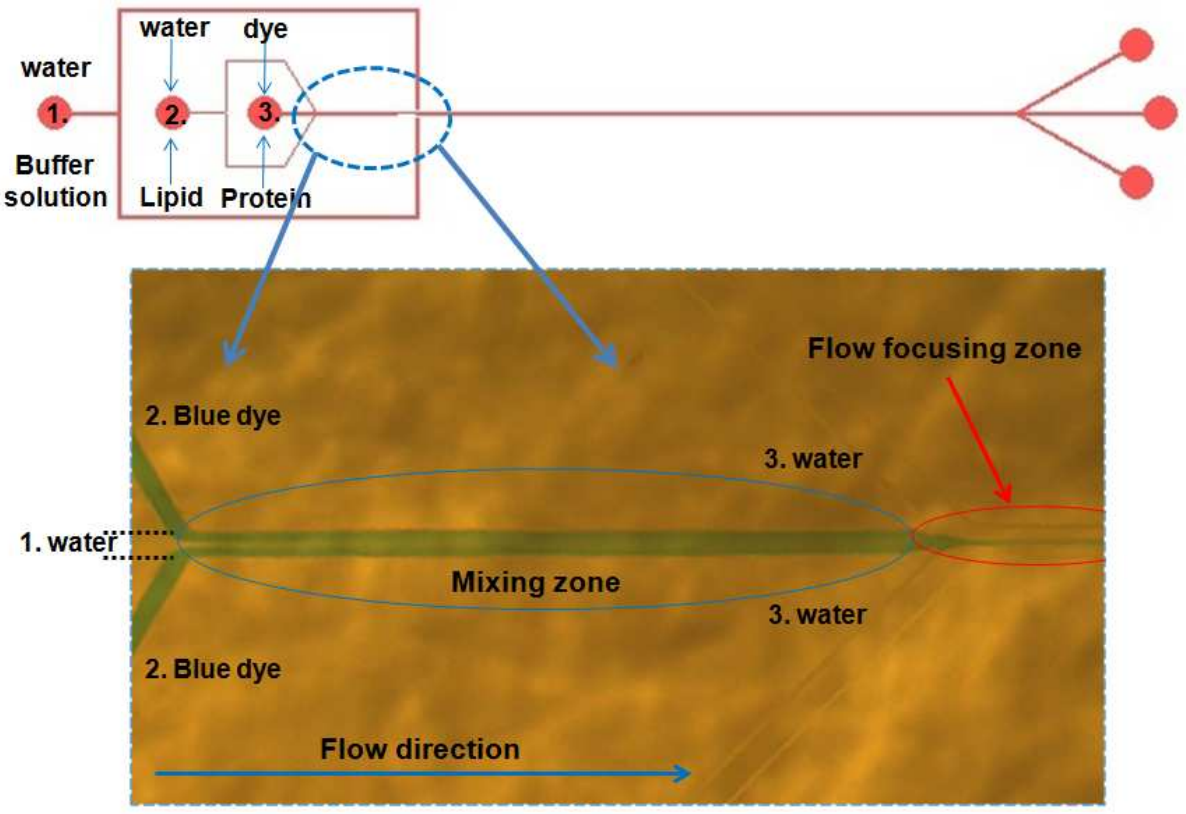


Figure 5.2. shows the designed scheme for the mixing chip. There are three inputs for 1. buffer solution/water, 2. lipid/water, 3. protein sample/blue dye. At the beginning, the input 2 and 3 started mixing completely in the mixing zone and then injected to the main channel merging with input 3 to perform a flow focusing phenomena for conductive-diffusive process.

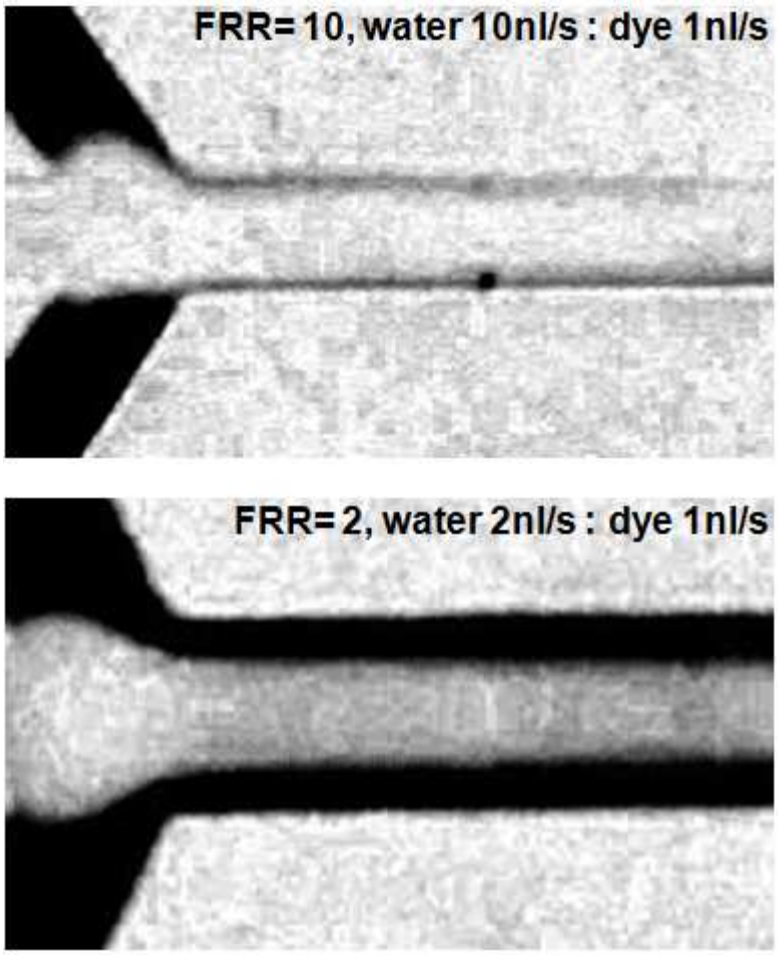


Figure 5.3 shows the close view of mixing zone in blue dye test. Top image is flow pattern in mixing zone when FRR of water and dye is 10. Bottom image is the flow pattern when FRR of water and dye is 2.

Figure 5.4 shows the result of various mixing ratio of water and blue dye from 1:1 to 6:1 by changing the flow rates. The test is repeated twice. The ratio of the widths between the blue dye and the water is measured. Ideally the ratio of widths has to be equal to the ratio of flow rates. Based on the two experimental results the measured ratio of widths are linear distribution and

completely followed by expectation. Therefore, this evidence confirmed the system stability that the variable mixing ratio in mixing chip can be precisely controlled by syringe pump. Moreover, because the water comes from both sides merging with the blue dye stream, the inside pressure will be more stable due to the balanced pressures. As shown by the resulting linear line, a varied mixing ratio can be stable and generated predictably. Based on this result we can produce a varying mixing ratio of protein and lipid by this microfluidic device instead of hand pipette.

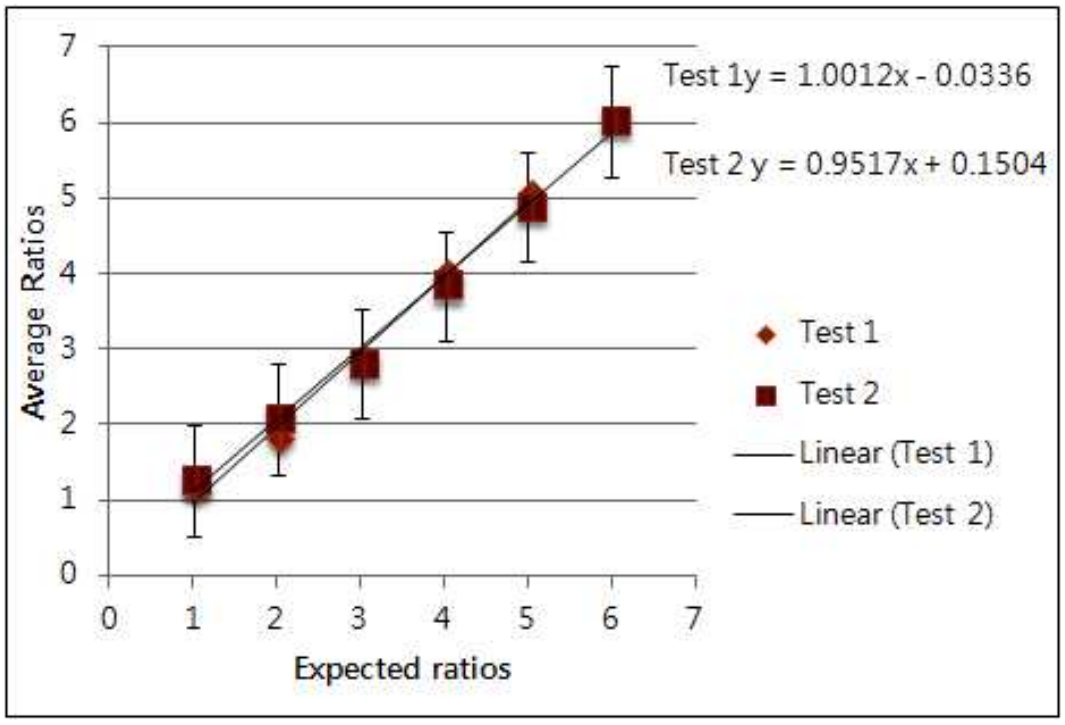


Figure 5.4 shows the result of mixing ratio stable test that two experiment results are both nearly linear lines from mixing rate are 1:1 to 6:1.

## 5.4 Membrane protein MscS experiment

Here we used the same membrane protein/detergent and lipid that are the *E. coli* mechanosensitive channel of small conductance (MscS), detergents Fos-Choline (FC-14) with initial concentration 2.5mM (millimolar), and lipids Phosphocholine (PC-14) with initial concentration 0.16mM. In previous study the initial mixture sample consists of pre-mixed 2mg/ml protein and 0.2mg/ml PC-14 lipid with lipid to protein/detergent ratio of 10:1. Figure 5.5 shows the protocol using in this mixing chip experiment, they being separated into two individuals tubes eppendorf A for MscS and eppendorf B for lipid PC-14. In order to test the stability and repeatability of mixing chip, there are 4 different concentration of protein/detergent samples, as 0.2, 0.4, 1.0, 2.0 (mg/ml), applying to experiment and lipid being always kept at 0.2mg/ml.

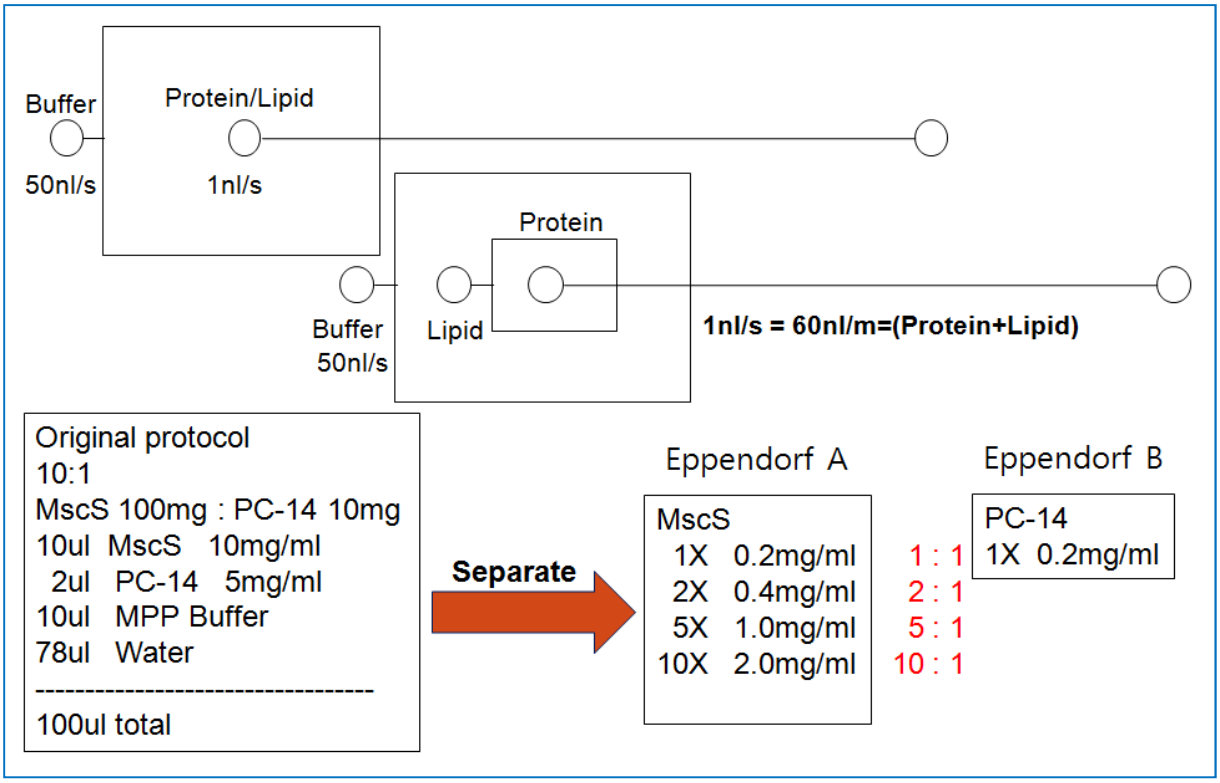


Figure 5.5. shows the illustration of mixing ratio for protein/detergent sample and lipid applied to individual input of mixing chip. The protein to lipid ratio in previous study were 10 to 1 (2mg/ml : 0.2 mg/ml). In this mixing chip experiment, they being separated into two individuals eppendorf A for MscS and eppendorf B for lipid PC-14.

According to previous results, the proper flow rates for buffer solution and pre-mixed protein/lipid sample are 50nl/s to 1nl/s. In order to verify the mixing ratio of protein and lipid in this mixing chip experiment, the sum of flow rates for protein and lipid keeps 1nl/s as same as 60nl/min. Therefore the protein to lipid ratio (PLR) equals to FRR of protein to lipid. The PLR 5

can be expressed the FRR 5 that flow rates for the protein and lipid are 50nl/min and 10nl/min. For example, in order to reach protein to lipid ratio (PLR) at 10, there are few combinations. When the initial protein and lipid concentration are 1.0 mg/ml and 0.2 mg/ml, the PLR was 5 at FRR of protein and lipid 1:1. However, the mixing chip has an ability to control the individual flow rate to match the desired final mixing ratio. In this case, increasing the FRR of protein and lipid for 2:1generates the concentration of lipid twice less in total volume. Therefore the concentrations of protein to lipid became 0.66mg/ml and 0.066mg/ml (PLR 10) when the flow rates of protein to lipid are 40nl/min and 20nl/min (FRR 2 ). Figure 5.6 shows the results of applying different initial concentration of MscS when FRR of buffer solution and protein/lipid mixture keeps at 50. The left image shows the initial concentration of PLR of MscS and lipid at 5 (1.0 mg/ml to 0.2 mg/ml) when FRR of protein to lipid at 2. Thus the final PLR is 10. The right image shows the other example of initial concentration of PLR of MscS and lipid at 10 (2.0 mg/ml to 0. 2mg/ml) when FRR of protein to lipid at 1. Thus the final PLR is 10 as well. The very similar membrane protein nanoparticle structures were observed in both results. Although the both cases are in same mixing ratios of protein to lipid at 10 (PLR 10), the total concentration of protein and lipid in the left image shows slightly less than the right image because the initial amount of protein and lipid in the left image is only 0.66mg/ml and 0.066mg/ml, and the initial amount of protein and lipid in right image is 2.0 mg/ml and 0.2 mg/ml.

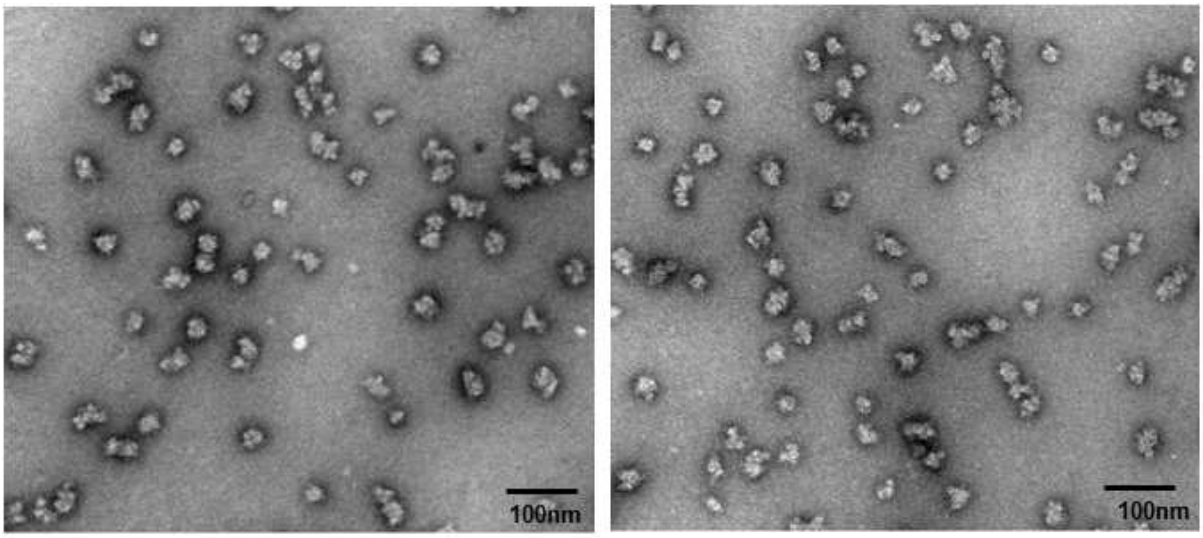


Figure 5.6 shows the results of applying different initial concentration of MscS when FRR of buffer solution to protein/lipid mixture is at 50 . The left image shows the initial concentration of PLR of MscS and lipid at 5 (1.0 mg/ml to 0.2 mg/ml) when FRR of protein to lipid at 2. Thus the final PLR is 10. The right image shows other example of initial concentration of PLR of MscS and lipid at 10 (2.0 mg/ml to 0. 2mg/ml) when FRR of protein to lipid at 1. The very similar membrane protein nanoparticles were observed in both results.

Moreover, comparing the result of the mixing chip with the result of using conventional dialysis method is also necessary. At the PLR 50, the membrane protein nanoparticles formed completely in mixing chip. Applying this PLR 50 into the conventional dialysis method is a way to verify the

functional stability of mixing chip.

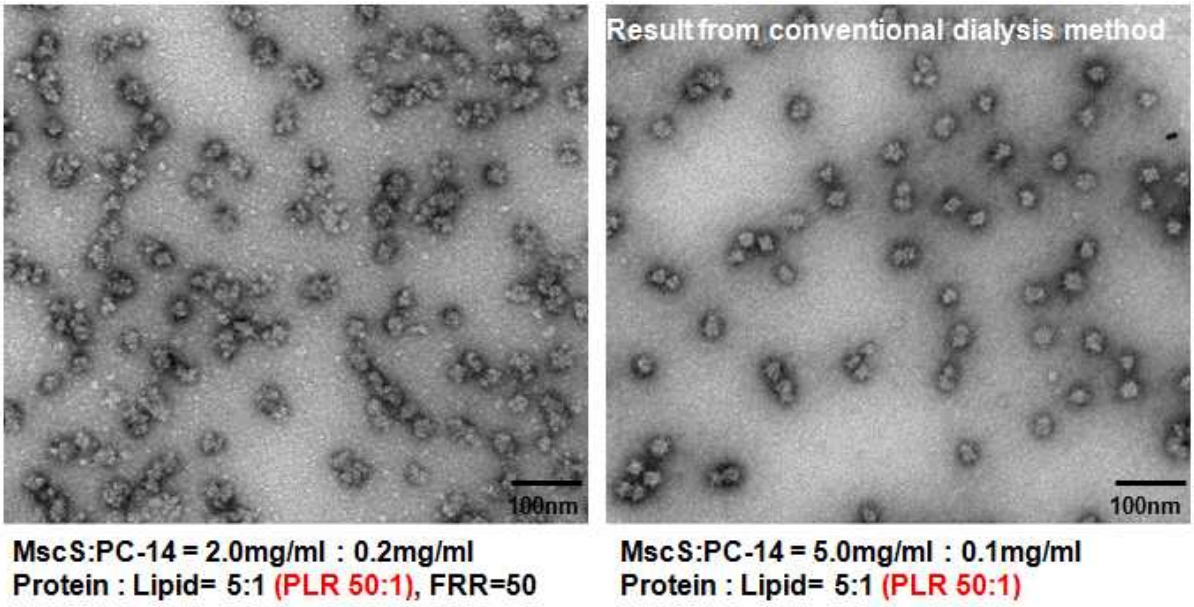


Figure 5.7. shows the compared results made from mixing chip and conventional dialysis method. The left image shows the initial concentration of PLR of MscS and lipid at 5 (2.0 mg/ml to 0.2 mg/ml) when FRR of protein to lipid at 5. Thus the final PLR is 50 (1.66 mg/ml to 0.033 mg/ml). The right image shows the PLR 50 made by conventional dialysis method. The very similar membrane protein nanoparticles are obvious observed in both results that strongly confirm the capability of mixing chip. .

Figure 5.7 shows the results comparing the mixing chip and conventional dialysis method. The left image shows the initial concentration of PLR of MscS and lipid at 5 (2.0 mg/ml to 0.2 mg/ml)

when FRR of protein to lipid at 5. Thus the final PLR is 50 (1.66 mg/ml to 0.033 mg/ml). The right image shows the result of PLR 50 by using conventional dialysis method. The membrane protein nanoparticles are observed in both cases. This compared result helped us confirm that microfluidic mixing chip for varying the possibility of mixing protein to lipid ratio is apparently reliable and also provide the solid evidence to allow testing other different types of membrane protein to form membrane protein nanoparticles in the future.

### 5.5 Membrane protein MscL experiment

In this section we used the membrane protein *E. coli* mechanosensitive channel of Large conductance (MscL) 2.1mg/ml, with the detergents *n*-dodecyl-β-D-maltopyranoside (DDM). The initial conditions for detergent DDM are initial concentration 0.39mM, CMC 0.17mM, and diffusion coefficient $2X10^{-8}$ $cm^2/s$. For the lipid, we used same lipid as previous study, Phosphocholine (PC-14), with initial concentration 0.16mM, CMC 0.006mM, and diffusion coefficient $2X10^{-8}$ $cm^2/s$.

To find the perfect condition for forming membrane protein nanoparticle was not easy. The

possible parameters include protein to lipid ratio, pH, and salt concentration. Based on the previous results, we can use the numerical simulation for modeling the convection-diffusion process of detergent and lipid in microfluidic channel to predict the approximate flow rate ratio range of buffer solution and protein/lipid sample in the crystallization zone.

Once the initial conditions of detergent and lipid are known, we apply these data into the simulation modeling to obtain the flow rate ratio of buffer solution and protein/lipid to determine the crystallization zone for forming membrane protein nanoparticle. In this MscL study, the initial concentration of *n*-dodecyl-β-D-maltopyranoside (DDM) applied into modeling is 0.39 mM and its CMC is 0.17mM with the diffusion coefficient $2X10^{-8}$ $cm^2/s$. Figure 5.8 shows the simulation results at different flow rate ratios of buffer solution and protein/lipid sample. When the FRR at 10, the concentration of detergent DDM at distance of 500um is below its CMC. However, based on the previous conclusion the slow flow speed is good to form better membrane protein nanoparticles. Thus Figure 5.8b shows the result when FRR at 5. At 500um, the concentration of detergent started to be lower than its CMC creating the beginning point of crystallization zone to form membrane protein nanoparticle. Once the concentration of detergent DDM reached its CMC, micelle detergents became the monomer detergents that being removed to outer buffer solution by convective-diffusive phenomenon. Therefore, the proper flow rate ratio of buffer solution and

protein/lipid sample can be predicted to FRR 5 as well as buffer solution at 5nl/s and protein/lipid sample at 1nl/s. In addition, in order to reduce the time consumption of experiment, adjusting the flow rates of buffer solution and protein/lipid sample and staying the same FRR are reachable. Figure 5.8c shows the simulation result in same FRR of 5 but at different flow rates of buffer solution and protein/lipid sample (20nl/s; 4nl/s). Comparing these results of Figure 5.8b and Figure 5.8c, the concentration distributions of detergent DDM are similar. Thus the FRR of 5 with 20nl/s for buffer solution and 4nl/s for protein/lipid sample has been chosen for the following test. Using this FRR from Figure 5.8c not only can generate a crystallization zone for forming membrane protein nanoparticle as well as Figure 5.8b, but also can reduce the experimental time consumption in order to do fast evaluation of nanoparticle.

Meanwhile, the lipid concentration is also a key issue for protein crystallization process in this microfluidic device that transformed into bi-layer structures and simultaneously aggregate with the proteins to form membrane protein crystals. Here we used the same lipids Phosphocholine (PC-14) as in the previous case to find the desired protein to lipid ratio for aggregating with MscL membrane protein to form nanoparticle. The initial conditions for the micelle lipids Phosphocholine (PC-14) are initial concentration 0.16mM, and CMC 0.0006mM. Figure 5.9a shows the concentration changing along the center flow. At a higher FRR of 150, the

concentrations in most of measured points are smaller than the lipid (PC-14) CMC which means that it is unable to keep a micelle structure as well as bi-layer membrane. When FRR equals 70, the concentrations in most of points are larger than its CMC which means the lipids still keep a micelle structure to form lipid bi-layer membrane. Therefore, based on this prediction result the maximum FRR for lipid PC-14 in micelle structure would not be higher than FRR 120.

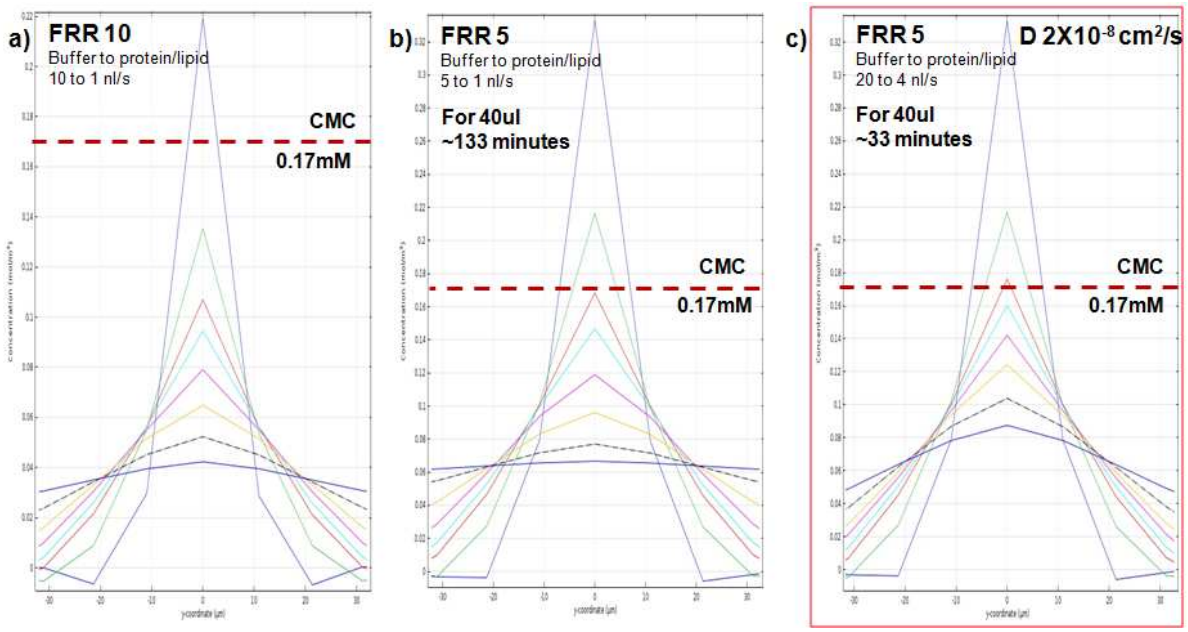


Figure 5.8. shows the concentration distribution of detergent *n*-dodecyl-β-D- maltopyranoside (DDM) in microfluidic channel. a) when FRR at 10 with buffer solution 10nl/s and protein/lipid sample 1nl/s, b) when FRR at 5 with buffer solution 5nl/s and protein/lipid sample 1nl/s, c) when FRR at 5 with buffer solution 20nl/s and protein/lipid sample 4nl/s.

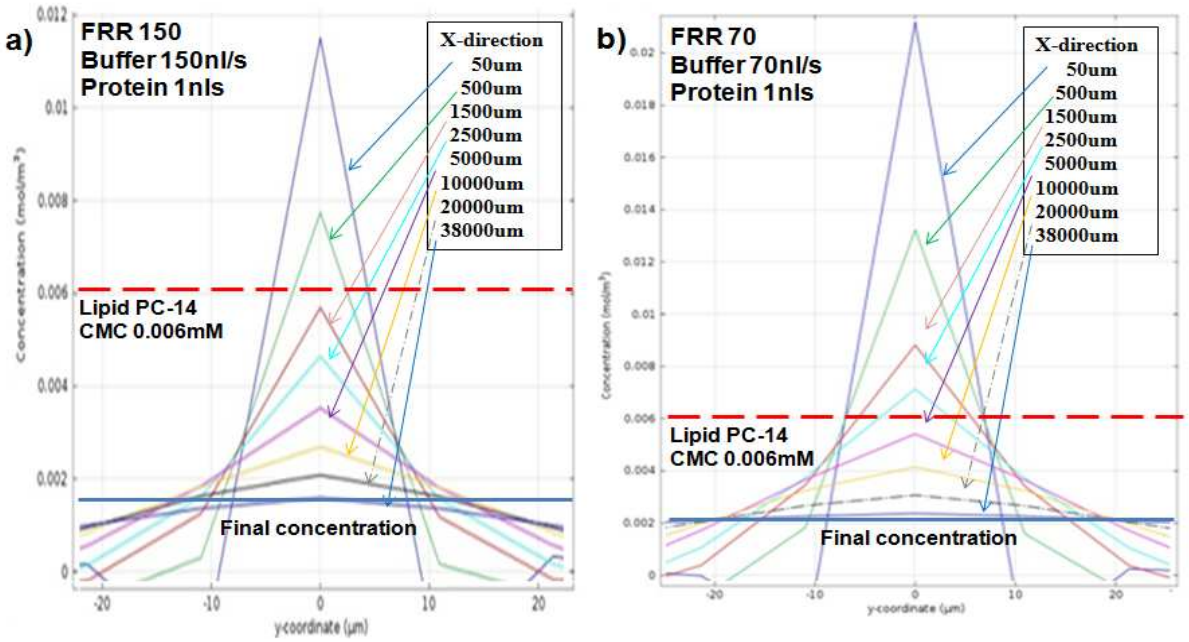


Fig 5.9. the left diagram shows the distribution of lipid PC-14 concentration when FRR at 150. The center flow concentration is mostly lower than its CMC that means lipids become monomer structure. The right diagram shows the distribution of lipid concentration when FRR at 70. The concentration is larger than its CMC meaning that the lipids retain a micelle structure.

Once we obtained the desired FRRs for both detergent DDM and lipid PC-14 from the simulation results, we can generate the flow rate ratio map to estimate the crystallization zone where FRR is between 5 and 120 (Figure 5.10). If the FRR is lower than 5, detergent micelle could not become detergent monomer. If the FRR is larger than 120, lipid micelle would become lipid monomer.

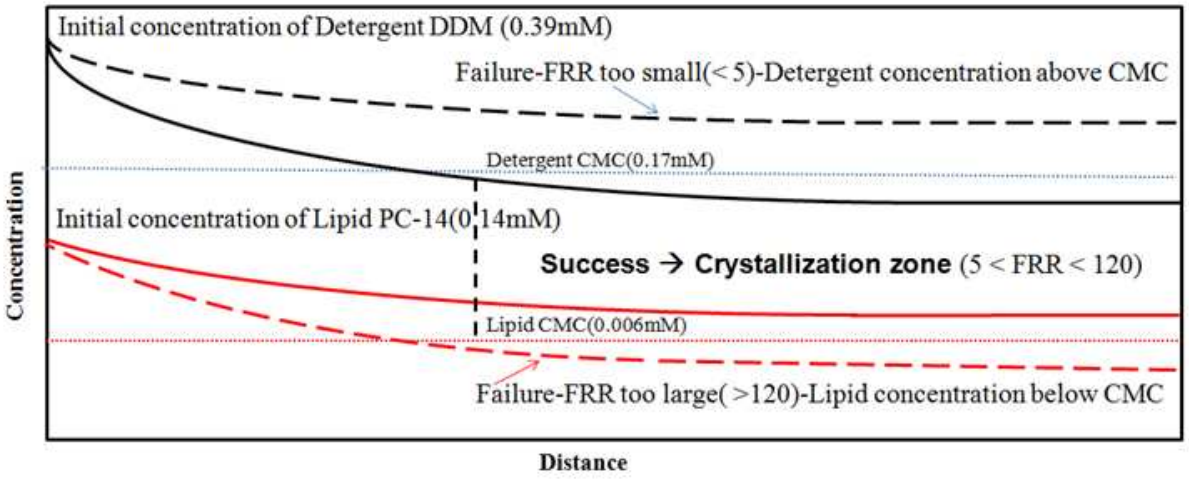


Figure 5.10 shows the estimated crystallization zone from the simulation result that indicates the possible FRR range for successfully forming the membrane protein nanoparticles. The minimum FRR is 5 and the maximum FRR is 120.

As described, the first step of forming membrane protein nanoparticle is to test the possibility of protein to lipid mixing ratio. The proper PLR might be obtained from any random combination. Here we started the tests of PLR from 1 to 1000. Once we found the similar nanoparticle from the electron microscope image to the particle seen using the conventional method at certain range of PLR, the experiment was repeated for this range and the results improved. Figure 5.12 shows the results from electron microscope at protein to lipid ratio of 30 (MscL 1.575 mg/ml; PC-14 0.05 mg/ml) at FRR of 5. From this image, well structure nanoparticles were not observed. After

the PLR reached 290 (MscL 2.03 mg/ml; PC-14 0.006 mg/ml) at FRR of 5, the nanoparticles were observed. The membrane protein MscL successfully aggregated with PC-14 lipid bi-layer structure to form the membrane protein nanoparticle at the proper PLR of 290.

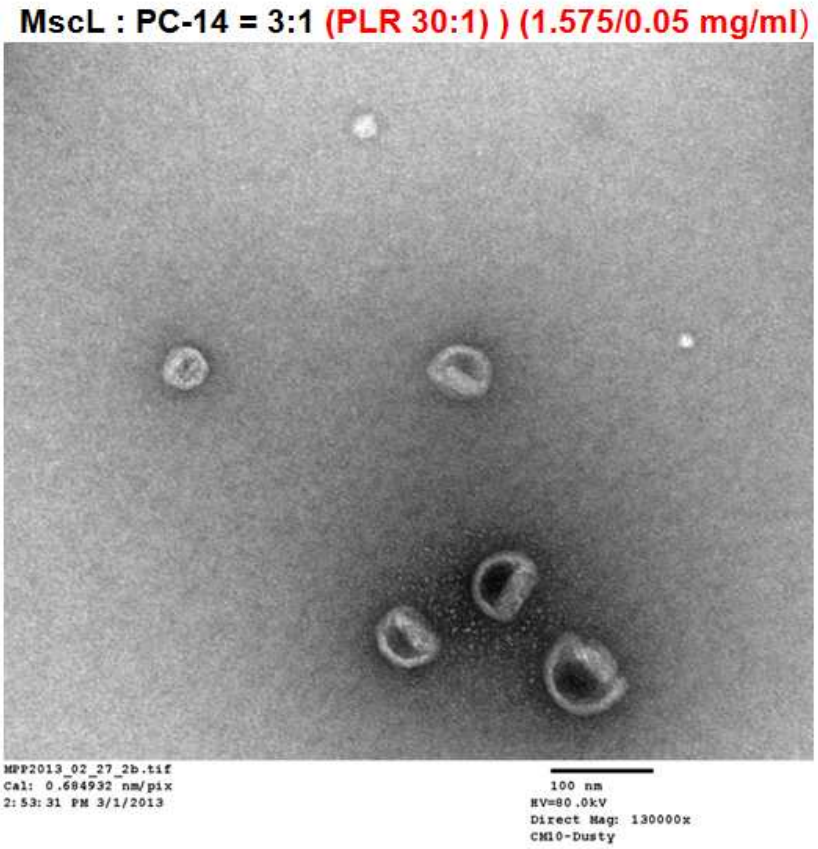


Figure 5.11 shows the image of MscL experimental result when protein to lipid ratio (PLR) at 30 and flow rate ratio (FRR) at 5. No acceptable membrane protein nanoparticle has been observed due to the incorrect protein to lipid ratio.

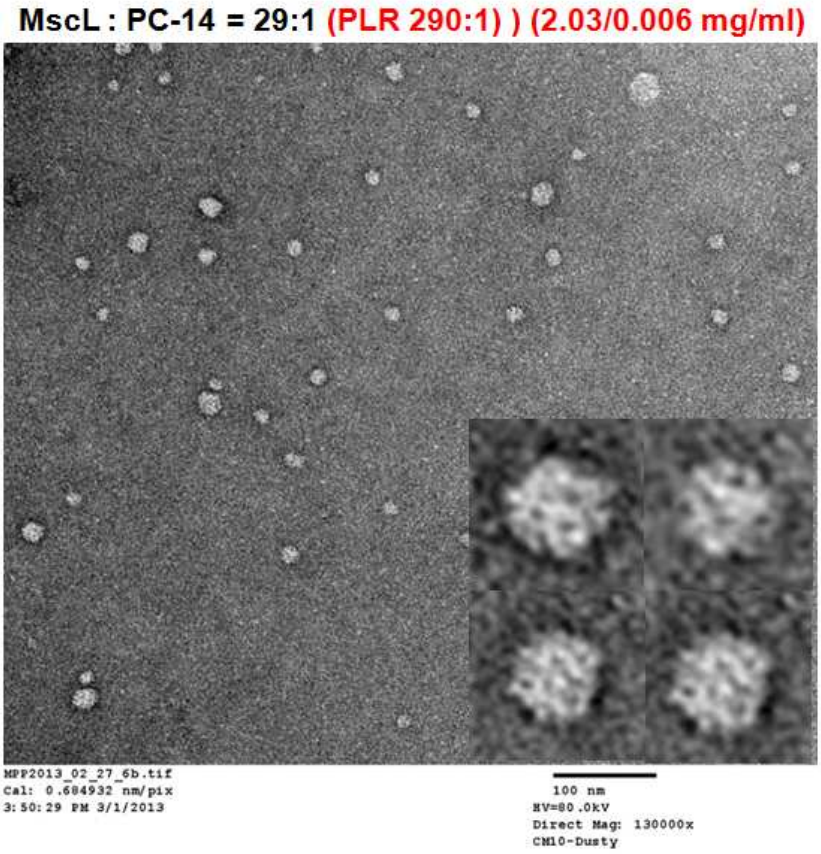


Figure 5.12 shows the image of MscL experimental result when protein to lipid ratio (PLR) at 290 and flow rate ratio (FRR) at 5. The MscL membrane protein nanoparticle has been observed. MscL membrane protein successfully aggregated with lipid bi-layer structure to form nanoparticles.

Moreover, these membrane protein MscL nanoparticles are uniform and size are almost within same diameter range. In the past, the nanoparticle of membrane protein MscL with lipid bilayer

structure has not been observed in any conventional dialysis method because the protein to lipid ratio is too large to reach. Also this result confirmed the hypothesis of numerical simulation method that can predict not only the flow rate ratio of buffer solution and protein/lipid/detergent sample but also the protein to lipid ratio for finding the correct condition to form membrane protein nanoparticles.

# CHAPTER 6

# CONCLUSION AND FURTHER WORK

## 6.1 Conclusion

Using a sample and a buffer solution well with a dialysis membrane in between, it takes between 7 days and a few weeks to form membrane proteins if the processing conditions are good. To generate membrane protein crystals successfully, we have to evaluate many combinations of: a) FRR, b) buffer solution and flow rate, c) concentration of the micelle detergents encapsulating the proteins, and d) concentration of the micelle lipids. It would take about a year and over 150 trials to achieve successful protein crystallization using a conventional dialysis approach.

In this study we demonstrated a novel membraneless microfluidic device that reduces the protein consumption from micro-liters to nano-liters. While also reducing each evaluation run from weeks

to minutes or seconds. In addition, the device can be automated with continuously varying concentrations and flow rates to cover a large number of combinations by using controllable syringe pumps.

Furthermore, we developed a novel microfluidic mixing chip for varying the combinations, such as protein to lipid ratio in order to find a proper protocol for crystallizing membrane protein nanoparticles. First, we successfully demonstrated that the MscS (Mechano-sensitive channel of Small conductance) membrane protein formed the membrane protein nanoparticle with two individual protein and lipid inputs mixed completely in the mixing zone of our mixing chip. Moreover, we tested a new membrane protein MscL **(**Mechano-sensitive channel of Large conductance) which has never been observed in a nanoparticle formation. In the chapter 5 we demonstrated the exciting result of the first MscL membrane protein nanoparticle following from our simulation and experiment of our mixing chip. The simulation result provided the ability to predict the crystallization zone for specific types of detergent and lipid forming membrane protein nanoparticles. For the mixing chip, it provided not only fast evaluation, but also the mixing function to find protein to lipid ratio for forming membrane protein nanoparticles.

Due to the formation changes of detergent and lipid occurred after CMC has been reached and

these reactions are self-assembled procedures followed by thermodynamic theory, the kinetics of monomer-to-micelle or micelle-to-monomer reactions in our microfluidic channel, such as the aggregation time between micelle and monomer transforms have to be considered. According to the previous results, the complete diffusion process for micelle detergent transited to monomer detergent finished in around 7 seconds depended on its diffusion coefficient. This diffusion time is relevantly important compared to aggregation time. For example, if the diffusion time is shorter than aggregation time the monomer will not form a micelle structure due to insufficient time for aggregation process. According to the literature, some studies pointed out the aggregation time is less than $10^{-3}$ seconds, typically range $10^{-3}$ – $10^{-6}$ seconds [56-61]. Based on the comparison, the diffusion time for micelle detergent to change to a monomer detergent in microfluidic channel is at least 3 order of magnitudes larger than the typical aggregation time that provides the sufficient time for detergent and lipid to change their formations. Therefore, the process of either the micelle-to-monomer or monomer-to-micelle in our microfluidic channel can be fully completed without any problem.

In conclusion, in this thesis we developed the numerical simulation method and demonstrated two types of microfluidic devices, a membraneless microfluidic device and a mixing chip, for evaluating membrane protein nanoparticle formation with tremendous improvements compared to

prior work in the field (Table 6.1). The results of our numerical simulation not only confirmed the theory of convection-diffusion phenomena in microfluidic channel but also supported the experimental results. We believe these two novel microfluidic devices for super-fast evaluation of membrane protein nanoparticle crystallization will make a transformative impact in the bio-nanotechnology field .

Table 6.1 The comparison of conventional dialysis method and membraneless microfluidic devices.

| **Comparison** | **Conventional dialysis membrane method** | **Membraneless microfluidic devices** | **Magnitude** |
|---|---|---|---|
| Nanoparticle growth | ~ 7 days | **~7 seconds** | **~ 5 orders** |
| Protein sample consumption | 50-100 mg | **20-400 ng** | **~ 3 orders** |
| No hand pipette needed | X | **Control by syringe pumps** | |
| Low Cost | One condition, one tube, | **One chip for many tests,** | |

| | | | |
|---|---|---|---|
| | dialysis membrane | **no dialysis membrane** | |
| Computational support | X | **Simulation support** | |

## 6.2 Further work

### Different types of membrane protein tests

In this thesis we successfully demonstrated a new method for forming membrane protein nanoparticles by using both numerical simulation and experiment of microfluidic devices. MscS membrane protein with detergent FC-14 and lipid PC-14 have been confirmed for forming membrane protein nanoparticles using conventional dialysis method. Thus, MscS membrane protein is a very suitable sample and reference to test the new concept of microfluidic device. Based on the experimental results of using MscS membrane protein with detergent FC-14 and lipid PC-14, we confirmed the stability and liability of this hypothesis by modeling the CMCs of detergent and lipid to define the crystallization zone for forming MscS membrane protein nanoparticles.

Furthermore, using different type of membrane proteins to form the structure of the nanoparticle is also a challenge. Here we successfully demonstrated the new membrane protein nanoparticle which is an MscL membrane protein with detergent DDM and lipid PC-14. This exciting result proved that this new method of microfluidic devices for forming membrane protein nanoparticles has tremendous abilities to rapidly evaluate varying conditions of membrane proteins and to find new types of membrane protein nanoparticles. Thus, to discover and examine new membrane proteins for forming nanoparticles of membrane protein embedded with a physiological lipid bi-layer structure will be the first priority for future research topics. For example, using the membrane proteins: Bacteriorhodopsin (BR), and Connexin (Cx 26).

**Multi-input microfluidic chip**

In this study, we only have two inputs to verify the combination of protein to lipid ratio due to the limitation of the syringe pump showed in Figure 6.1.

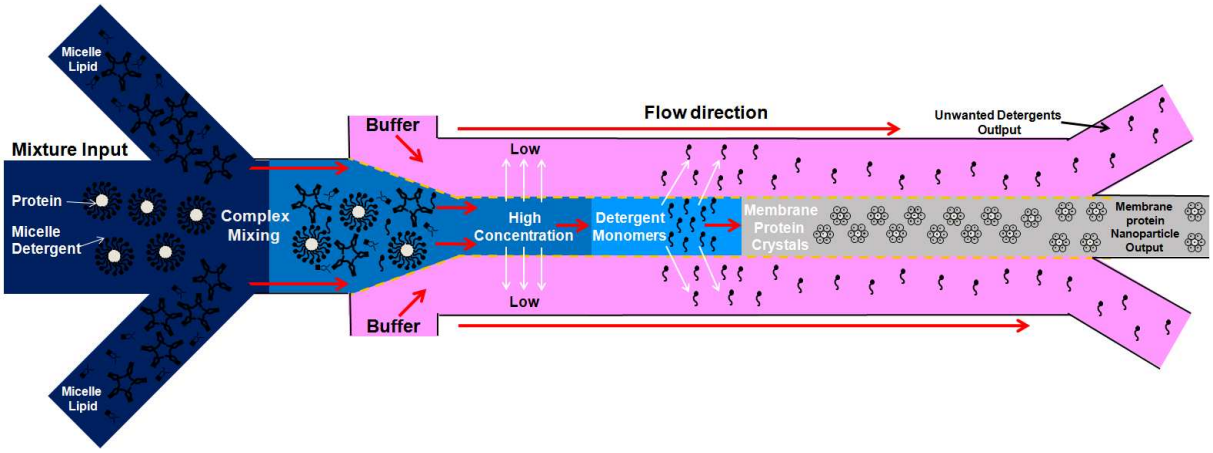


Figure 6.1 Example of membrane protein nanoparticle formation with mixing function. The protein sample with micelle detergent can be adjustably mixed with lipid by using controllable syringe pump.

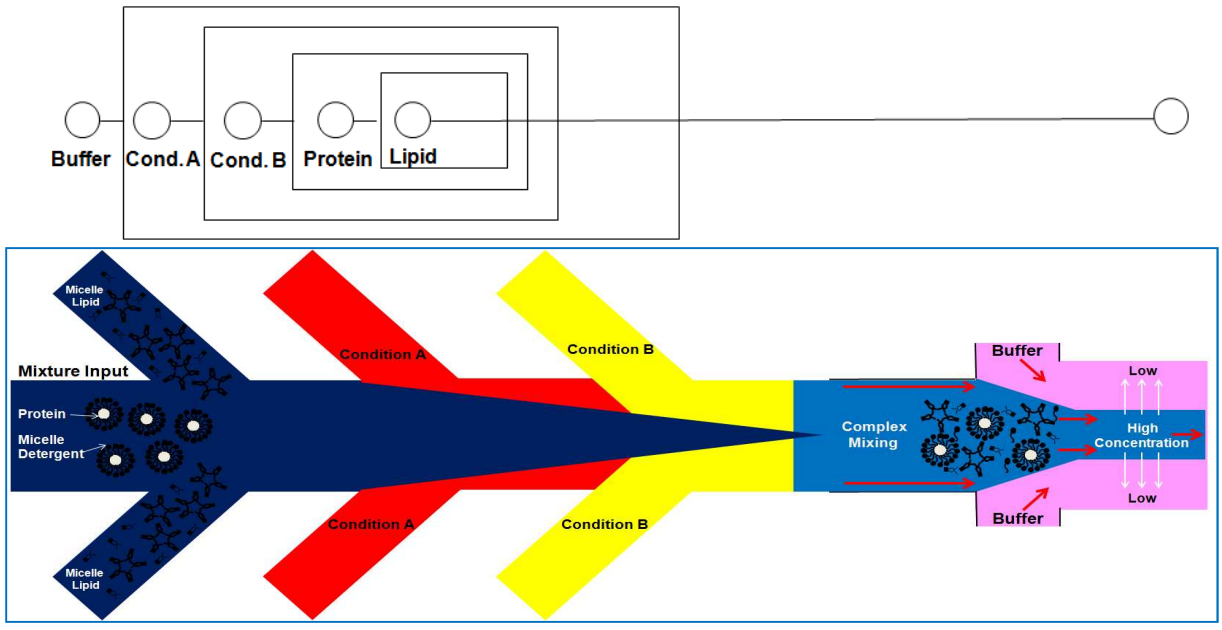


Figure 6.2 shows the multi-input microfluidic device design for verifying the possible combinations of different conditions such as protein to lipid ratio, ph, and salt concentrations.

As previously discussed, a successful membrane protein crystallization is affected by a combination of several conditions such as protein to lipid ratio, and pH and salt concentration in both buffer and protein solutions. Thus, the multi-input microfluidic device is desired for verifying the combinations with more different conditions.

Figure 6.2 shows the potential design for multi-input microfluidic device. By adding more inputs into the beginning of flow focusing microfluidic device, it is possible for the different conditions mixed in the mixing zone to generate a combination of conditions to find a good structure of membrane protein nanoparticles. This multi-input microfluidic device can not only improve the efficiency of verifying the condition for membrane protein nanoparticles, but also provide the ability to find the best combination of conditions for nanoparticle uniformity.

**REFERENCE**


1. Shia-Yen Teh, Robert Lin, Lung-Hsin Hung, and Abraham P. Lee, “Droplet microfluidics”, *Lab Chip*, **2008**, 8, 198–220

2. Axel Gunther, and Klavs F. Jensen, “Multiphase microfluidics: from flow characteristics to chemical and materials synthesis”, *Lab Chip*, **2006**, 6, 1487–1503

3. Todd M. Squires, and Stephen R. Quake, “Microfluidics: Fluid physics at the nanoliter scale”, *REVIEWS OF MODERN PHYSICS*, **2005**, 77

4. Kiichi Sato, Akihide Hibara, Manabu Tokeshi, Hideaki Hisamoto, and Takehiko Kitamoria, “Microchip-based chemical and biochemical analysis systems”, A*dvanced Drug Delivery Reviews*, **2003**, 55, 379–391

5. Adam R. Abatea, Tony Hunga, Pascaline Marya, Jeremy J. Agrestib, and David A.

Weitz, ”High-throughput injection with microfluidics using picoinjectors”, *PNAS,* **2010**, vol. 107, no. 45, 19163–19166

6. Ashleigh B. Theberge, Fabienne Courtois, Yolanda Schaerli, Martin Fischlechner, Chris Abell, Florian Hollfelder, and Wilhelm T. S. Huck, “Microdroplets in Microfluidics: An Evolving Platform for Discoveries in Chemistry and Biology”, *Angew. Chem. Int. Ed*., **2010**, 49, 5846 – 5868

7. T. Thorsen, R.W. Roberts, F. H. Arnold, and S. R. Quake, “Dynamic Pattern Formation in a Vesicle-Generating Microfluidic Device”, *Phys.Rev. Lett*., **2001**, 86, 4163 – 4166

8. Bo Zheng, L. Spencer Roach, and Rustem F. Ismagilov, “Screening of Protein Crystallization Conditions on a Microfluidic Chip Using Nanoliter-Size Droplets”, *J. AM. CHEM. SOC*., **2003**, 125, 11170-11171

9. Bo Zheng, Joshua D. Tice, L. Spencer Roach, and Rustem F. Ismagilov, “A Droplet-Based, Composite PDMS Glass Capillary Microfluidic System evaluating Protein Crystallization Conditions by Microbatch and Vapor-Diffusion Methods with On-Chip

X-Ray Diffraction", *Angew. Chem. Int. Ed*., **2004**, 43, 2508 –2511

10. Bo Zheng, Joshua D Tice, and Rustem F. Ismagilov, "Formation of Arrayed Droplets by Soft Lithography and Two-Phase Fluid Flow, and Application in Protein Crystallization", *Adv. Mater*., **2004**, 16, No. 15

11. Thomas Ward, Magalie Faivre, Manouk Abkarian, and Howard A. Stone, "Microfluidic flow focusing Drop size and scaling in pressure versus flow-rate-driven pumping", *Electrophoresis*, **2005**, 26, 3716–3724

12. Linas Mazutis, Jean-Christophe Baret, Patrick Treacy, Yousr Skhiri, Ali Fallah Araghi, Michael Ryckelynck, Valerie Taly, and Andrew D. Griffiths, "Multi-step microfluidic droplet processing: kinetic analysis of an in vitro translated enzyme", *Lab Chip*, **2009**, 9, 2902–2908

13. D. R. Link, S. L. Anna, D. A.Weitz, and H. A. Stone, "Geometrically Mediated Breakup of Drops in Microfluidic Devices", *Physical Review Letters*, **2004**, v 92, n 5, 545031-545034

14. Wei-Heong Tan, and Shoji Takeuchi, “A trap-and-release integrated microfluidic system”, *PNAS*, **2007**, vol. 104, no. 4, 1146–1151

15. Kosuke Iwai, Wei-Heong Tan, and Shoji Takeuchi, “A RESETTABLE DYNAMIC MICROFLUIDIC DEVICE”, *MEMS 2008*, January 13-17, **2008**, Tucson, AZ, USA

16. Weiwei Shi, Jianhua Qin, Nannan Ye, and Bingcheng Lin, “Droplet-based microfluidic system for individual Caenorhabditis elegans assay”, *Lab Chip*, **2008**, 8, 1432–1435

17. James P. Brody and Paul Yager, “Diffusion based Extraction in a Microfabricated Structure.” *Sensors and Actuators A: Physical*, **1997**, 58, 13 – 16

18. Rui Hua, Xiaojun Feng, Pu Chen, Meng Fu, Hong Chen, Lin Guo, and Bi-Feng Liu, “Rapid, highly efficient extraction and purification of membrane proteins using a microfluidic continuous-flow based aqueous two-phase system”, *Journal of Chromatography A*, **2011**, 1218, 171–177

19. Andrew P. Yeh, Andy McMillan, and Michael H. B. Stowell, “Rapid and simple

protein-stability screens: application to membrane proteins", *Acta Cryst.*, **2006**, D62, 451–457

20. Henning Stahlberg, Dimitrios Fotiadis, Simon Scheuring, Herve Remigy, Thomas Braun, Kaoru Mitsuoka, Yoshinori Fujiyoshi, and Andreas Engel, "Two-dimensional crystals a powerful approach to assess structure function and dynamics of membrane proteins", *FEBS Letters*, **2001,** 504, 166-172

21. Liang Li, and Rustem F. Ismagilov, "Protein Crystallization Using Microfluidic Technologies Based on Valves, Droplets, and SlipChip", *Annu. Rev. Biophys.*, **2010**, 39, 139–58

22. Iban Ubarretxena-Belandia, and David L. Stokes, "Membrane protein structure determination by electron crystallography", *Current Opinion in Structural Biology*, **2012**, 22, 520–528

23. Renault L, Chou HT, Chiu PL, Hill RM, Zeng X, Gipson B, Zhang ZY, Cheng A, Unger V, and Stahlberg H., "Milestones in electron crystallography", *J Comput Aided Mol Des.*, **2006**,

20(7-8), 519-27

24. Liang Li, Debarshi Mustafi, Qiang Fu, Valentina Tereshko, Delai L. Chen, Joshua D. Tice, and Rustem F. Ismagilov, “Nanoliter microfluidic hybrid method for simultaneous screening and optimization validated with crystallization of membrane proteins”, *PNAS*, **2006**, vol. 103, no. 51, 19243–19248

25. Stefan Raunser, and Thomas Walz, “Electron Crystallography as a Technique to Study the Structure on Membrane Proteins in a Lipidic Environment”, *Annual Review of Biophysics*, **2009**, v 38, 89-105

26. Martin Vink, KD Derr, James Love, David L. Stokes, and Iban Ubarretxena-Belandia, “A high-throughput strategy to screen 2D crystallization trials of membrane proteins”, *Journal of Structural Biology*, **2007**, 160, 295–304

27. Jessamine M. K. Ng, Irina Gitlin, Abraham D. Stroock, and George M. Whitesides, “Components for integrated poly(dimethylsiloxane) microfluidic systems”. *Electrophoresis*, **2002**, 23, 3461–3473

28. Javier Atencia, and David J. Beebe, “Controlled microfluidic interfaces”, *NATURE*, **2005**, Vol 437

29. Helen Song, Delai L. Chen, and Rustem F. Ismagilov, “Reactions in Droplets in Microfluidic Channels”, *Angew. Chem. Int. Ed*., **2006**, 45, 7336 – 7356

30. Gotz Munchow, Friedhelm Schonfeld, Steffen Hardt, and Karlheinz Graf, “Protein Diffusion Across the Interface in Aqueous Two-Phase Systems”, *Langmuir*, **2008**, 24, 8547-8553

31. Mariana Surmeian, Maxim N. Slyadnev, Hideaki Hisamoto, Akihide Hibara,Kenji Uchiyama, and Takehiko Kitamori, “Three-Layer Flow Membrane System on a Microchip for Investigation of Molecular Transport”, *Analytical Chemistry,* **2002**, Vol. 74, No. 9

32. G. Munchow, S. Hardt, J.P. Kutter, and K.S. Drese, “Protein Transport and Concentration by Electrophoresis in Two-phase Microflows”, *Journal of the Association for Laboratory Automation*, **2006**, v 11, n 6, 368-373

33. Andreas Jahn, Samuel M. Stavis, Jennifer S. Hong, Wyatt N. Vreeland, Don L. DeVoe, and Michael Gaitan, “Microfluidic Mixing and the Formation of Nanoscale Lipid Vesicles”, *ACS Nano*, **2010**, v 4, n 4, 2077-2087

34. Robert J. Meagher, Yooli K. Light, and Anup K. Singh , “Rapid, continuous purification of proteins in a microfluidic device using genetically-engineered partition tags”, *Lab Chip*, **2008**, 8, 527–532

35. C.P. Arthur and M.H.B. Stowell, “Structure of synaptophysin: A hexameric MARVEL domain channel protein”, *Structure*, **2007**, vol. 15, 707–714

36. Yong Tae Kim, Bomy Lee Chung, Mingming Ma, Willem J. M. Mulder, Zahi A. Fayad, Omid C. Farokhzad, and Robert Langer, “Mass Production and Size Control of Lipid−Polymer Hybrid Nanoparticles through Controlled Microvortices”, *Nano Lett.*, **2012**, 12, 3587−3591

37. J.-L. Rigaud, “Membrane proteins functional and structure studies using reconstituted proteoliposomes and 2-D crystals”, *Brazilian Journal of Medical and Biological Research*, **2002**, vol 35, 753-766

38. D.B. Weibel, and G.M. Whitesides, “Applications of microfluidics in chemical biology”, *Current Opinion in Chemical Biology*, **2006**, vol. 10, 584–591

39. K. Sato, A. Hibara, M. Tokeshi, H. Hisamoto, and T. Kitamoria, “Microchip-based chemical and biochemical analysis systems”, A*dvanced Drug Delivery Reviews*, **2003**, 55, 379–391.

40. A. B. Theberge, F. Courtois, Y. Schaerli, M. Fischlechner, C. Abell, F. Hollfelder, and W. T. S. Huck, “Microdroplets in Microfluidics: An Evolving Platform for Discoveries in Chemistry and Biology”, *Angew. Chem. Int. Ed.*, **2010**, 49, 5846 – 5868

41. A. Gunther, and K.F. Jensen, “Multiphase microfluidics: from flow characteristics to chemical and materials synthesis”, *Lab Chip*, **2006**, vol *6*, 1487–1503

42. A. Jahn, S.M. Stavis, J.S. Hong, W.N. Vreeland, D.L. DeVoe, and M. Gaitan, “Microfluidic Mixing and the Formation of Nanoscale Lipid Vesicles”, *ACS Nano,* **2010,** vol 4, 2077-2087

43. J.S. Hong, S.M. Stavis, S.H.D. Lacerda, L.E. Locascio, S.R. Raghavan, and M. Gaitan, “Microfluidic Directed Self-Assembly of Liposome-Hydrogel Hybrid Nanoparticles”, *Langmuir*, **2010**, 23, 13, 11581-11588

44. Jinjun Shi, Alexander R. Votruba, Omid C. Farokhzad, and Robert Langer, “Nanotechnology in Drug Delivery and Tissue Engineering: From Discovery to Applications”, *Nano Lett*., **2010**, 10, 3223–3230

45. Rohit Karnik, Frank Gu, Pamela Basto, Christopher Cannizzaro, Lindsey Dean, William Kyei-Manu, Robert Langer, and Omid C. Farokhzad, “Microfluidic Platform for Controlled Synthesis of Polymeric Nanoparticles”, *Nano Lett*., **2008**, 8, 9, 2906-2912

46. Meagher, R.J., Light, Y.K., and Singh, A.K.: ‘Rapid, continuous purification of proteins in a microfluidic device using genetically-engineered partition tags’, *Lab chip*, **2008**, 8, 527-532

47. Serdar Ozturk, Yassin A. Hassan, and Victor M. Ugaz, “Interfacial Complexation Explains Anomalous Diffusion in Nanofluids”, *Nano Lett.*, **2010**, 10, 665-671

48. Randal B. Bass, Pavel Strop, Margaret Barclay, and Douglas C. Rees, “Crystal Structure of *Escherichia coli* MscS, a Voltage-Modulated and Mechanosensitive Channel”, *Science*, ***2002***, 298, 1582-1587

49. Elizabeth S. Haswell1, Rob Phillips, and Douglas C. Rees, “Mechanosensitive channels: what can they do and how do they do it?”, *Structure*. **2011**, 19, 10, 1356–1369

50. Valeria Vásquez, Marcos Sotomayor, Julio Cordero-Morales, Klaus Schulten, Eduardo Perozo, “A Structural Mechanism for MscS Gating in Lipid Bilayers”, *Science*, ***2008***, 321, 1210

51. Luis F. Padilla-Morales, Claudio L. Morales-Pérez, Pamela C. De La Cruz-Rivera, Guillermo Asmar-Rovira, Carlos A. Báez-Pagán, Orestes Quesada, José A. and Lasalde-Dominicci,

"Effects of Lipid-Analog Detergent Solubilization on the Functionality and Lipidic Cubic Phase Mobility of the *Torpedo californica* Nicotinic Acetylcholine Receptor", *J Membr Biol.*, **2011**, 243(1-3), 47–58

52. Paulo F. F. Almeida, Winchil L. C. Vaz,y and T. E. Thompsonz, "Lipid Diffusion, Free Area, and Molecular Dynamics Simulations", *Biophysical Journal*, **2005**, 88, 4434–4438

53. Christopher D. Pivetti, Ming-Ren Yen, Samantha Miller, Wolfgang Busch, Yi-Hsiung Tseng, Ian R. Booth, and Milton H. Saier, Jr., "Two Families of Mechanosensitive Channel Proteins", *MICROBIOLOGY AND MOLECULAR BIOLOGY REVIEWS*, **2003**, 67, 1, 66–85

54. Paul Wiggins and Rob Phillips, "Analytic models for mechanotransduction: Gating a mechanosensitive channel", *PNAS*, **2004**, 101, 12, 4071–4076

55. Paul Wiggins and Rob Phillipsy, "Membrane-Protein Interactions in Mechanosensitive Channels", *Biophysical Journal*, **2005**, 88, 880–902

56. Jacob N. Israelachvili, “Intermolecular and Surface Forces”, **1991**, chapter 16, ISBN 0-12-375181-0.

57. Charles Tanford,”Micelle Shape and Size”, *Journal of Physical Chemistry*, **1972**, 76,21, 3020-3024.

59. Charles Tanford, “Thermodynamics of Micelle Formation: Prediction of Micelle Size and Size Distribution”, *Proc. Nat. Acad. Sci.*, **1974**, 71, 5, 1811-1815.

60. A. G. Lee, “Lipid-protein Interactions in Biological Membranes: a Structural Perspective”, *Biochimca et Biophysica Acta*, **2003**, 1612, 1-40.

61. Alexander Patist, James R. Kanicky, Pavan K. Shukla, and Dinesh O. Shah, “Importance of Micellar Kinetics in Relation to Technological Processes”, *Journal of Colloid and Interface Science*, **2002**, 245, 1-15.

# Appendix A

## Numerical Simulation by Comsol Multiphysics 4.2

### Introduction

In the flow focusing phenomena the higher concentration of protein/lipid/detergent complex being injected into the center of main channel merging by two buffer solutions with equal flow velocity from both perpendicular sides (Figure A.1). The contact interface in between a center and both side streams generated a concentration gradient in which the diffusive transport happened from the higher concentration of a center protein/lipid/detergent complex stream to the low concentration of buffer solution stream in both sides. The mixing phenomena in the main channel of center stream and both side buffer solutions were dominated by convective-diffusive transport. Such gradients offer us an opportunity to form membrane protein crystals.

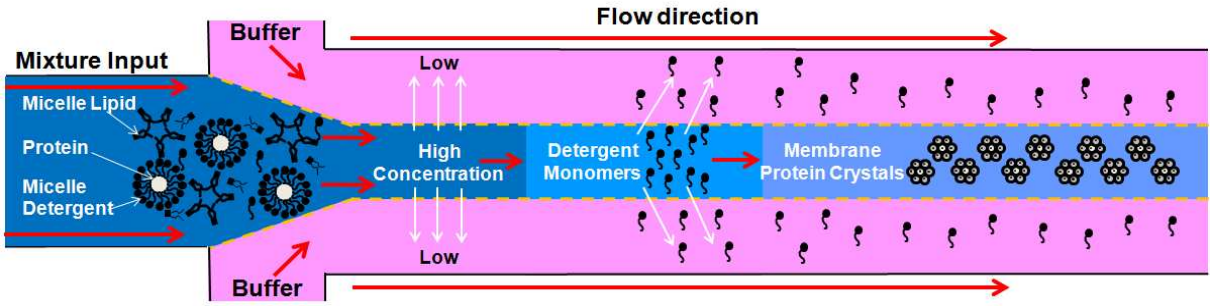


Figure A.1. Diagram of the flow focusing in microfluidic channel.

The numerical result of the mixing concentration distribution of the injected central protein/lipid complex stream merging by two side adjoining buffer solution streams were simulated with two-dimensional laminar flow model using COMSOL Multiphysics 4.2a( COMSOL, Inc., Burlington, MA). The laminar flow and mixing behaviors were governed by the continuity and Navier-Stoke equations for the single phase incompressible flow combining with convection-diffusion equation for the concentration transport of diluted species in flow focusing. The following equations were set up and solved at steady-state.

$$-\nabla \cdot \eta(\nabla u + (\nabla u)^T) + \rho u \cdot \nabla u + \nabla p = 0 \quad (1)$$

$$\nabla \cdot u = 0 \quad (2)$$

$$\nabla \cdot (-D\nabla c + cu) = 0 \quad (3)$$

Where η, u, ρ, and p represent the viscosity, velocity, density and pressure. D is diffusion

coefficient and c is concentration. Applying the no-slip boundary condition to all boundaries except inlets and outlet; it presents the velocity is zero at the walls as well as zero diffusive flux through the wall. For a given set of concentration factors optimized by other studies, the formation of the crystals is affected by the flow rate ratio (FRR) between the buffer (phosphate buffered saline) and the mixture streams.

**Step by step instruction for modeling flow focusing phenomena in microfluidic channel by using COMSOL**

1. Create a new file, select 2D axisymmetric in Dimension window, and click next.

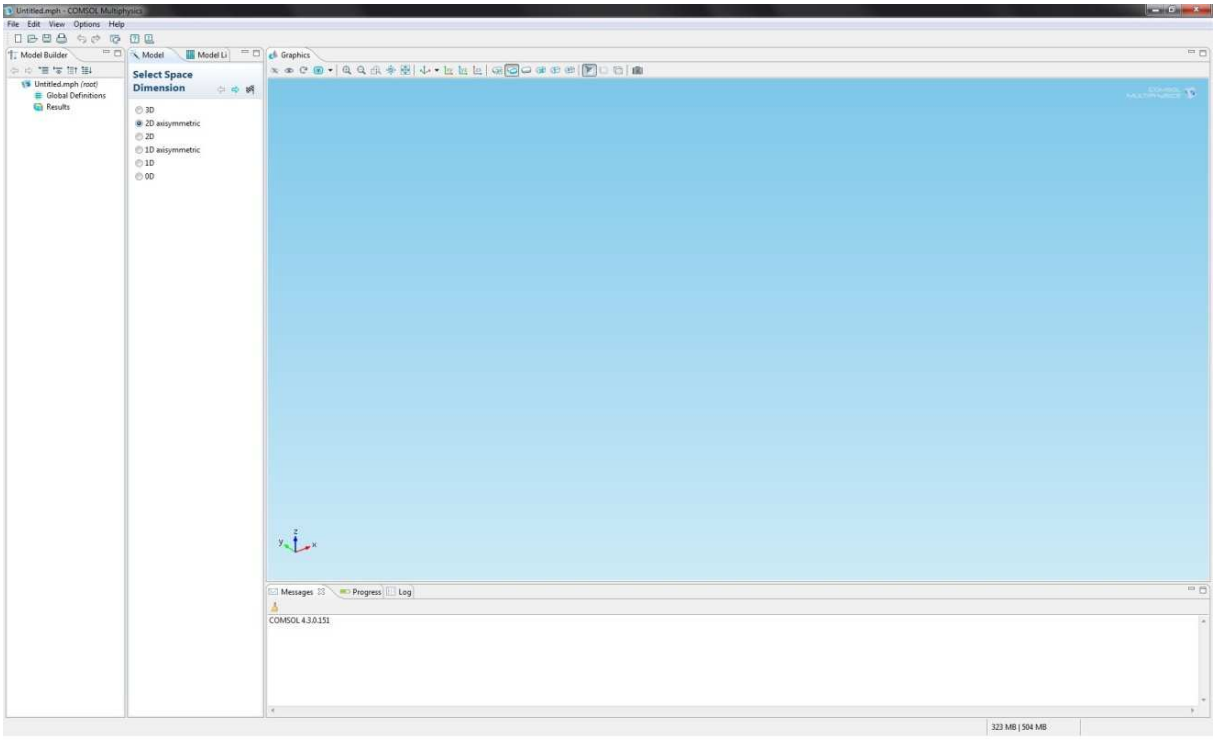


Figure A.2. shows to create a new file and choose the space dimension.

2. In the add physics tree, select Chemical Species Transport > Transport of Diluted Species(chds), and Click Selected

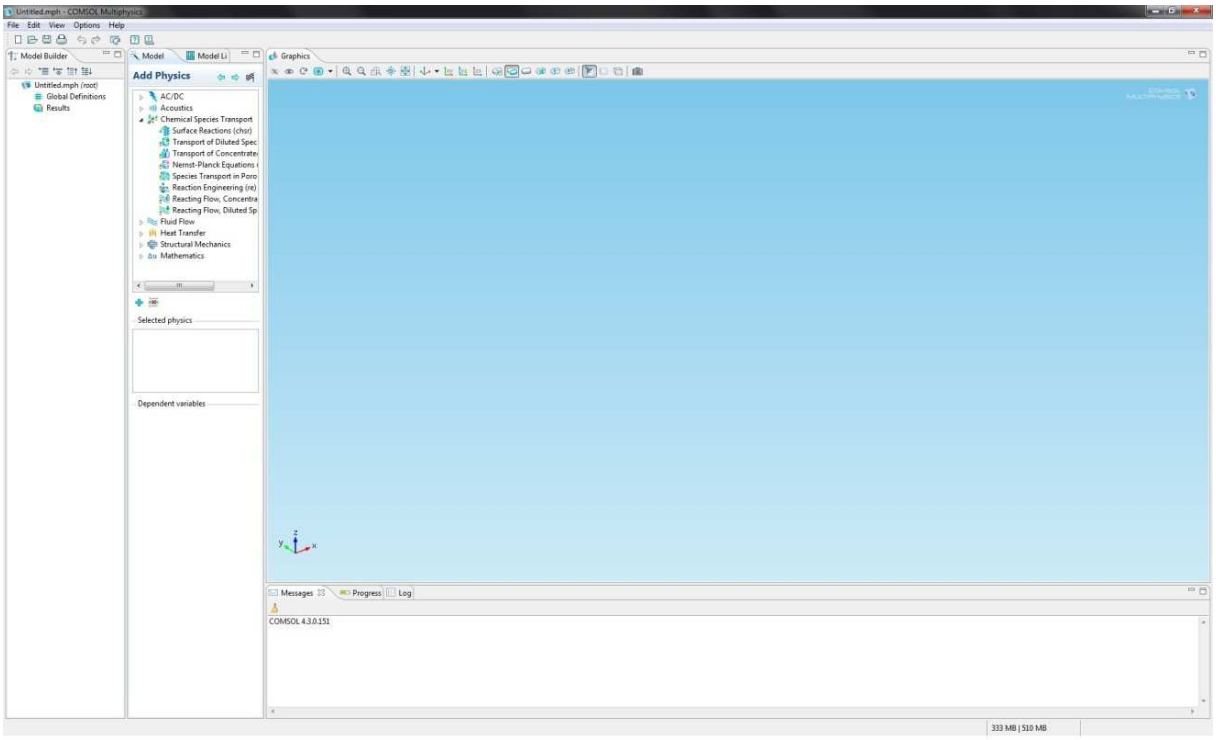


Figure A.3 shows to add the physics functions for modeling.

3. In the add physics tree, select Fluid Flow > Single-Phase Flow > Laminar Flow (spf), click Selected, and Next

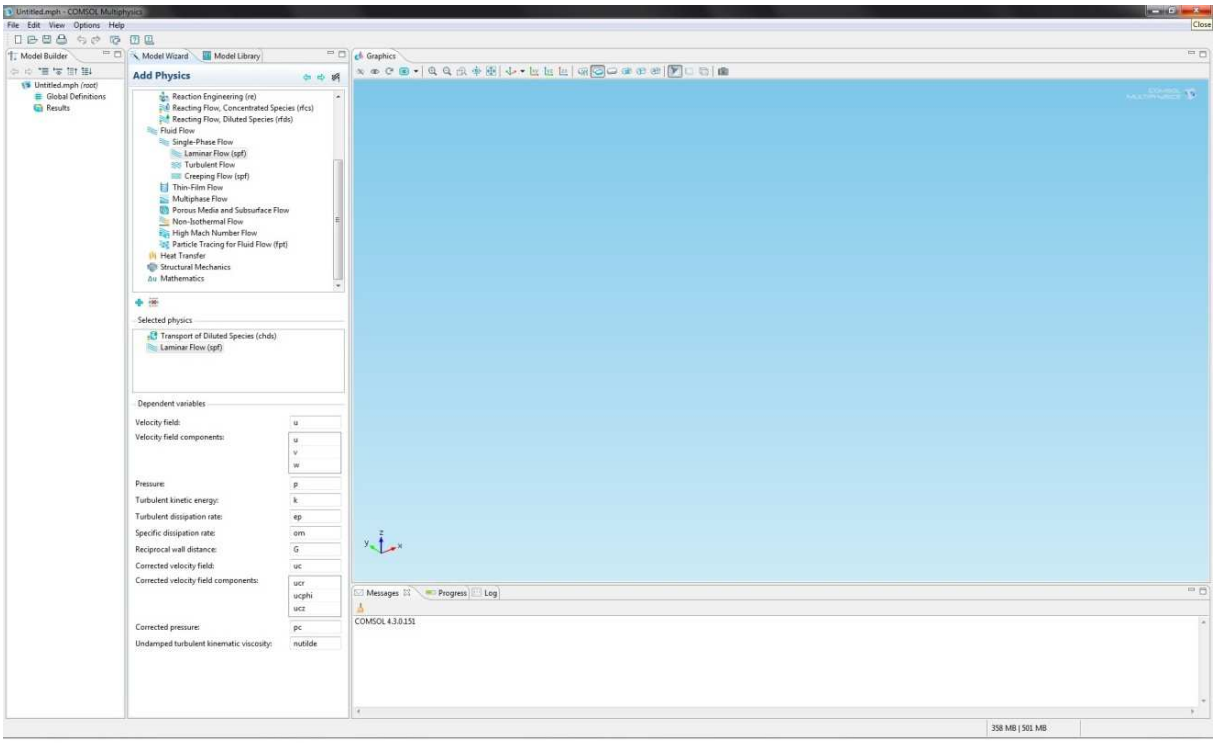


Figure A.4 shows adding the Laminar Flow (spf) from Single-Phase Flow and Transport of Diluted Species(chds) from Chemical Species Transport in physics tree.

4. In the Studies tree, select Preset studies for Selected Physics > Stationary, and click Finish.

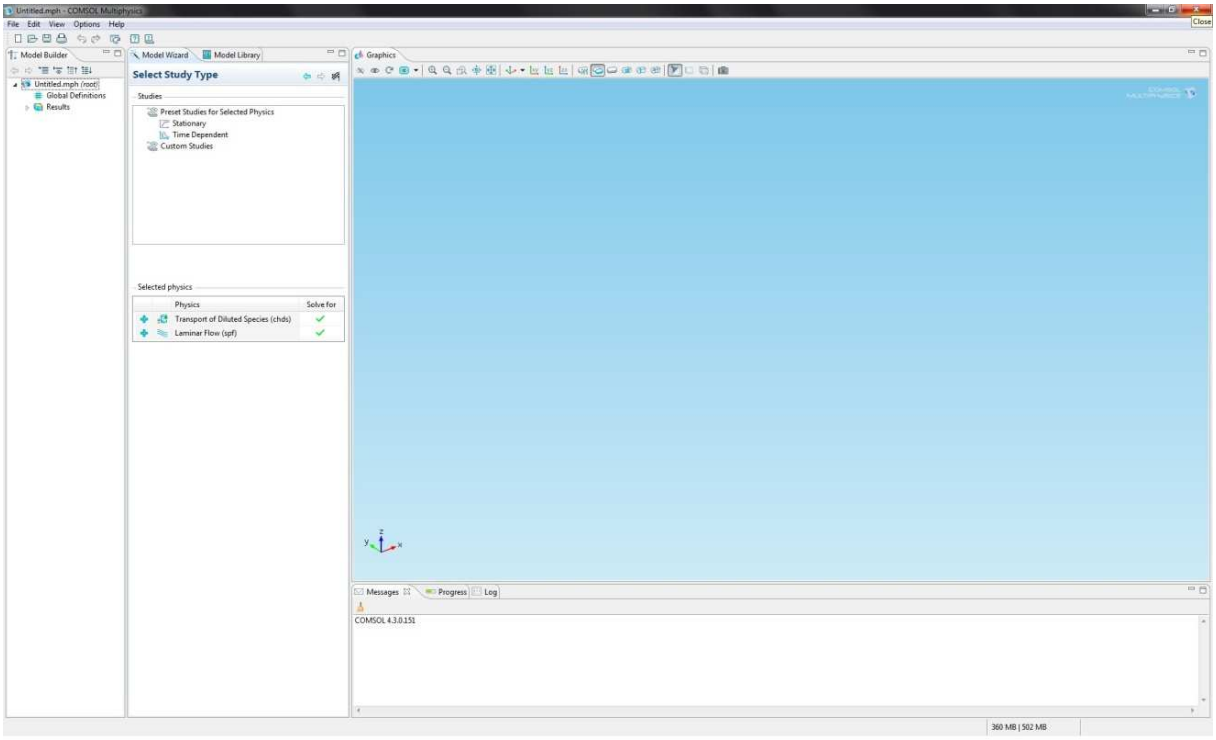


Figure A.5 shows to select the study type as stationary.

5. In geometry 1, set micro meter in Units tree. Then in the Model Builder window right-click Model 1 > Geometry 1 and choose Work Plane, then build up the your designed geometry

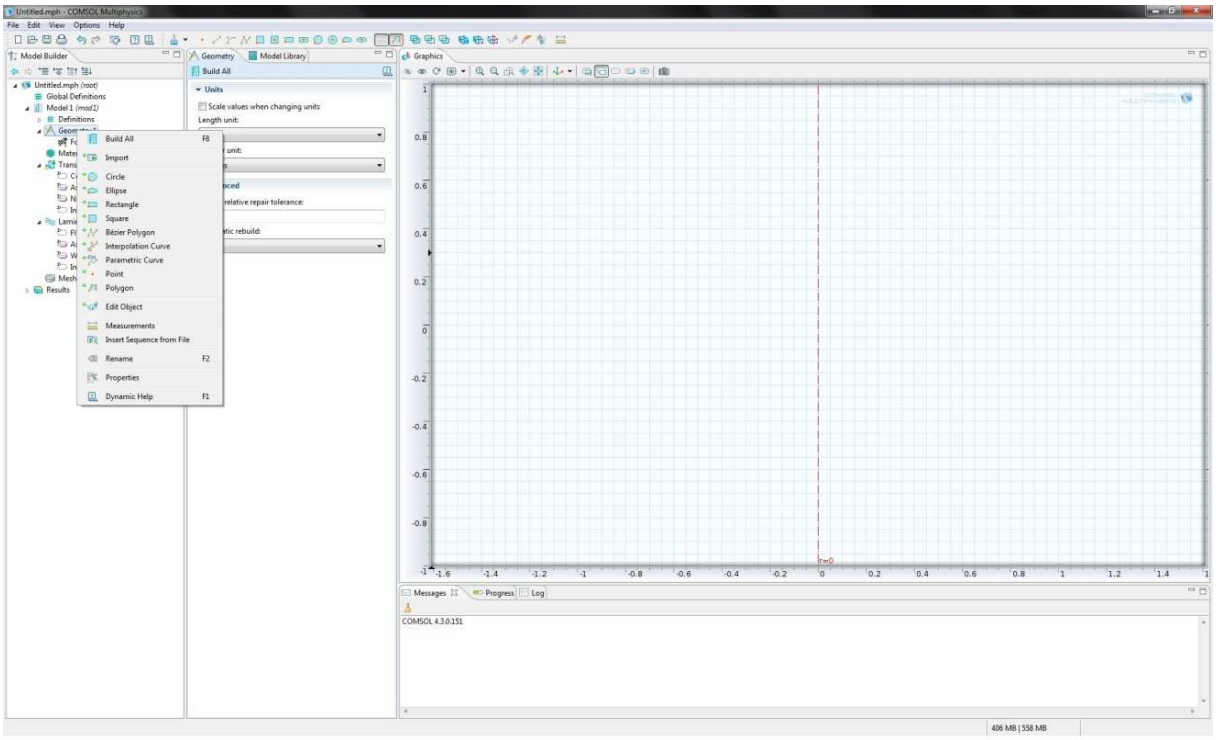


Figure A.6 shows drawing tools for creating the modeling geometry.

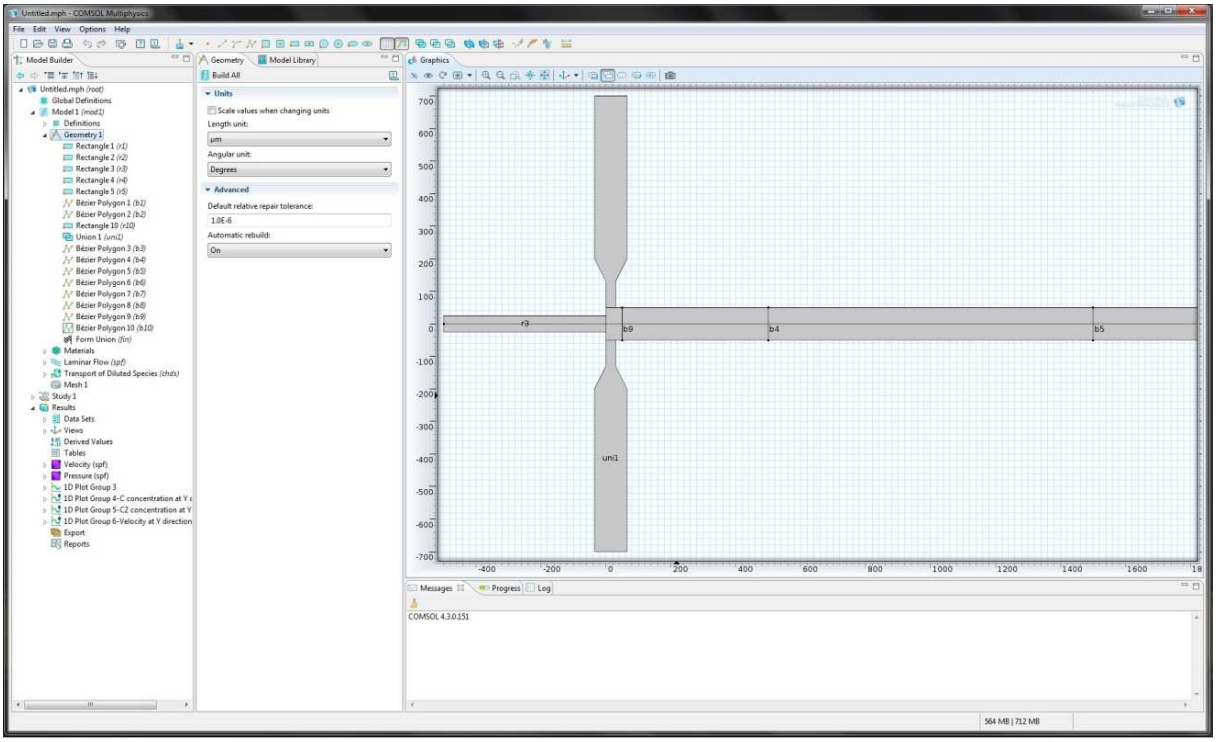


Figure A.7 shows the final designed geometry for micro channel.

6. Materials, In the Model Builder window, right-click Materials, in the Materials tree, select Built-In > Water, liquid.

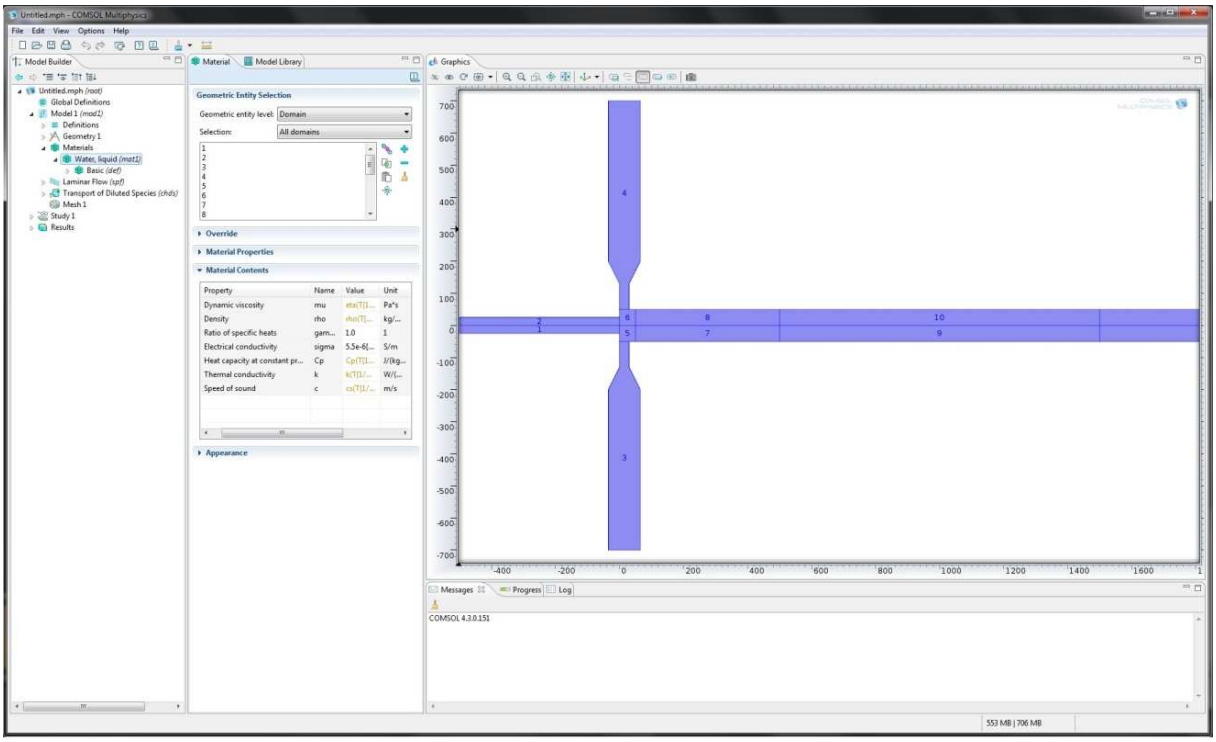

Figure A.8 shows how to choose the material and check the material properties.

7. Laminar flow set up. In the Model Builder window,

a. Select Wall 1 to choose walls for the boundary selection and set up no slip for boundary condition.

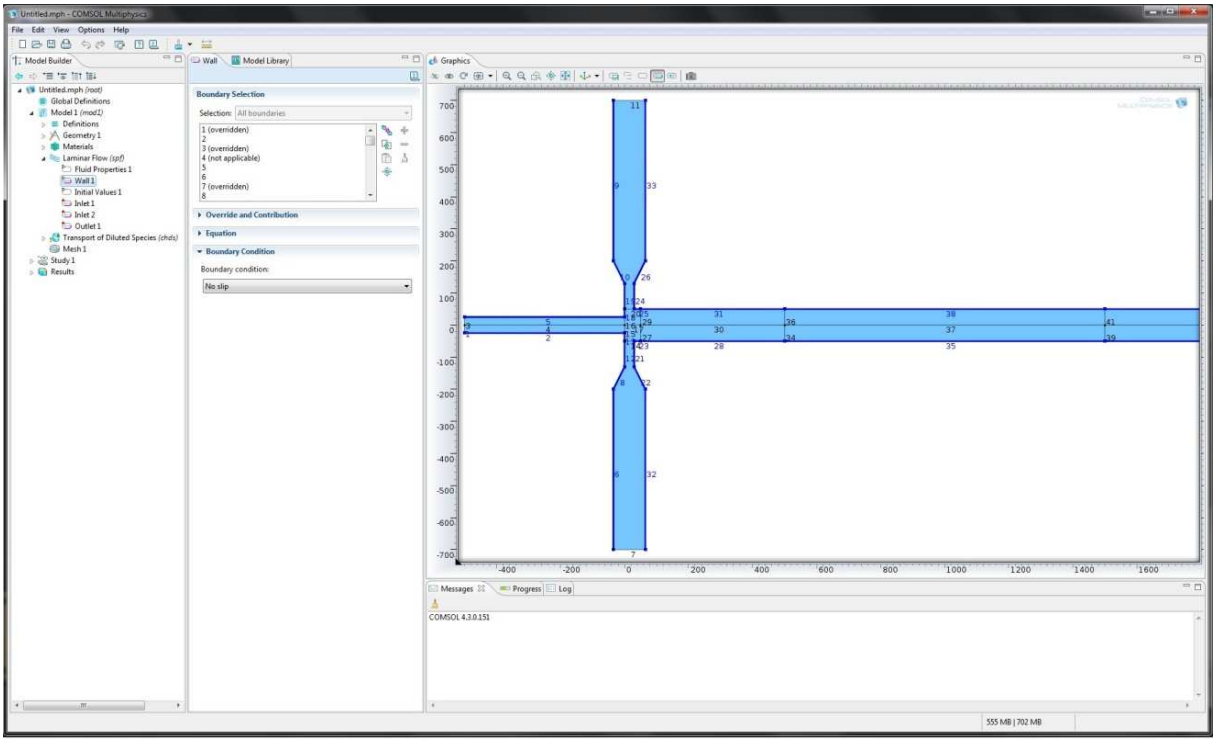


Figure A.9 shows how to select the walls as defined boundaries.

b. Right-click Model 1 > Laminar Flow and choose input and output boundaries for Inlet 1, Inlet 2 and Outlet 1. Then choose the flow rate in laminar inflow section to be initial condition for Inlet 1 and 2. And locate the Pressure, No Viscous Stress section. In the *p*0 edit field, type p0 for Outlet 1

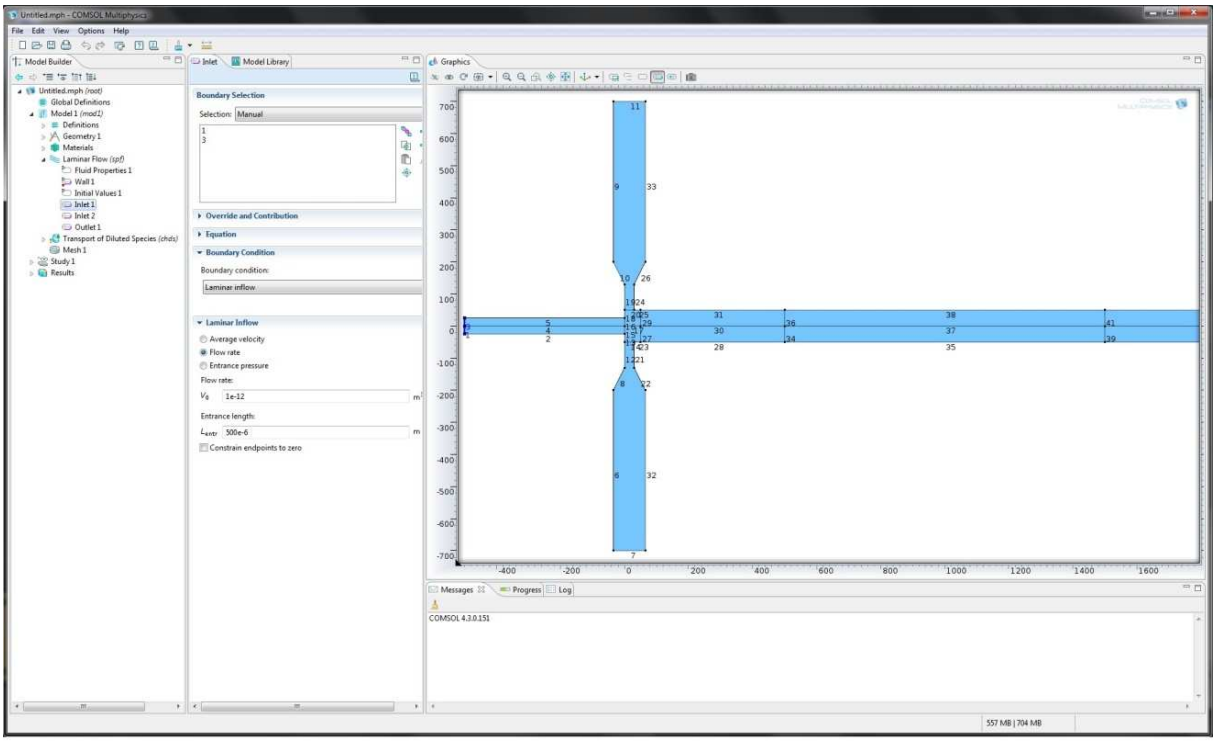


Figure A.10 shows how to define the inlet for liquid input.

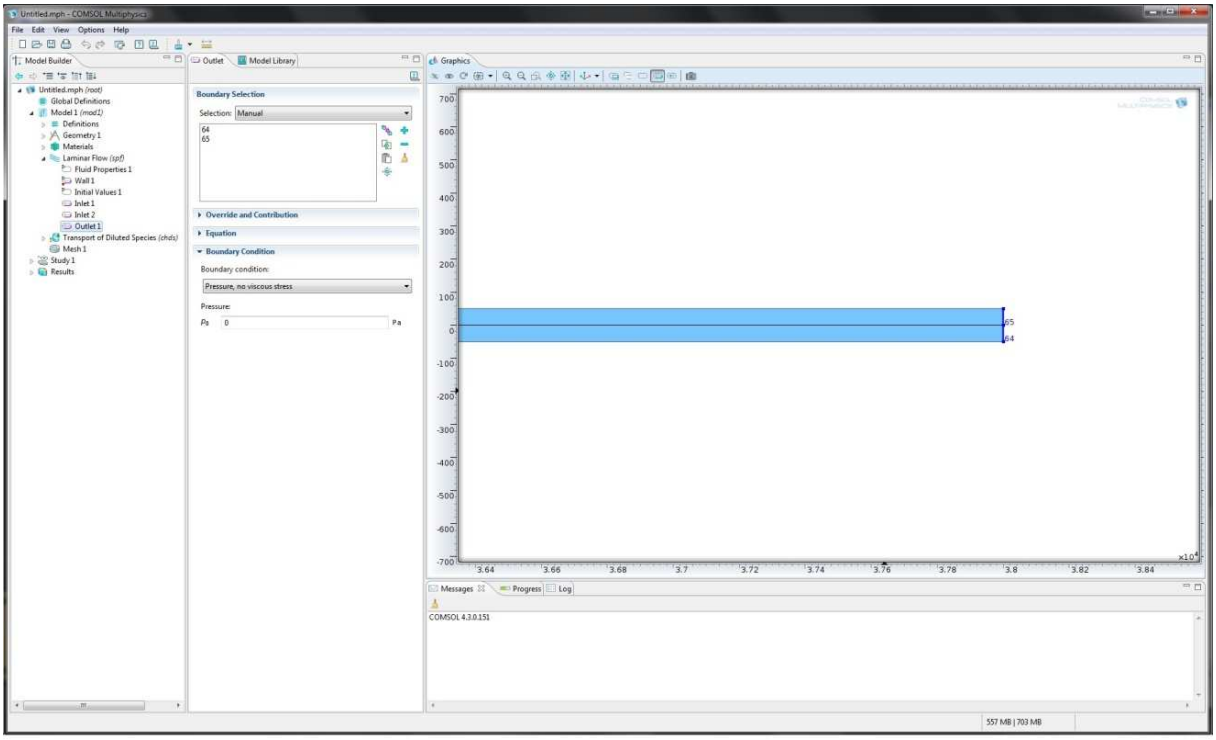


Figure A.11 shows how to define the outlet.

8. Transport of Diluted Species(chds)set up, in the Model Builder window,

*a.* Click Convection and Diffusion 1. Select the areas in Domain Selection.

b. Locate the Model Inputs section, choose velocity field(spf/fp1), and locate the Diffusion section, type diffusion coefficient for $D_c$ and $D_{c2}$

c. Click the Inflow 1, select boundaries for flow input 1, and then set up the initial concentration for $C_{0,c}$ and $C_{0,c2}$ since there are two species 1 and 2 inputted through from Inlet 1. And for Inflow 2, select boundaries for flow input 2, and then initial concentration type 0 for both $C_{0,c}$ and $C_{0,c2}$ since no any concentration of species added in buffer solution. for the outflow 1, select boundaries for the flow outlet 1.

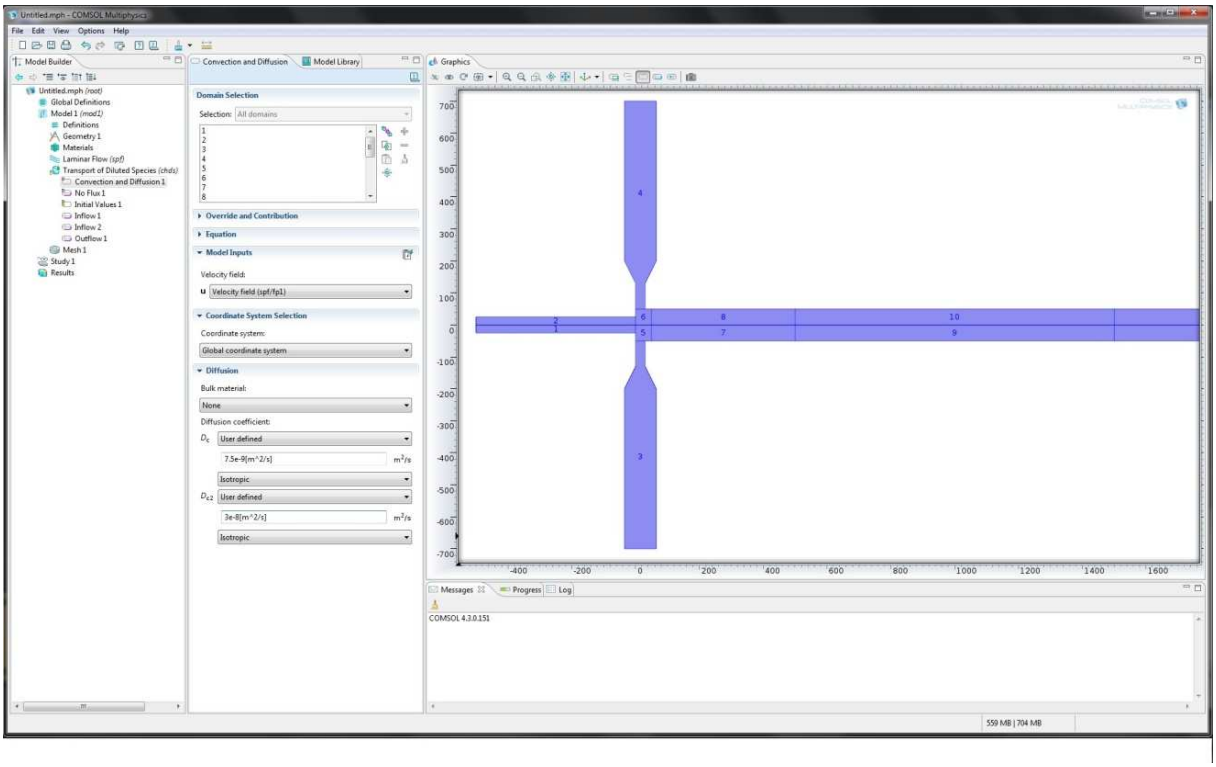


Figure A.12 shows the parameters of convection and diffusion in Transport of Diluted Species.

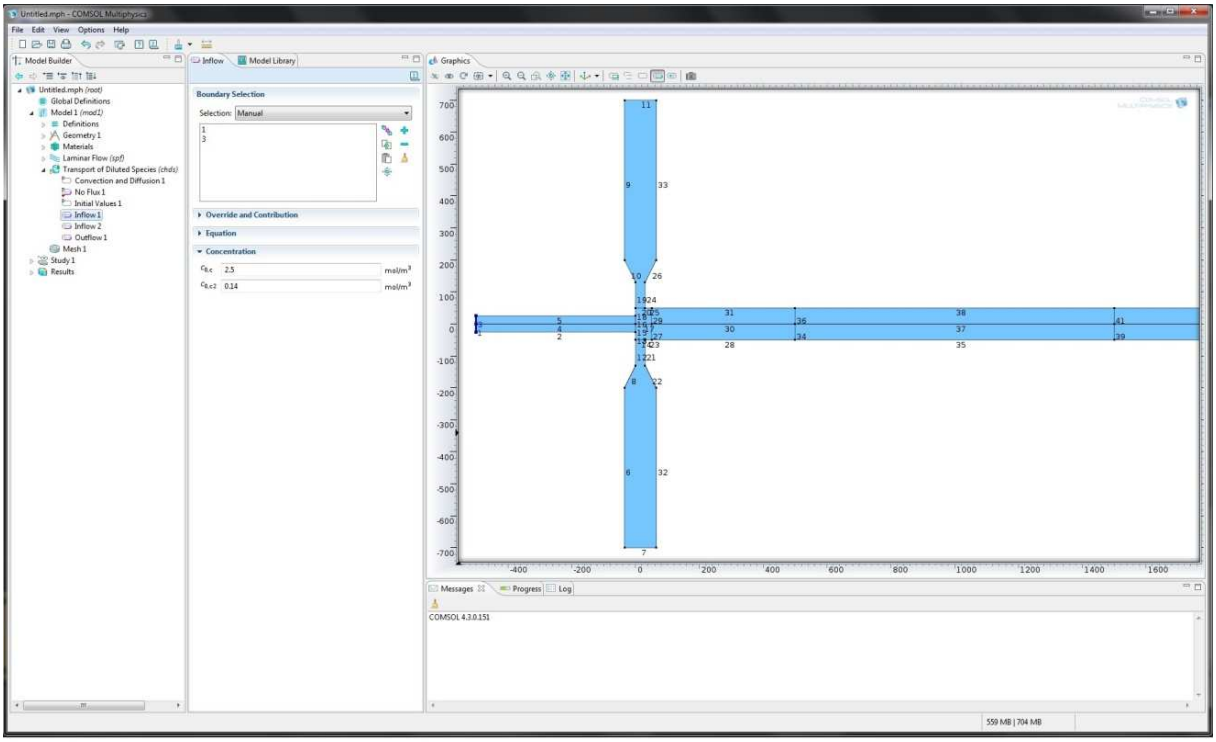


Figure A.13 shows how to define the inflow 1 inlet and initial concentration.

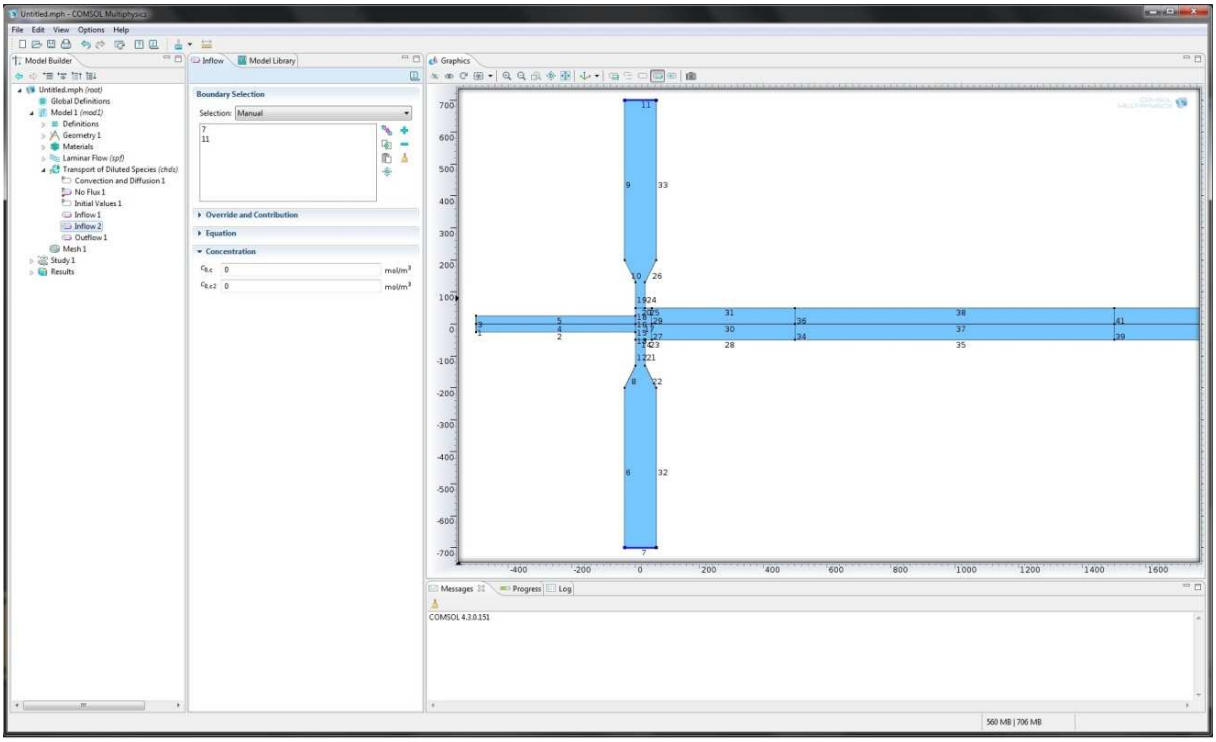

Figure A.14 shows how to define the inflow 2 inlet and initial concentration.

9. Mesh, In the Model Builder window, right-click Model 1 > Mesh 1 and choose Free Tetrahedral. Then locate the Element Size section and choose Extremely fine. Then click the Build All button.

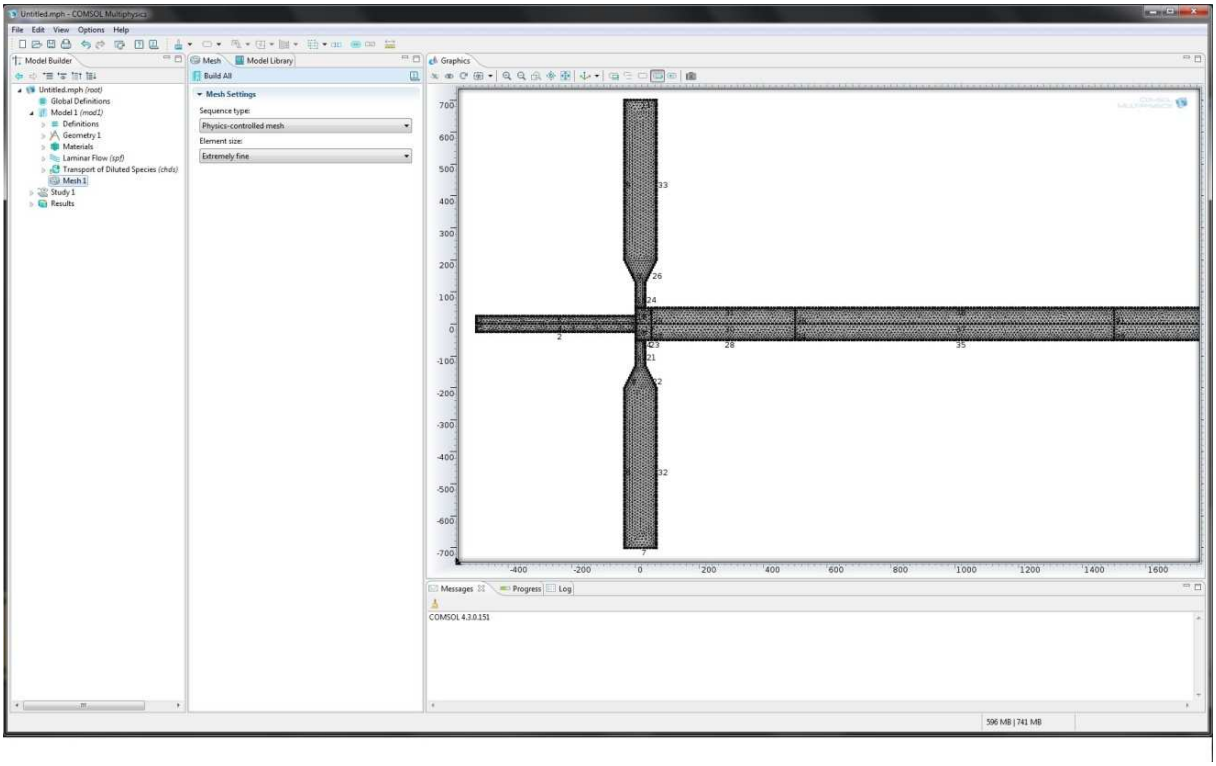


Figure A.15 shows the mesh map for designed geometry.

10. Study, in the Model Builder window, right-click Study and choose Compute.

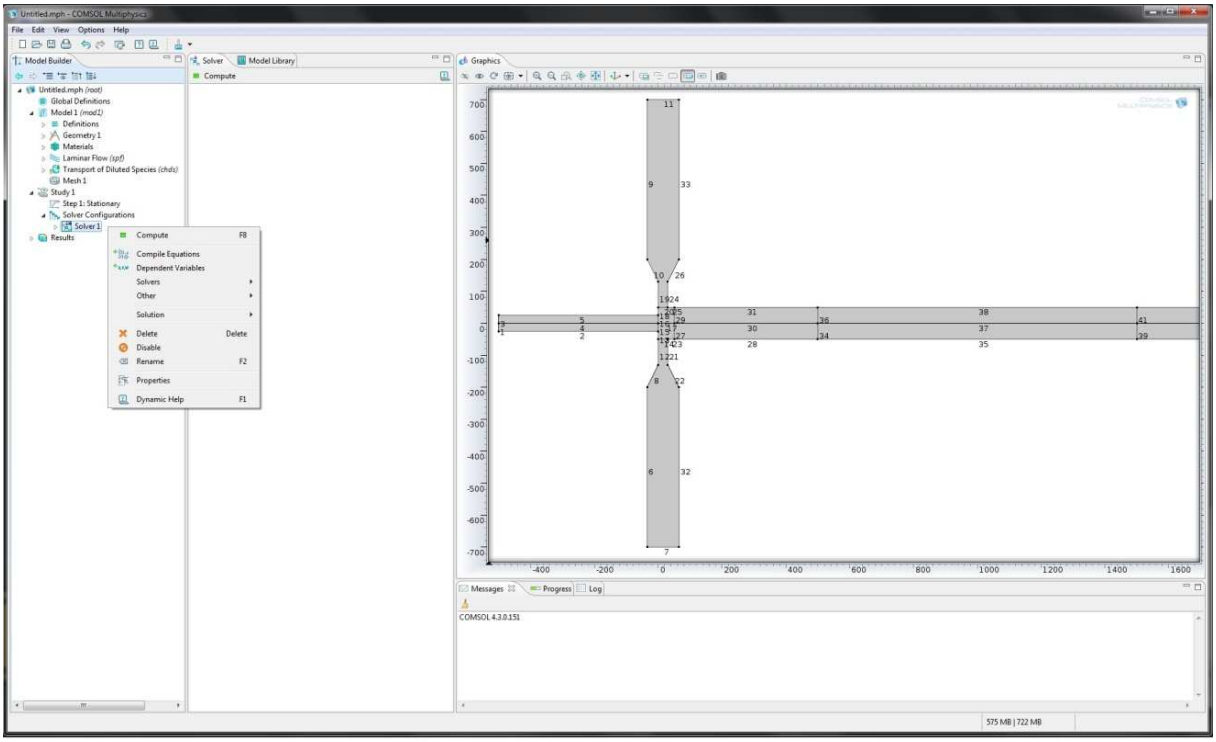


Figure A.16 shows how to compute the simulation modeling.

11. Results, in the in the Model Builder window,

a. right-click Results, then choose whatever 3D, 2D and 1D plots you want to generate.

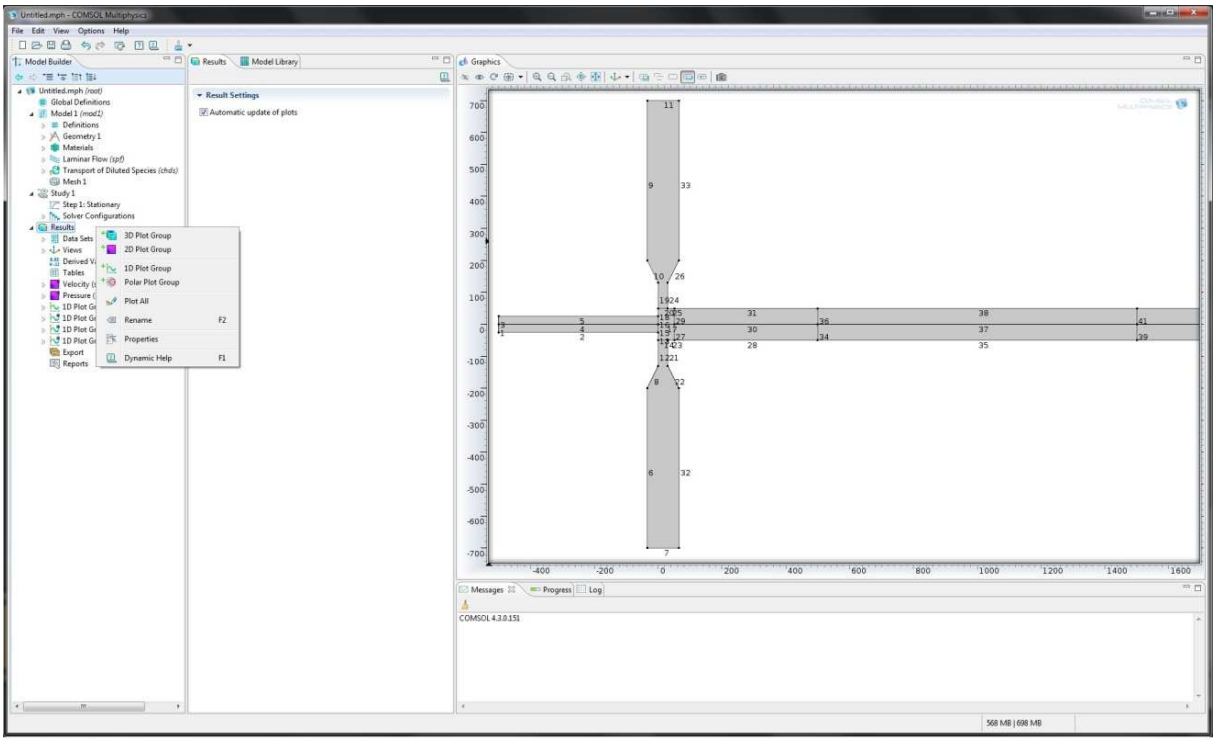


Figure A.17 shows the options of different plots when right-click Results.

b. In the Model Builder window, expand Velocity > Surface 1, and then go to the Setting window. Locate the expression section, from the expression list, choose concentration C and from the unit list, choose mol/$m^3$ for generating concentration distribution map.

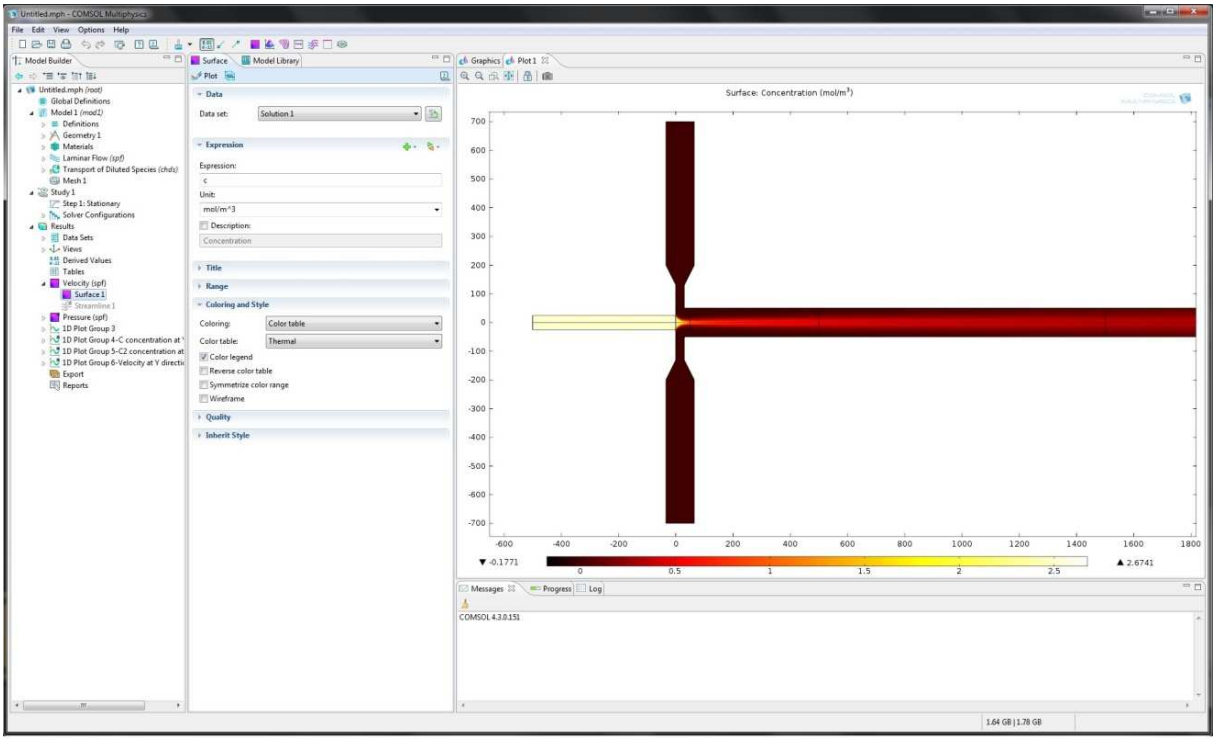


Figure A.18 shows the concentration map of designed model.

12. In the Model Builder window, right-click the results and choose 1D plot. Then right-click 1D plot Group 3 and choose Line Graph for importing data to generate the concentration distribution for center line in micro channel.

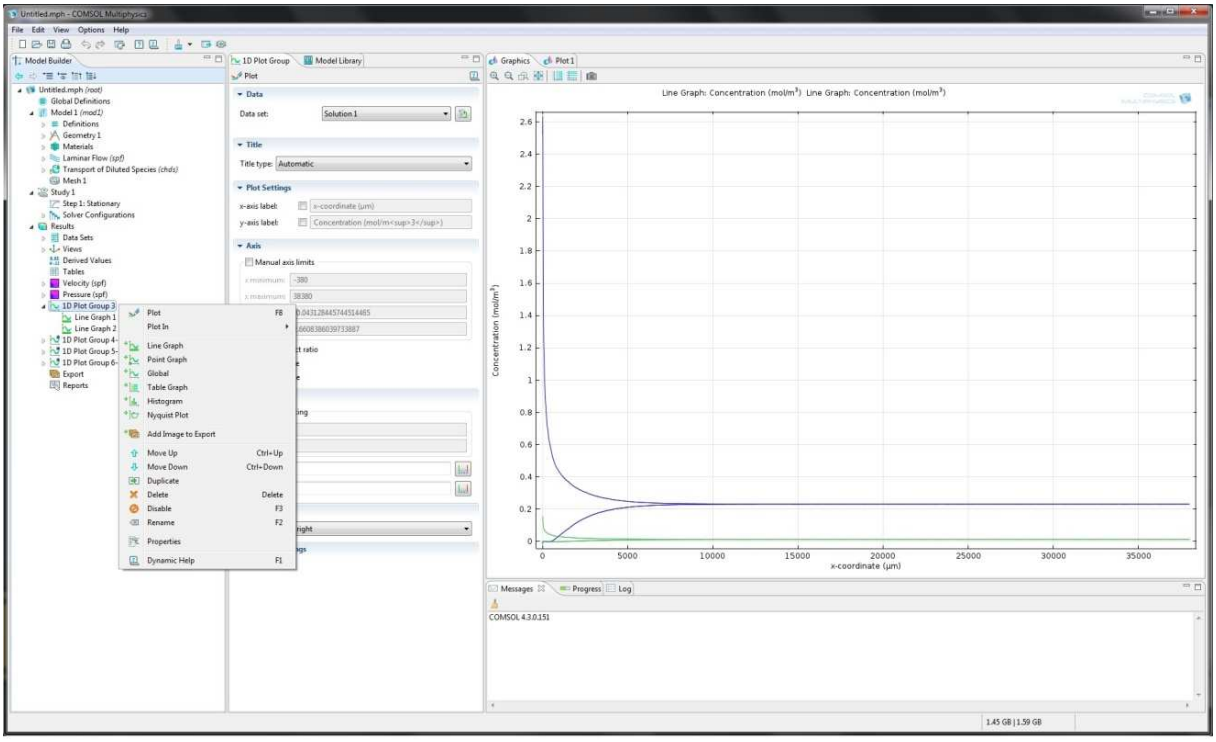


Figure A.19 shows the different type of 1D plot when you right-click 1D Plot.

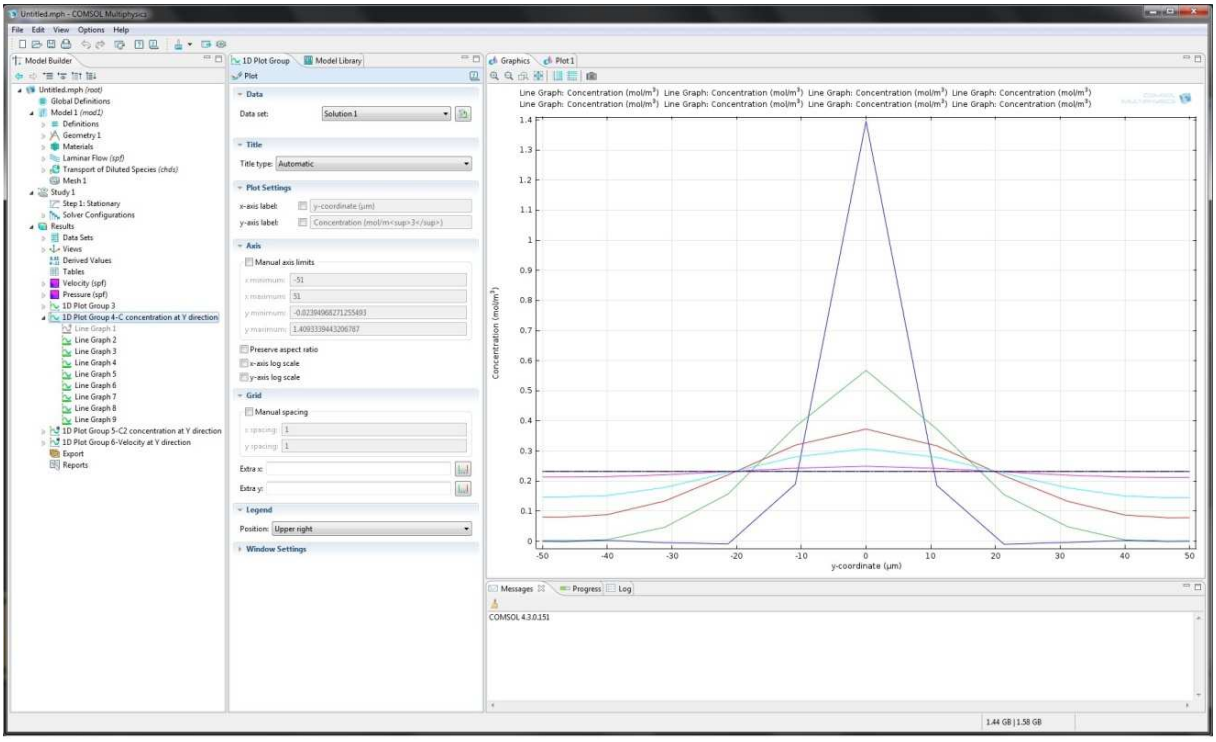


Figure A.20 shows the 1D plot for Detergent concentration distribution of cross-section along the vertical direction

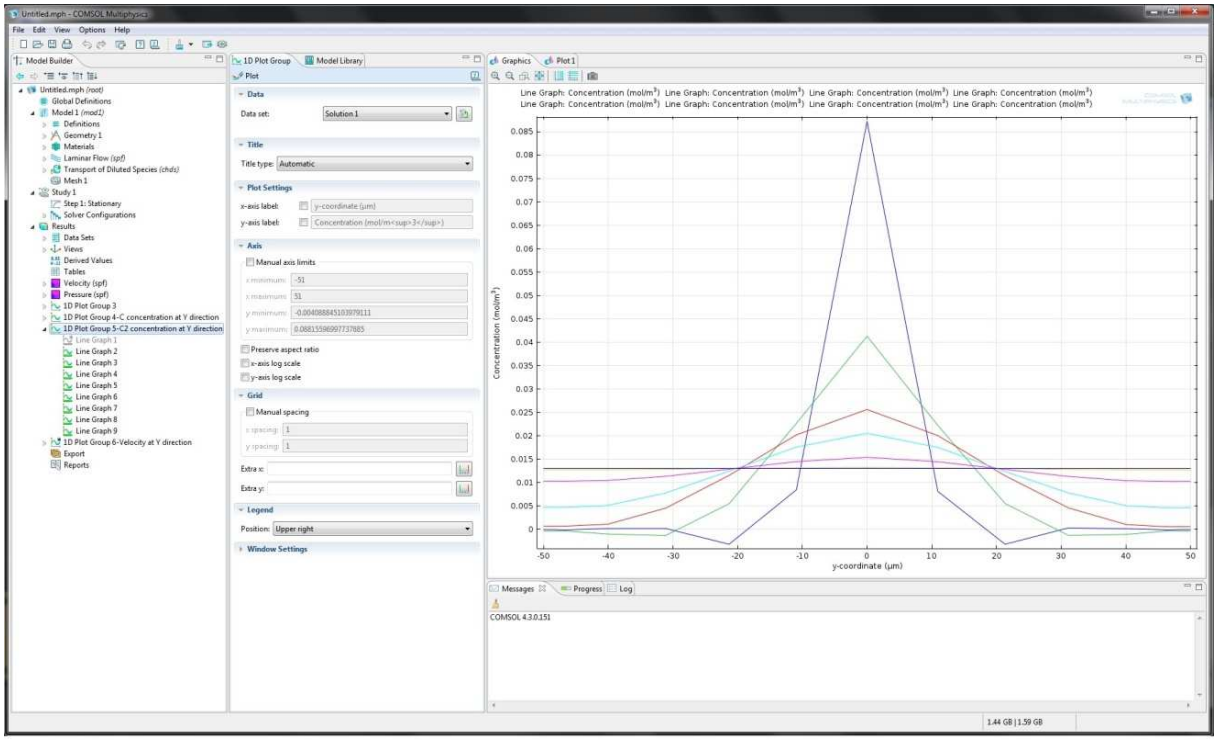


Figure A.21 shows the 1D plot for Lipid concentration distribution of cross-section along the vertical direction

# Appendix B

## Instruction of Microfluidic Experiment

### Introduction

The test vehicle for the membrane protein nanoparticle formation in microfluidic devices consists of 4 individual controllable syringe pumps with a main controller to drive fluids that can precisely adjust flow rate down to 1nl/min (Figure B.1). And then the protein/detergent, lipid, and buffer solution delivered through the connecting tube injected into the inlets of PDMS microfluidic device (Figure B.2).

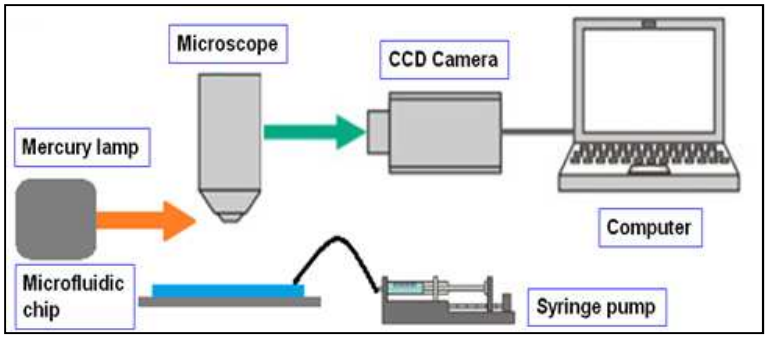


Figure B.1 shows the equipments of the entire experiment set up.

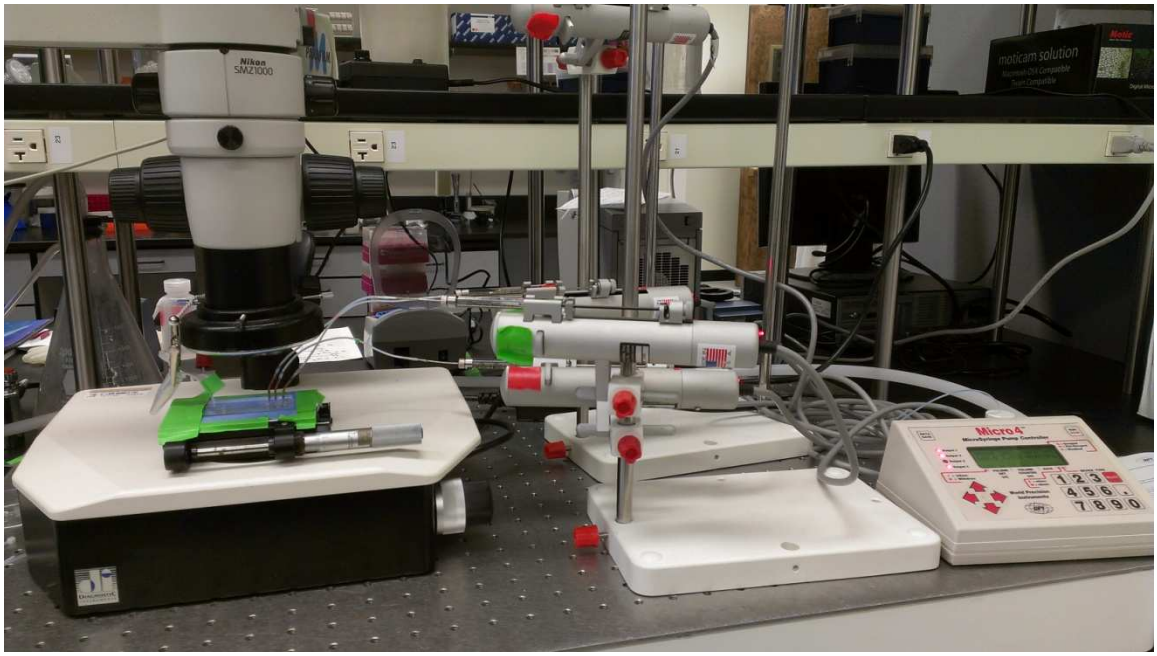

Figure B.2 shows the entire equipments placed on the leveled optic table. The main controller is on the right side.

The size of the inlets in the PDMS microfluidic device is around 1.5mm diameter connected with copper tube making a good seal to inlet. The eppendorf pipet was used for collecting the sample

from output through commercial plastic tube.

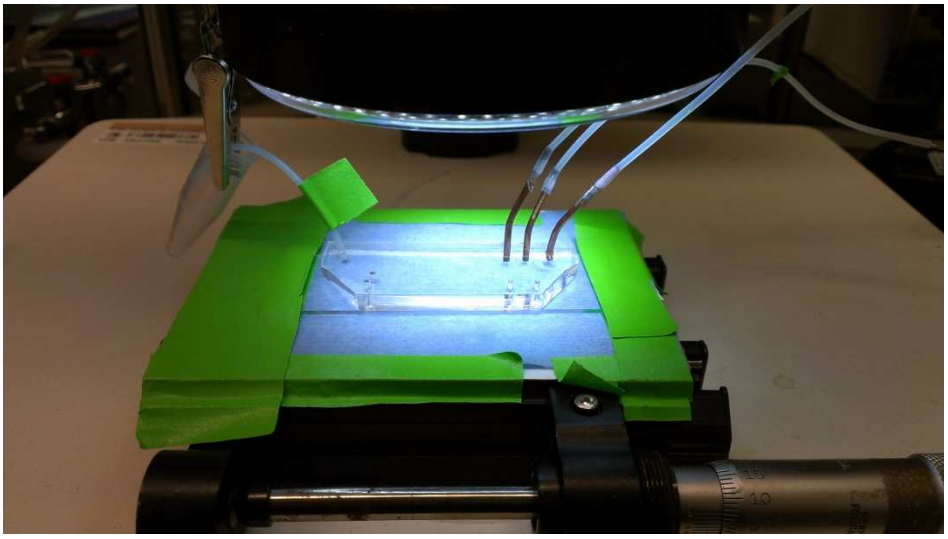

Figure B.3 shows the tubes connected from syringe pump to inlets(right) and outlet(left) of PDMS microfluidic device.

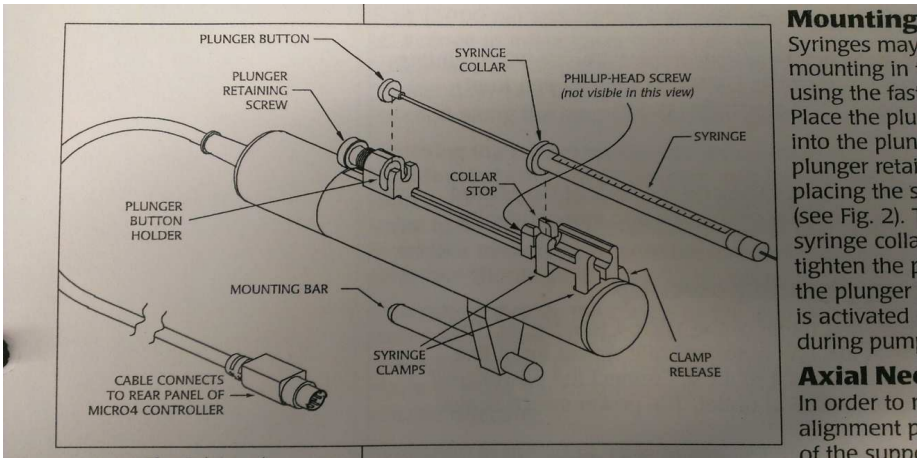


Figure B.4 shows the detail component of individual syringe pump and the method for placing the syringe onto the pump.

For preparation of the sample into the syringe, be careful to slowly load sample in for avoiding the bubble generated.

Those each 4 syringe pumps were individually controlled by the main controller (Figure B.5). When we started to run the experiment, the first step is checking the size of the syringes you are going to use. Figure B.5 shows the different volumes of syringes with different type codes. For example, 50ul syringe is type F and 100ul syringe is type G.

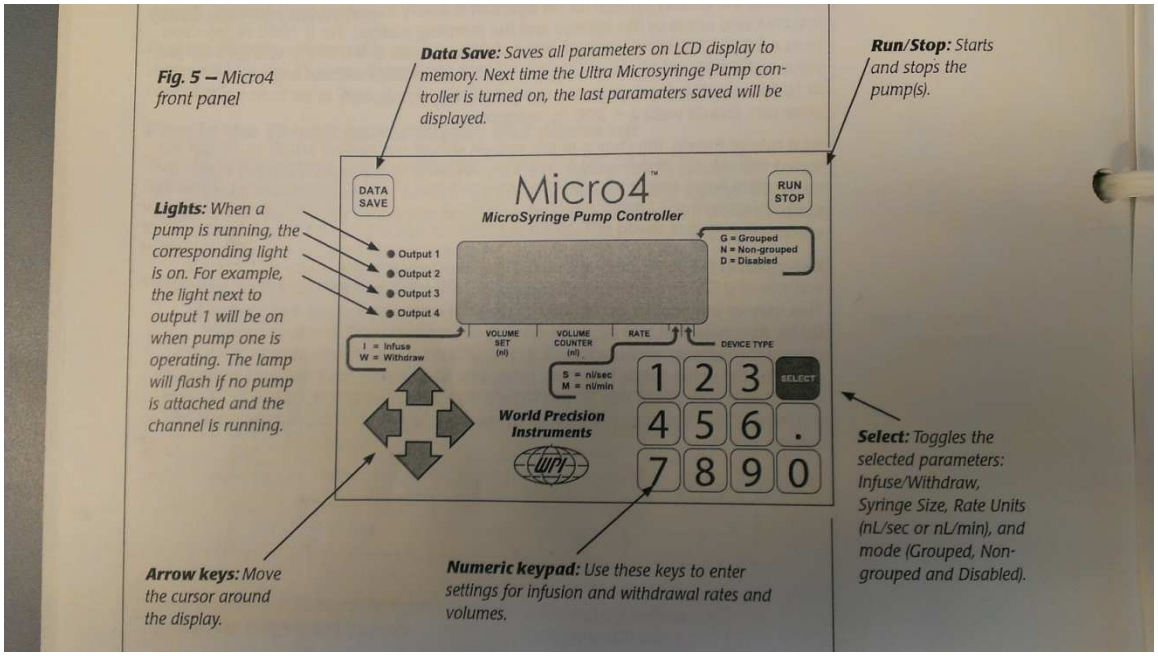


Figure B.5 shows the functions on the control panel of the main controller for controlling each individual syringe pump.

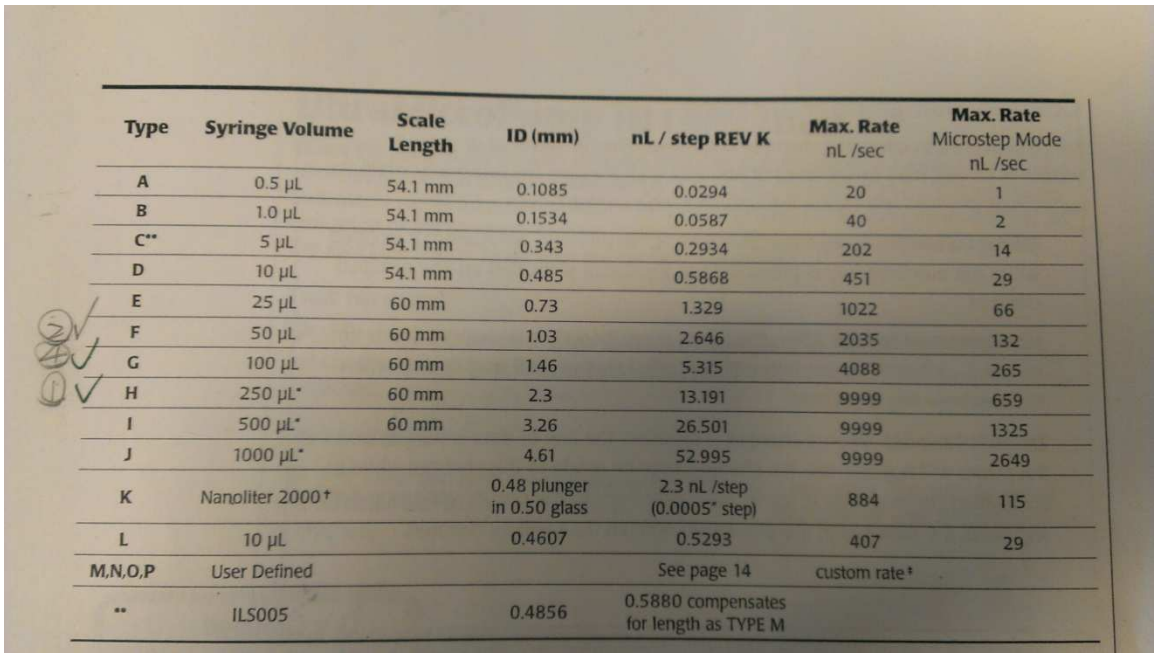

| Type | Syringe Volume | Scale Length | ID (mm) | nL / step REV K | Max. Rate nL /sec | Max. Rate Microstep Mode nL /sec |
|---|---|---|---|---|---|---|
| A | 0.5 µL | 54.1 mm | 0.1085 | 0.0294 | 20 | 1 |
| B | 1.0 µL | 54.1 mm | 0.1534 | 0.0587 | 40 | 2 |
| C** | 5 µL | 54.1 mm | 0.343 | 0.2934 | 202 | 14 |
| D | 10 µL | 54.1 mm | 0.485 | 0.5868 | 451 | 29 |
| E | 25 µL | 60 mm | 0.73 | 1.329 | 1022 | 66 |
| F | 50 µL | 60 mm | 1.03 | 2.646 | 2035 | 132 |
| G | 100 µL | 60 mm | 1.46 | 5.315 | 4088 | 265 |
| H | 250 µL* | 60 mm | 2.3 | 13.191 | 9999 | 659 |
| I | 500 µL* | 60 mm | 3.26 | 26.501 | 9999 | 1325 |
| J | 1000 µL* | | 4.61 | 52.995 | 9999 | 2649 |
| K | Nanoliter 2000† | | 0.48 plunger in 0.50 glass | 2.3 nL /step (0.0005" step) | 884 | 115 |
| L | 10 µL | | 0.4607 | 0.5293 | 407 | 29 |
| M,N,O,P | User Defined | | | See page 14 | custom rate† | |
| ** | ILS005 | | 0.4856 | 0.5880 compensates for length as TYPE M | | |

Figure B.6 shows the calibration for different types of desired syringes by volume. Most of commercial syringe are included.

Figure B.6 is the closer view of display panel from the controller. The functions from the left to right of display panel are

1. Infuse/withdraw, which control the syringe pump to moving forward or backward

2. Volume set(nl), which you can set up the maximum volume. Once the amount of volume counter reached the amount of volume set, the individual pump will automatically stop.

3. Volume counter(nl), counting the volume during injection.

4. Rate, set up the flow rate with two different unit, one is nl/sec (S) and othe is nl/min (M).

5. Device type, check the type code from the Figure B.6 depending on the volume of syringe.

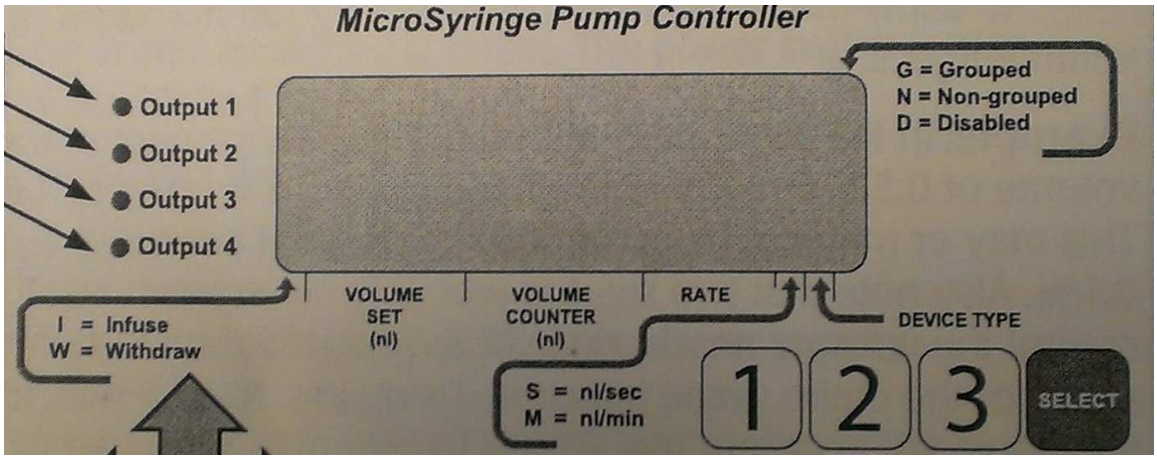


Figure B.6 show the closer view of display panel where has infuse/withdraw, volume set, volume counter, rate (nl/sec, nl/min), and device type.